

A FUZZY MODELING PLATFORM FOR FLOW
AND TRANSPORT IN ALLUVIAL AND
FRACTURED PORUS MEDIA

By

JON LANSFORD LaRUE

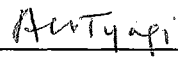
Bachelor of Science
University of Cincinnati
Cincinnati, Ohio
1979

Master of Business Administration
University of Texas
Austin, Texas
1981

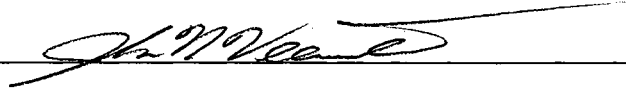
Submitted to the Faculty of the
Graduate College of the
Oklahoma State University
in partial fulfillment of
the requirements for
the Degree of
DOCTOR OF PHILOSOPHY
July, 1997

A FUZZY MODELING PLATFORM FOR FLOW
AND TRANSPORT IN ALLUVIAL AND
FRACTURED PORUS MEDIA

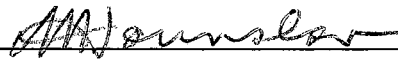
Thesis Approved:

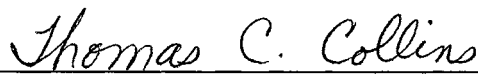


Dissertation Adviser









Dean of Graduate College

PREFACE

This research was conducted to provide new knowledge regarding the utilization of fuzzy mathematical methods to simulate groundwater flow and transport. Sensitivity analysis of traditional groundwater modeling platforms involves considering different levels of parametric uncertainty; however, the true uncertainty associated with any hydrogeologic parameter should be recognized to be a combination of two distinct types of uncertainty, the *vagueness* of a parameter, and the statistical *randomness* of the parameter. Most groundwater simulation platforms erroneously assume that the uncertainty associated with any parameter can be completely accounted for with statistical methods. In reality, the dominate type of uncertainty existing in the hydrogeological modeling environment results from the inherent vagueness of parametric values, not the randomness of the values. Fuzzy mathematical methods allow the vagueness of parameter values to be incorporated into simulation.

ACKNOWLEDGMENTS

I wish to express my sincere appreciation to my major advisor, Dr. Avdhesh Tyagi for his supervision, assistance, and encouragement in this effort. My sincere appreciation is also extend to the other committee members: Dr. John Veenstra, Dr. Arthur Hounslow, and Dr. Greg Wilber. Moreover, I wish to express my sincere gratitude to the Environmental Institute for their financial support through the Water Presidential Fellowship.

I would also like to express my special appreciation to my entire family for their support and encouragement throughout this entire effort.

TABLE OF CONTENTS

Chapter	Page
I. INTRODUCTION.....	1
II. TRADITIONAL MODELING PLATFORMS.....	5
Deterministic Platform.....	5
Analytical Solution Form.....	6
Numerical Solution Form.....	6
Stochastic Platforms.....	7
III. FUZZY MODELING PLATFORM	11
Classical Set Theory.....	12
Fuzzy Set theory.....	15
Fuzzy Numbers.....	22
IV. DETERMINISTIC, PROBABILISTIC, AND FUZZY OPERATIONS.....	25
V. ANALYTICAL GROUNDWATER FLOW APPLICATION.....	29
Comparison of Deterministic and Stochastic Realization.....	30
Deterministic Platform Solution.....	32
Stochastic Platform Solution.....	32
Fuzzy Platform Solution.....	34
VI. GROUNDWATER VELOCITY APPLICATION.....	41
Connecticut Tobacco Field Crisp Parameters.....	41
Connecticut Tobacco Field Fuzzy Parameters.....	43
Connecticut Tobacco Field: Realization Comparison.....	46
VII. ONE-DIMENSIONAL TRANSPORT APPLICATION.....	47
Governing Equations.....	47
Analytical Solution Form.....	52
Brine Lagoon Example.....	53
Analytical Platform Solution.....	54
Fuzzy Platform Solution.....	54
Comparison and Contrast of Results.....	58
VIII. BORDEN SITE EXPERIMENT.....	59
Scope of Experiment.....	59
Site Description.....	61
Experimental Methodology.....	66

Observed Chloride Plume Development.....	67
Observed Chloride Plume Trajectory.....	69
Observed Chloride Plume Vertical Displacement.....	71
Observed Chloride Plume Velocity.....	72
Summary: Borden Experiment	75
Transport Modeling Platform Comparison, Analytical vs. Fuzzy at the Borden Site.....	75
Borden Analytical Groundwater Model.....	77
Data Preparation.....	78
Mass Balance.....	84
Summary: Analytical Realization.....	96
 IX. BORDEN SITE FUZZY MODELING.....	 99
Crisp and Fuzzy Realizations.....	99
Discussion of Fuzzy Realizations.....	106
Conclusion: Borden Experiment.....	108
 X. FRACTURED MEDIA TRANSPORT APPLICATION.....	 109
Characteristics of Fractured Media.....	109
Conceptual Modeling in Fractured Media.....	112
Governing Equations.....	115
Laboratory Trial.....	117
Fuzzy Analytical Models.....	120
 XI. SUMMARY AND CONCLUSIONS.....	 129
Summary.....	129
Conclusions.....	130
 REFERENCES.....	 132
 APPENDIXES.....	 139
APPENDIX A - FUZZY MATHEMATICAL OPERATIONS.....	139
APPENDIX B - TABLE VI - NORMAL FUZZY DATA.....	142
APPENDIX C - TABLE VI - LOGNORMAL FUZZY DATA.....	148
APPENDIX D - NUMERICAL DATA FOR REDUCED 1-D DATA.....	155
APPENDIX E - CHLORIDE PLUME CENTER OF MASS.....	156
APPENDIX F - COMPLEMENTARY ERROR APPROXIMATION.....	157
APPENDIX G - FIGURE 37 DIGITIZED DATA.....	158
APPENDIX H - FIGURE 5a AND 5b DATA.....	159
APPENDIX I - FIGURE 39 FUZZY CALCULATIONS.....	160

LIST OF TABLES

Table	Page
I. Crisp Core Sample Permeabilities.....	13
II. Fuzzy Core Sample Permeabilities.....	14
III. Fuzzy Set Ordered Pairings.....	19
IV. Deterministic and Stochastic Modeling Platform Comparison.....	31
V. Percentage Difference: Monte Carlo vs. Latin Hypercube Travel Time.....	34
VI. Fuzzy Modeling Platform Parametric Distributions.....	37
VII. Percentage Difference in Fuzzy Platform Travel Time Realizations.....	38
VIII. Connecticut Tobacco Field, Crisp Hydrogeological Parameters.....	41
IX. Connecticut Tobacco Field, Fuzzy Hydrogeological Values.....	43
X. Connecticut Tobacco Field, Fuzzy Realization.....	46
XI. Summary: One-Dimensional Transport Example (mg/L).....	55
XII. Borden Aquifer Mineralogy.....	63
XIII. Borden Background Groundwater Parameters.....	64
XIV. Estimated Borden Aquifer Properties.....	65
XV. Injected Non-Reactive Tracer Composition.....	66
XVI. Results of Methods of Estimating Average Linear Groundwater Velocity.....	74
XVII. Plume Concentration Data and Realizations.....	77
XVIII. Relative Concentration Data.....	121
XIX. "Normal" Fuzzy Model Realizations: Relative Concentration.....	123
XX. "Lognormal" Fuzzy Modeling Realizations: Relative Concentrations.....	125

LIST OF FIGURES

Figure	Page
1. Fuzzy Membership Function of 25 md.....	19
2. Core Sample Number One's Degree of Membership in Fuzzy Set F.....	20
3. Overlapping Membership Functions, Fuzzy Sets Good and Pretty Good Permeability.....	21
4. Crisp Membership Function for Real Number Five.....	23
5a. "Normal" Fuzzy Distribution Travel Time vs Stochastic Realization.....	39
5b. "Lognormal" Fuzzy Distribution Travel Time vs Stochastic Realization.....	40
6. Fuzzy Hydraulic Gradient of Connecticut Bedrock.....	44
7. Fuzzy Hydraulic Conductivity of Connecticut Bedrock.....	45
8. Fuzzy Groundwater Velocity in Connecticut Bedrock.....	45
9. Membership Function of Crisp Analytical Solution	56
10. Membership Function of Fuzzy Analytical Solution.....	56
11. Membership Function of Initial Concentration.....	57
12. Membership Function of Fuzzy Longitudinal Dispersion Coefficient.....	57
13. Borden Site Geological Cross Section.....	62
14. Chloride Concentration Contours after 462 days.....	68
15. Chloride Plume Horizontal Trajectory.....	69
16. Chloride Plume Vertical Trajectory.....	71
17. Chloride Plume Horizontal Displacement vs. Time.....	73
18. Profile of Reduced 1-D Concentration Data.....	80
19. Profile of Analytical Realization.....	80

20. Analytical Solution at 1.25 meter Increments.....	82
21. Difference Between the Observed Concentration Data and the Analytical Realization.....	83
22. Ellipsoid Profile.....	85
23. Digitized Chloride Plume Data.....	88
24. Digitized Chloride Plume Data with Isopleth Overlay.....	90
25. Rough Three-Dimensional Chloride Plume Structure.....	92
26. Smoothed Three-Dimensional Chloride Plume Structure.....	94
27. Reduced 1-D Concentration Data, Analytical Realization and the Difference Between the Two.....	96
28. Crisp Analytical Realization and Fuzzy Endpoints (+/- 10%).....	100
29. Crisp Realization less Fuzzy Realization Endpoints (+/- 10%).....	101
30. Reduced 1-D Data with Analytical and Fuzzy Realizations (+/- 10%).....	102
31. Reduced 1-D Data less Fuzzy Realization Endpoints (+/- 10%).....	103
32. Reduced 1-D Data with Analytical and Fuzzy Realizations(+/- 20%).....	104
33. Crisp Analytical Realization less Fuzzy Realization Endpoints (+/- 20%).....	105
34. Reduced 1-D Data less Fuzzy Realization Endpoints(+/- 20%).....	106
35. Percentage Difference Between the Two Fuzzy Realizations.....	107
36. Physical Basis of Analytical Solution for Solute Transport in Fractured Media..	114
37. Experimental Chloride Breakthrough Data and the Analytical Solution.....	119
38. TRAFRAP-WT Solution Comparison.....	122
39. Analytical Solution and "Normal" Fuzzy Solution.....	124
40. Difference Between Centroids Obtained with Normal and Lognormal Input.....	126
41. Analytical Solution and Lognormal Fuzzy Solution.....	127

I. INTRODUCTION

Groundwater represents the single largest source of freshwater readily available to the human race, and by one estimate accounts for 98% of the world's drinking water supply [Fetter, 1988]. Unfortunately, a large percentage of the groundwater available as a public water supply has been found to be contaminated with organic chemicals, [Westrick *et al.*, 1984] while the contamination in industrialized areas has been found on a regional scale. [Fusillo *et al.*, 1985]

In order to successfully manage this critical resource we need the ability to accurately predict certain behavioral aspects of the subterranean fluid flow system. To do this various mathematical computer models have been developed to replicate and simulate the varied conditions of *in situ* groundwater flow. In most instances, it is not possible to quantify the initial mass of contaminant which entered the groundwater, nor is it possible to locate the emission source precisely in space and time. Additionally, financial and confidentiality considerations usually dictate only sparse amounts of monitoring data become publicly available. This makes it very difficult to determine an accurate delineation of a contaminant plume's concentration distribution as a function of time.

When performing any mathematical modeling simulation it is important for a user to recognize the distinction between an accurate realization and a precise realization.

Unfortunately, a computer model's *precise* output is often incorrectly assumed to be an *accurate* realization. The seminal question that must be asked of any simulation model's realization is "How accurate is the model's output?" not, "How precise is the model's output?" Notwithstanding the number of significant digits generated in a model's realization, the overall accuracy of any mathematical model is a direct function of the model's applicability, validity, and the quality and quantity of the input data.

The success of any groundwater modeling program depends largely on an accurate understanding of the subsurface environment's physical parameters. Modelers of underground flow systems are often confronted with the problem of accurately quantifying the uncertainties recognized as inherent in almost every hydrogeologic parameter's estimate. This problem becomes especially acute when a modeler must estimate parametric variables such as aquifer thickness or porosity, which usually vary both spatially and gradually. After the significant problem of accurately estimating input parameters is overcome, the modeler must then address the problem of accurately reflecting the intrinsic uncertainty in the model's output realization.

The reality of the situation is our simulation modeling abilities and resources often fall short of what is necessary to accurately characterize and mathematically recreate a

real subsurface flow system. Traditionally, the gap between our mathematical methods and the requirements for an accurate simulation has been bridged via one of two major modeling platform types, 1) deterministic modeling platforms, or 2) stochastic modeling platforms.

Each of these platforms can perform well when properly utilized, but each has its own innate limitations. Deterministic platforms are usually applied when sufficient data is available to allow the calculation of a single precise answer. Stochastic based platforms are used when input data is scarce or the modeler is attempting to account for some uncertainty in the parametric value estimates. Most groundwater simulation platforms assume all the uncertainty associated with any parameter can be completely and accurately accounted for with statistical techniques. Unfortunately, this is often an unrealistic or erroneous assumption [*Dverstorp et al.*, 1992]

The true overall uncertainty inherent in hydrogeological modeling should be recognized as originating from two different sources; 1) the randomness of parametric values and, 2) the vagueness of parametric values. Traditionally, the two major groundwater modeling platforms treat both the randomness and the vagueness of parametric values as a single type of uncertainty [*Beckie et al.*, 1994; *Berkowitz and Balberg*, 1993; *Neuman*, 1993].

Fuzzy mathematics, or possibility theory [*Dubois and Prade, 1988*] allows the recognition of the difference between these two types of uncertainty, and can be used to develop an alternative modeling platform which can bridge the oftentimes large gap laying between modeling resources constraints and accurate simulations.

The fuzzy modeling approach has been applied very successfully in other fields, and only very recently been applied to the area of groundwater modeling. This approach has been applied on a very limited basis in the areas of geomechanics [*Valliappan and Pham, 1993; Johnson and Ayyub, 1996*] and groundwater infiltration [*Bardossy and Disse, 1993*].

A fuzzy modeling approach will be applied to saturated groundwater flow and transport in this research, with the unique aspect of this research being the application of a fuzzy modeling platform to one-dimensional contaminant transport. Basic computer software utilized in this research include Lotus 123(4.1) spreadsheets, the @Risk(2.1) spreadsheet addin, and FuziCalc(1.5). Specialized software which was also used is identified in the text.

II. TRADITIONAL MODELING PLATFORMS

Deterministic Platform

A deterministic modeling platform assumes a system can be so uniquely defined that the governing differential flow equations can be solved for a single precise realization. Major simplifying assumptions must be made regarding certain input parameters in order to do this; more importantly, these assumptions must be accepted as the reality of the flow system. Recent laboratory and field experiments; however, have shown some of these key assumptions are suspect in certain situations. [*Persoff and Pruess*, 1995; *McKay et al.*, 1993; *Fourar et al.*, 1993; *Unger and Mase*, 1993; *Ewing and Jaynes*, 1995]

An example of two of the more common and significant assumptions required by many deterministic models would be the suppositions that an aquifer's media is homogenous and isotropic. There are not many homogenous and isotropic aquifers in the real world, and the mandatory simplifying assumptions such as these are commonly accepted, then quickly forgotten. Real world hydrogeologic flow systems usually exist with highly variable hydrogeological characteristics, and many of these parameter values can have a dramatic impact on localized or regional groundwater flow. Consequently, the reduced accuracy in a model's realization resulting from the

erroneous simplifying assumptions often goes unrecognized or unacknowledged by the modeler. This holds true for both of the two dominant types of deterministic solution constructs; analytical and numerical solution forms.

Analytical Solution Form

The differential flow equations which serve as the foundations for all groundwater modeling platforms can be solved via either a numerical or analytical solution form.

Analytical solution forms can provide accurate realizations when the initial and boundary conditions of a groundwater system are relatively simple, and the hydrogeologic parameters can be correctly assumed to be constant. These solutions produce an *exact* closed-form solution which is continuous in both time and space.

While the analytical solution form provides an exact answer to a well defined problem, the constraining and simplifying assumptions required to produce an analytical solution make it imperative the initial assumptions be verified. [Javandel *et al.*, 1984]

Numerical Solution Form

When complex reservoir and boundary conditions exist, a numerical solution form can provide much greater modeling flexibility than the analytical solution form.

However, the increased flexibility of a numerical solution form requires much more data and computational effort than the analytical form, and produces only an *approximate* solution to the governing differential flow equations. When numerical

solution forms are utilized it is very important the modeler make well reasoned and appropriate choices regarding model input grid spacing and time step increments. The improper selection of either of these two input parameters can cause simulation errors such as: mass imbalances, numerical oscillations, or incorrect velocity distributions.[*Remson et al.*, 1971; *Javendal et al.*, 1984] In an attempt to address these potential problems alternative numerical mathematical techniques, such as simulated annealing [*Maudon et al.*, 1993] and the method of decomposition [*Serrano*, 1995a/1996b] have recently been proposed. To address the fundamental limitations of the deterministic platforms, stochastic modeling platforms were developed.

Stochastic Platforms

Stochastic, or probability-based, modeling platforms attempt to characterize the inherent variability found in physical system parameter estimates with statistical methods. [*Hoeksma and Kitandis*, 1985; *Warrick et al.*, 1986] This type of modeling platform attempts to represent all the uncertainty of modeling as either a function of the mathematical randomness of a parameter's value, or as the uncertainty created when limited sample data is used to represent and characterize an entire flow system. These platform models typically use some form of the normal distribution function shown below to represent the various input parametric distributions.

$$F(x) = \frac{1}{\sigma\sqrt{2\pi}} \int_{-\infty}^{(x-\mu)/\sigma} e^{-u^2/2} \sigma du \quad (1)$$

One of the more basic and popular solution forms used with the stochastic modeling platform is Monte Carlo simulation.[*White and Gehman, 1979*] The term "Monte Carlo" came about during World War II as the code name for modeling simulations used in the development of the atomic bomb. Today, the words "Monte Carlo simulation" are considered synonymous with any number of techniques used to repeatedly sample probability distributions by any sort of random or pseudo-random method. Most of these types of solution forms use each individual sampling iteration to produce a single simulation realization, and present the final output result as a compilation of all of the individual realizations. The output realization is usually presented in the form of a probability distribution or a cumulative frequency distribution.

Theoretically, Monte Carlo sampling is based on an entirely random process, and proves statistically that with enough sampling iterations one can accurately create an output realization distribution which is representative of the entire range of possible realization outputs. While this may be true from a mechanical sense, the key to obtaining accurate output realizations with a Monte Carlo solution form, or any other statistics based solution form, is the modeler's ability to accurately describe each modeling parameters' input distribution. This, unfortunately, is extremely difficult to achieve when working with real world hydrogeological parameters.

One of the functional disadvantages of the Monte Carlo solution form is the computational aspect. Complex Monte Carlo models require a great deal of computational effort and can require hours of computer processing time. Consequently, other solution forms were developed on the stochastic modeling platform to address this short fall.

Latin Hypercube solution forms are similar to Monte Carlo solution forms in that they rely upon repeated random sampling of input parameter probability distributions. The key difference is that the Latin Hypercube sampling technique requires fewer iterations than Monte Carlo methods to accurately reproduce parameter input distributions. This is achieved by segmenting the cumulative probability distribution curve of each input variable into equally sized intervals. Each interval is then randomly sampled only once during processing, and this sample is used to produce an output realization. This sampling technique forces samples to be taken from every area of a parameter's cumulative distribution, and consequently, insures both high and low probability events are represented in the simulation realization. While Latin Hypercube sampling provides for faster computations and shorter computer processing time, the limitations of this sampling technique are the same as those which must be associated with all stochastic modeling platforms. Namely, accurate output realizations can only be obtained if accurate statistical descriptions of the input parameters are used in the model.

The greatest strength of the stochastic modeling platform is also its greatest weakness. Specifically, a certain level of statistical uncertainty must always be associated with any model's output. By its very nature, this type of modeling platform output cannot produce a precise realization, and may not produce an accurate one, as experience teaches us that many real world groundwater modeling situations do not lend themselves well to either gross simplifying assumptions or stochastic based modeling.

A similar, but fundamentally different, platform based on the fuzzy mathematical modeling concept has been used in this research to address the above problems.

Fuzzy mathematical modeling platforms are based upon the fundamental concepts of fuzzy sets; however, before fuzzy sets are discussed, a brief review of classical set theory is in order.

III. FUZZY MODELING PLATFORM

While the term fuzzy logic is very much in vogue, these days one rarely hears the term fuzzy modeling. The reality of the situation is fuzzy modeling is one of the most critical, if not the pivotal, issue in the broader concept of fuzzy theory.

The foundation of fuzzy modeling was laid by Zadeh [Zadeh, 1965] more than 20 years ago in his early works regarding fuzzy mathematics and fuzzy theory.

Historically, one of the issues in the recognition and acceptance of fuzzy modeling lies with the definition and interpretation of the concept of what really is fuzzy modeling. One practice considers a fuzzy set to be a fuzzy model of a human concept, while another considers fuzzy modeling to be a qualitative modeling technique whereby system behavior is described with natural language concepts. This latter consideration of fuzzy modeling is a narrower view of the fuzzy concept whereby systems are described with fuzzy quantities. Fuzzy quantities are described by fuzzy numbers associated with linguistic labels or characterizations.

This work suggests a qualitative model should be regarded as a generalized fuzzy model wherein linguistic terms are used to describe system behavior. This approach requires accepting the precept that natural language terms approximate fuzzy sets under the fuzzy modeling platform, and that linguistic terms can be used to describe

relationships of state variables in system definition and behavior. Accepting this precept allows the use of linguistic terms to describe system behavior in qualitative and quantitative terms. The qualitative concept is an extremely important one to grasp and was promoted through the concept of the fuzzy algorithm [Zadeh, 1965].

A specific example of a fuzzy algorithm is:

Set "Y" approximately equal to 10 if "X" is approximately equal to 5.
If "X" is large, increase "Y" by several units.

This algorithm can be viewed in its most basic sense as a qualitative description of the human decision making process. Mundane activities such as hitting a golf ball, parking a car, treating medical conditions, or cooking beef stew can be described via fuzzy algorithms. The necessity of fuzzy algorithms became apparent to Zadeh after he observed:

"Most realistic problems tend to be complex, and many complex problems are either logarithmically unsolvable, or if solvable in principle, are computationally infeasible."

Fuzzy algorithms could not exist without fuzzy sets, and fuzzy sets form the basis and foundation of fuzzy theory and fuzzy modeling. The relationship of fuzzy sets to classical set theory is discussed below.

Classical Set Theory

Classical set theory defines a set as a collection of objects in which each object shares a common and specific membership property. Subset "S" of the universal set "U"

could be defined with traditional mathematics as sets of ordered pairs. A singular pair of two numerical elements exists for each element in U , and by definition consists of only two real values. The first element of any ordered pair is the individual item in set U , while the second portion of any pair is an element of the set $\{0,1\}$. The second part of the ordered pair, either 0 or 1, is used to indicate if the item exists in subset S . A zero as the second element in the pair indicates the pair does not exist or belong within subset S , while a 1 indicates the item does belong in subset S .

For example, let's assume we obtain 5 different core samples from a single well drilled into a non-fractured, limestone aquifer. Each core sample is analyzed for permeability, and the following values are obtained;

TABLE I
CRISP CORE SAMPLE PERMEABILITIES

Core Sample	<u>#1</u>	<u>#2</u>	<u>#3</u>	<u>#4</u>	<u>#5</u>
Permeability "k" (md)	18	23	26	29	37

Set " T " is then designated to contain "*tight*" core samples, and tight core samples are defined as those samples which exhibit a permeability lying somewhere between 20 and 30 millidarcies ("md").

The ordered pair membership mapping function for T can thus be written as:

$$M(T) = \begin{cases} 20 \leq k \leq 30, & 1 \\ \text{Otherwise,} & 0 \end{cases} \quad (2)$$

and yields the membership pairings as shown in Table II.

TABLE II
FUZZY CORE SAMPLE PERMEABILITIES

<u>Sample #1</u>	<u>Sample #2</u>	<u>Sample #3</u>	<u>Sample #4</u>	<u>Sample #5</u>
(18, 0)	(23, 1)	(26, 1)	(29, 1)	(37, 0)

These pairings indicate the core samples with permeability less than 20 md or more than 30 md exist with a membership grade of 0, and therefore must lie outside the "tight" set T . Samples exhibiting permeability between 20 md and 30 md are included in set T as dictated by the membership grade of 1. Thus, set T contains only three members, core samples #2, #3, and #4, as samples #1 and #5 do not belong in set T . These pairings simply state set T has been defined so that the individual elements of the sample universe have been dichotomized as either members or nonmembers.

The validity of the statement, "Sample #2 is tight" can be evaluated by simply examining sample #2's ordered pair. Table II shows the first element of the pair is 23 md, and the second element is the real value 1. The statement can be considered

to be valid as the second element of the pair requires the sample to belong within Set T . Fuzzy set theory is based on a similar evaluation process, and all of the operations traditionally performed with classical set theory can be utilized and applied to fuzzy set theory.

Fuzzy Set Theory

Fuzzy sets and fuzzy mathematics were originally developed in an attempt to mathematically represent the vagueness of the human language [Zadeh, 1965]. Zadeh noticed human beings use many words as if the words are mathematical concepts. Words such as "few" and "many" are often used to represent numbers, while words such as "frequently" and "rarely" are commonly employed to represent probabilities. Traditional mathematical operations cannot be performed using words as variables because identical words have different, but fundamentally similar meanings to different people. Simply put, exacting definitions of words are "fuzzy," because there is no universal agreement as to a single common and precise definition for every word. For example, what specifically characterizes a fracture as being "long" or an aquifer as "thick." The vague nature of common agreement of descriptive words lies at the heart of fuzzy theory. Both fuzzy theory and traditional mathematics can trace their roots back to the logical nature of set theory.

Fuzzy set theory, like classical set theory, can also describe the elements in a universe with sets of ordered pairs. The first element of any pair is interpreted identically as

in classical set theory; the difference in the interpretation of the second element of the pair is what makes fuzzy set theory fundamentally different.

The unique aspect of fuzzy set theory is that the infinite number of values lying within the *interval* 0 and 1 can be used to represent various *degrees of membership* in the set [Zimmermann, 1985]. It is true fuzzy sets also use a 0 value as the ordered pair's second element to indicate complete non-membership in a set, and a numerical value 1 to indicate complete membership in a set; however, the second element of the ordered pair does not always limit an item to being exclusively a member or a non-member of the set, but rather indicates the degree to which an item belongs to the set. Fuzzy sets do not have clear limits or boundaries and, in effect, are collections of objects which vary continuously and discretely. In the final analysis the fuzzy mathematical concept of *degrees of membership* is simply a numerical conception used to indicate how much an element belongs to a particular set. Mathematically speaking, the formal definition [Kaufmann and Gupta, 1985] of a fuzzy set is:

If T is the set universe, F is a fuzzy subset of T if F exists as sets of ordered pairs such that $\mu_F(t)$ is the membership grade of t in fuzzy set F , when the value $\mu_F(t)$ takes its values in the closed interval of $[0,1]$.

$$F = \{(t, \mu_F(t)); t \in T, \mu_F(t) \in [0,1]\} \quad (3)$$

The closer $\mu_F(t)$ is to 1, the more t belongs to F and conversely, the closer $\mu_F(t)$ is to zero, the less t belongs to F . The fuzzy subset F can be viewed as a conventional

subset of T if the closed interval $[0,1]$ is replaced by the two element set of $\{0,1\}$.

The remainder of this paper will consider fuzzy subsets as if they are fuzzy sets for the sake of simplifying the discussion.

Fuzzy sets can be used to answer the types of questions classical set theory cannot address, such as; "If you remove the rocks from a pile of rocks one rock at a time, when does a pile of rocks cease to be a pile of rocks?" The fuzzy answer is, "The pile of rocks leave the set of piles of rocks as smoothly as each individual rock is taken away." Classical set theory demands an abrupt transition from being either in or out of the pile of rocks set. The difference between the fuzzy set answer and classical set answer to this rocky question helps illustrate why fuzzy mathematics can be useful to model variables which can vary continuously and spatially, such as hydraulic conductivity or aquifer thickness.

One example of a fuzzy set could be the set of "deep" groundwater aquifers located in the United States. Some U.S. aquifers would certainly belong in this set, while others clearly would not. If the word "deep" is not crisply defined, i.e. $\text{deep} \geq 45$ feet below the earth's surface, many U.S. aquifers would exist in the somewhat fuzzy transition zone of "somewhat deep."

A fuzzy Set "F" of the previously discussed five core samples shown in Table I could be defined as the set of samples whose permeability is *approximately* 25md. The

definition of the word "*approximately*" is fuzzy, and being fuzzy cannot be interpreted universally with a commonly agreed upon unique membership function.

Common sense dictates some of the five core samples will have a greater degree of "belonging" in set F than some of the other samples. As the membership grade of each sample approaches 1.0, the permeability value of each sample must move closer to 25 md. Set "F" would clearly include the value 25 md as a member of the set, and most people would agree the value 24 md is close to the value 25md. Most people would also agree the numerical value 20 is closer to the numerical value 25 than is the numerical value 17. The overall agreement regarding of what is close to 25 allows a fuzzy Set "F" to be represented by a wide variety of membership functions. This example will use the isosceles triangle defined below as equation 4, and represented as Figure 1 for the fuzzy membership function. Fuzzy membership functions are also commonly referred to as fuzzy belief graphs.

$$M_F(t) = \begin{array}{|l|l|} \hline k \leq 10, & 0 \\ \hline 10 \leq k \leq 25 & (k-10)/15 \\ \hline 25 \leq k \leq 40 & (40-k)/15 \\ \hline P \geq 40, & 0 \\ \hline \end{array} \quad (4)$$

By definition, an infinite number of membership functions could be developed to describe fuzzy Set "F." The fact is that although the uniqueness of Set "F" is sacrificed when Set "F" is defined as a fuzzy set, the same fuzziness provides for much greater mathematical modeling flexibility than can traditional mathematics.

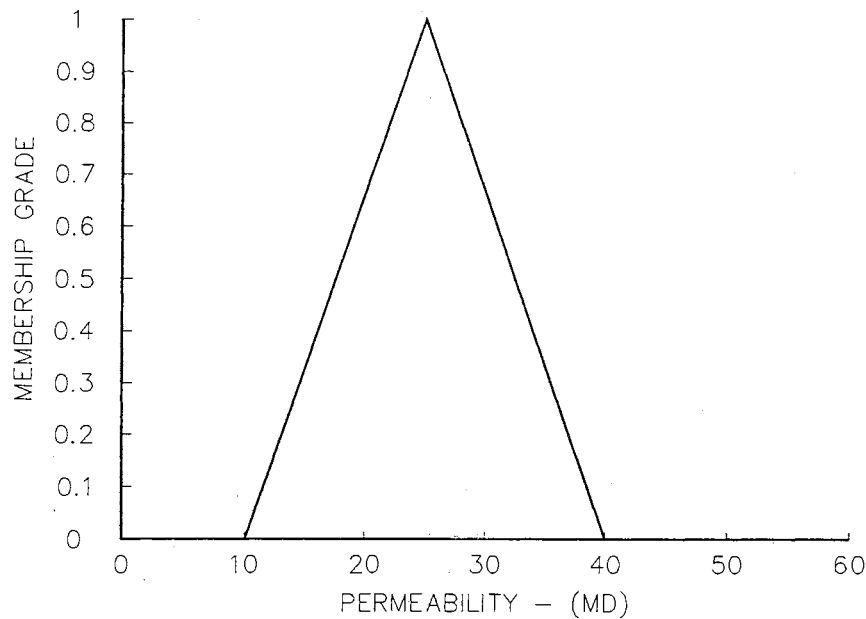


Figure 1. Fuzzy Membership Function of 25 md.

The membership function for the "*approximately*" 25md fuzzy set F yields the ordered membership pairings of:

TABLE III

FUZZY SET ORDERED PAIRINGS

<u>Sample #1</u>	<u>Sample #2</u>	<u>Sample #3</u>	<u>Sample #4</u>	<u>Sample #5</u>
(18, 0.53)	(23, 0.87)	(26, 0.93)	(29, 0.73)	(37, 0.20)

Each sample's second element indicates the degree of membership the sample has, or can claim, in the fuzzy set. For example, in Sample #1 the second element is 0.53; this number indicates the degree of membership which sample #1 has in fuzzy set F ,

and can also be thought of as the degree of truth of the statement "Sample #1 (18 md) lies in set F." This statement is represented graphically as the membership function or belief graph shown as Figure 2.

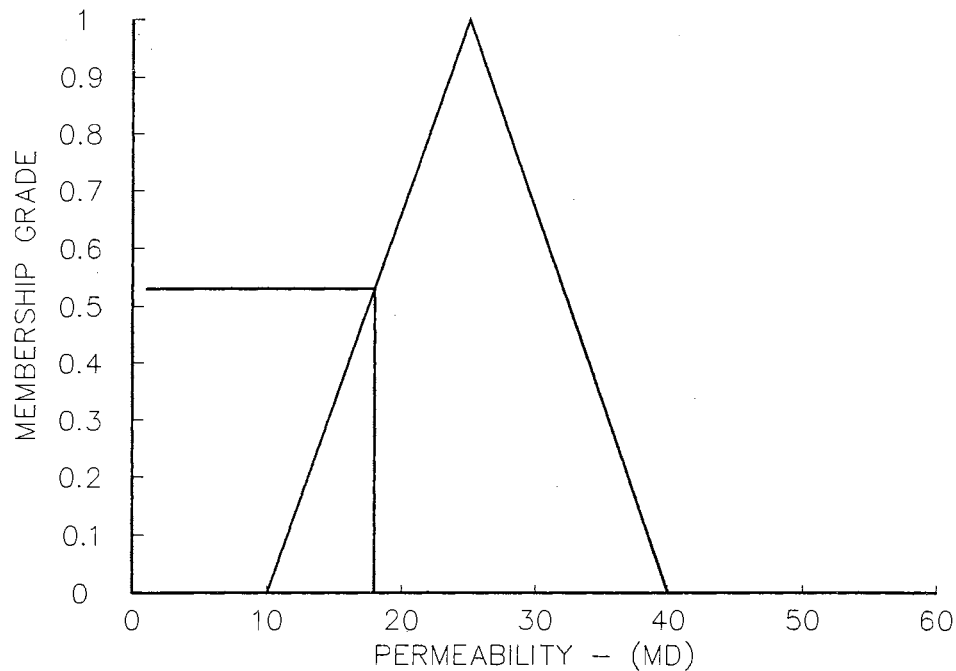


Figure 2. Core Sample Number One's Degree of Membership in Fuzzy Set F

Figure 3, shown on the following page, shows the fuzzy set of "good" permeability, and the fuzzy set of "pretty good" permeability. The set of *good* permeability is defined as the set permeability exhibiting values close to 40 md, and is represented in the membership graph by the larger triangle with endpoints of 15 md and 65 md. The smaller triangle, having endpoints at 10 md and 40 md represent the fuzzy set *pretty good* permeability.

Samples #4 and #5 can be seen to have greater degrees of membership in the fuzzy *good* permeability set than do core samples #1, #2, or #3 as $\mu_F(g)$'s 0.49 and 0.72 are larger than $\mu_F(g)$'s 0.10, 0.25, or 0.36. However, all five samples are members of both the *pretty good* and *good* permeability set as the respective membership grades fall within the 25 md to 65 md support of the *good* permeability membership graph, as well as the 10 md to 40 md support of the *pretty good* permeability membership graph.

The ability of multiple fuzzy sets to overlap and contain element items having concurrent membership in multiple fuzzy sets is one of the major strengths of fuzzy modeling.

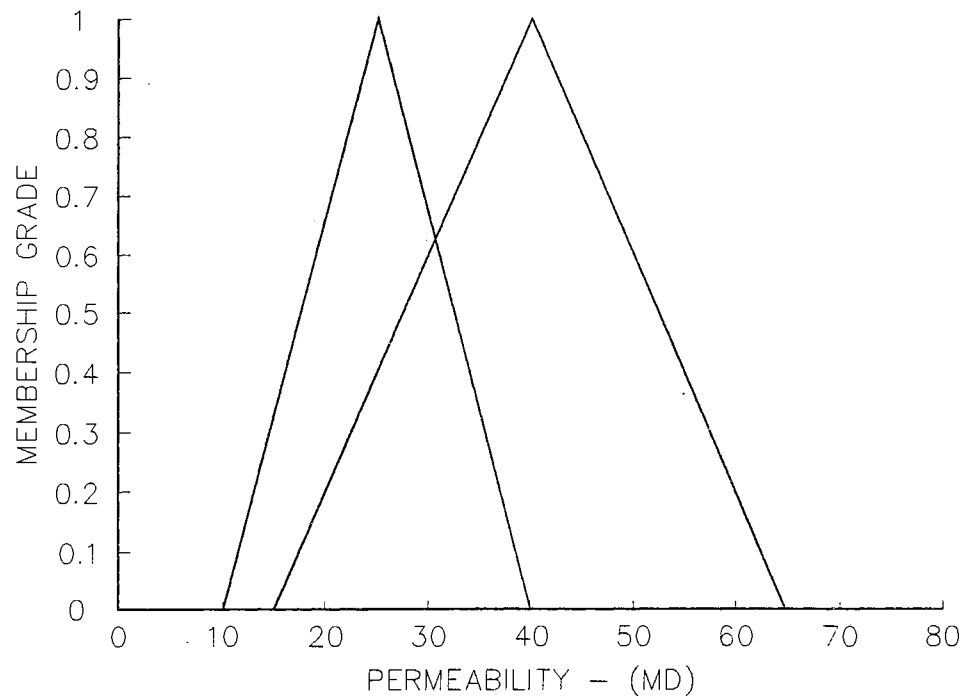


Figure 3. Overlapping Membership Functions, Fuzzy Sets *Good* and *Pretty Good* Permeability.

Fuzzy Numbers

Fuzzy numbers are a special case of fuzzy sets [Zimmermann, 1985] and because fuzzy numbers are numbers, it is possible to perform standard mathematical calculations with them. Mathematically speaking, fuzzy numbers are defined as follows:

A fuzzy subset F of a set of real numbers can be considered a fuzzy number if there is at least one z such that $\mu_F(z)=1$, and such that for every real number a, b, c , with $a < c < b$.

$$\mu_F(z) \geq \min (\mu_F(a), \mu_F(b)) \quad (5)$$

The membership function of a fuzzy number, like that of a fuzzy set, usually consists of an increasing and a decreasing part, and one of the simplest types of fuzzy numbers is a triangular fuzzy number. Any fuzzy number can be used as a "crisp" number when it is necessary to represent the fuzzy number as a single real value.

In fuzzy mathematics a "crisp" number may be thought of as a fuzzy number existing with a single point base line support. Figure 4 shows the support for the crisp, real number five.

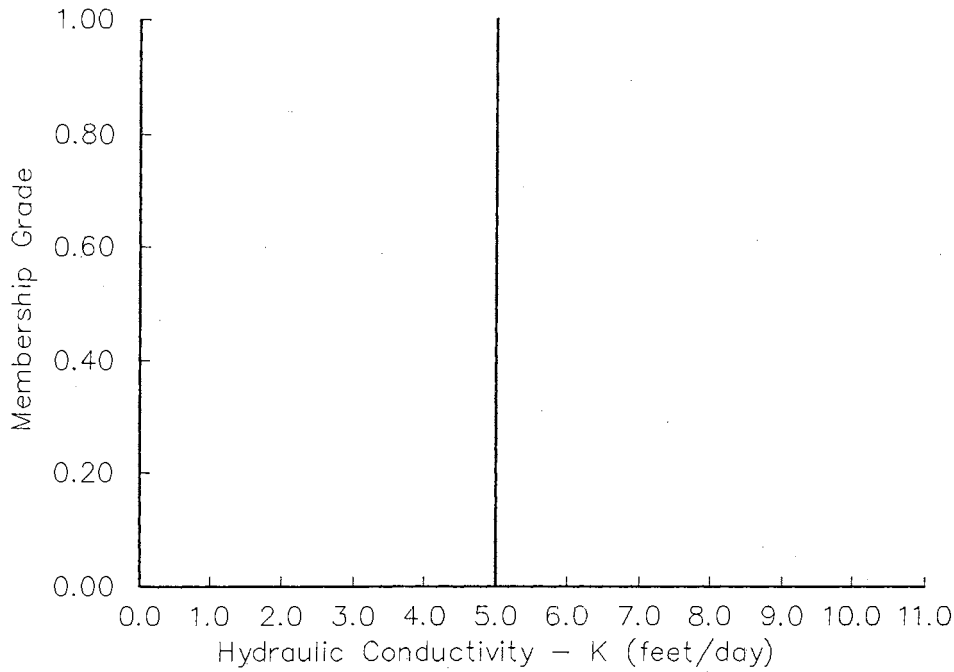


Figure 4. Crisp Membership Function for Real Number Five

The base line support of a fuzzy set contains all the elements which have non-zero membership grades. Mathematically speaking, the support of the fuzzy set F is defined as:

$$\text{supp}(F) = \{t; \mu_F(t) > 0\} \quad (6)$$

The support for the fuzzy "*approximately*" 25md set represented by the triangular membership graph shown in Figure 3 ranges from 10 to 40.

The "defuzzifying" of a fuzzy number into a representative single real value can be accomplished in a multitude ways, and [Mizumoto, 1982] has documented over thirty

such methods. One of the most common defuzzifying methodology is the "fuzzy mean" technique.

The fuzzy mean of a fuzzy subset F is the number $M(F)$ for which:

$$\int_{-\infty}^{M(F)} (M(F) - t) \mu_F(t) dt = \int_{M(F)}^{+\infty} (t - M(F)) \mu_F(t) dt \quad (7)$$

One of the major advantages of the fuzzy mean defuzzifying methodology is that the calculation is extremely fast and simple and is quite suitable for computer simulation modeling.

IV. DETERMINISTIC, PROBABILISTIC, AND FUZZY OPERATIONS

Accurate deterministic modeling solutions are predicated on utilizing accurate and precise variable parameters in the appropriate underlying modeling algorithm. The fundamental structural errors which can be introduced into the modeling solutions by the improper choice of parameter values often goes unexamined. Fuzzy modeling; on the other hand, is predicated upon using vaguely defined parameters. One of the primary tenants of fuzzy modeling is that the uncertainty introduced into a modeling platform's solution by the use of fuzzy parameters is relatively small when compared to the uncertainty introduced by traditional parameter estimation techniques and the requisite models' assumptions. The recognition and acknowledgment of some of the limitations and effects of parameter estimation in simulation modeling lead to the development of stochastic based modeling platforms. When the traditional modeling platforms approach their limitations, fuzzy methods can be used.

While cursory inspection of fuzzy mathematical theory could give one the incorrect impression fuzzy mathematics is simply another statistical technique, probability and fuzzy theory are not only conceptually different, they are also mathematically distinct. Fuzzy mathematics, like classical probability theory, does deal with uncertainty, and does operate with the numerical values 1 and 0. However, fuzziness portrays

uncertainties in a less tightly defined nature than probability theory, and therefore is more amenable to addressing a broader degree of uncertainty. This allows fuzzy mathematics to deal with the subjective uncertainty or the *vagueness* of parameters; whereas probability theory is limited to dealing with the *frequency* or the *randomness* of parameters. Vagueness results from the difficulty in making clear or sharp distinctions, whereas randomness is associated with the degree of frequency of occurrence. Vagueness is usually the dominate type of uncertainty in a geophysical environment as insufficient information usually exists to estimate the frequency distributions required for probability based models.

One of the base mathematical requirements of probability theory is the axiom of additivity. All the probabilities of a given event must sum to 100%, or stated another way, the integral of a cumulative density curve must always equal one. Fuzziness does not carry this restriction because membership distributions are not probability distributions, nor are they frequency values determined from repeated trials. Despite the fact that probabilities and possibilities appear to take on similar values, it is vitally important to realize membership grades are not probability density functions. Belief graphs, unlike probability distribution, decrease in width as uncertainty is removed from a fuzzy number. Fuzzy membership functions simply represent the similarities of objects having imprecisely defined properties, whereas probabilities convey information regarding the chance of a specific event, or the occurrence of a relative frequency.

From the purely mathematical perspective, some authors have contended both fuzzy sets and probability theory exist as parts of a greater Generalized Information Theory. [Klir, 1991] This theory postulates that while fuzzy sets are not probability sets, the converse is true, that is; all probability distributions are fuzzy sets. Broadly inclusive theories regarding fuzzy mathematics such as Klir's upset many people and some raise seemingly valid objections. [Haack, 1979] However, the undisputable fact is that fuzzy based methods have recently found their way into real world products such as: cement kilns, dishwashers, and automobiles. The successes fuzzy methods have achieved in the real world marketplace validates the fuzzy modeling platform concept as one of practical value and worth expanded investigation.

One significant advantage fuzzy based mathematical platform has over other modeling platforms is the ability to be initialized without well defined input variables. This attribute has been found to allow fuzzy based platforms to work well with both limited and non-linear input data,[Bardossy and Disse, 1993] and data exhibiting large degrees of non-statistical uncertainty. [Johnson and Ayyub, 1996]

When modeling subsurface flow systems important hydrogeologic parameters often end up being described as either a stochastic distribution or a simple range of crisp values. An alternative method can be used when the lack of high quality real data becomes a major problem, namely describing the input parameters with fuzzy numbers. The following example demonstrates that the fuzzy modeling platform is

quite flexible in that the information from a few crisp data points can easily be combined with assumed relationships based on experience and judgement. The following one-dimensional groundwater Darcy flow modeling problem contrasts a fuzzy based modeling platform realization with the realizations derived from the more traditional deterministic and stochastic modeling platforms.

V. ANALYTICAL GROUNDWATER FLOW APPLICATION

Assume a fresh water aquifer has been contaminated with a highly miscible and toxic substance, and a drinking water supply well is located down gradient from the last known location of the contaminant plume. If we assume away dispersion, degradation, and retardation effects, the time of arrival of the plume at the drinking water supply well can be expressed by coupling a simplified one-dimensional darcy saturated flow model (eq. 8), with a linear rate-time relationship (equ. 9).

$$V = \frac{(H * K)}{P} \quad (8)$$

and

$$T = \frac{D}{V} \quad (9)$$

Combining equations 8 and 9 yields:

$$T = \frac{D}{\frac{H * K}{P}} \quad (10)$$

where: V= Ground water velocity (ft/sec)
H= Hydraulic gradient (ft/mile)
K= Hydraulic conductivity (ft/day)
P= Effective porosity (%)
T= Travel time (days)
D= Distance between well and leading edge of plume (ft)

Hydrogeologic parameter values obtained from the drinking water supply well located 2,000 feet down gradient from the contamination indicate the aquifer porosity to be 20%, the hydraulic conductivity of the aquifer to be 5 ft³/ft²/day, and the groundwater gradient to be a uniform 300 ft/mile.

Of the three model input parameters necessary to calculate the darcy groundwater velocity, two of the variables, porosity and hydraulic conductivity, are highly spatially variable.

Comparison of Deterministic and Stochastic Realizations

Table IV shows the input parameters and the resulting realizations for an analytical deterministic platform solution, as well as four different stochastic platform solutions. Two of the stochastic platform solutions assumed normally distributed parameters, while the other two assumed lognormally distributed parameters.

TABLE IV

DETERMINISTIC AND STOCHASTIC MODELING PLATFORM COMPARISON

DETERMINISTIC PLATFORM MODEL

<u>INPUT</u>			<u>OUTPUT</u>
<u>Porosity (%)</u>		<u>Hydraulic Conductivity (ft/day)</u>	<u>Travel Time (days)</u>
20 (crisp)		5 (crisp)	1,407

STOCHASTIC PLATFORM MODEL

	<u>Normal Distribution Input</u>						<u>OUTPUT</u>		
	<u>Porosity (%)</u>			<u>Hydraulic Conductivity (ft/day)</u>			<u>Travel Time (days)</u>		
	min.	mean	max.	min.	mean	max.	min.	mean	max.
Monte Carlo	16.5	20.0	23.4	1.5	5.0	9.0	741	1,474	4,957
Latin Hypercube	16.1	20.0	23.6	1.3	5.0	8.8	803	1,472	5,232

	<u>Lognormal Distribution Input</u>						<u>OUTPUT</u>		
	<u>Porosity (%)</u>			<u>Hydraulic Conductivity (ft/day)</u>			<u>Travel Time (days)</u>		
	min.	mean	max.	min.	mean	max.	min.	mean	max.
Monte Carlo	16.6	20.0	24.2	2.3	5.0	12.8	522	1,466	3,092
Latin Hypercube	16.7	20.0	23.8	2.6	5.0	10.6	627	1,454	3,392

Deterministic Platform Solution

Each realization discussed in this paper was obtained from simulations run on the identical 486 microprocessor computer. The analytical solution realization for the crisp saturated darcy flow model indicates the required travel time for the contaminant plume to reach the water well to be 1,407 days. A numerical solution was not required, nor used, in this example due to the simplicity of the problem's initial structure. While the realization obtained from the deterministic platform model is simple and computational appealing, its practical limitations are obvious. No reasonably intelligent person would consider waiting 1,407 days before finding another drinking water supply.

Stochastic Platform Solution

Two different stochastic modeling platform scenarios were evaluated using both of the two sampling techniques discussed in Section II. One scenario assumed a normal distribution for both porosity and hydraulic conductivity input values, while the other scenario assumed a lognormal distribution for the same parameters. Both the Monte Carlo and Latin Hypercube sampling simulations were run using 5,000 iterations with a three percent auto-stop convergence mode [*Palisades Corp*, 1995]. Table IV shows the input parametric values derived from both the Monte Carlo and the Latin Hypercube sampling of normally distributed variables having a standard deviation of one. Table IV also shows similar sampling realizations obtained from sampling lognormally distributed variables with each variable's distribution also exhibiting one

standard deviation. The table also shows the resulting travel time realizations obtained by utilizing the input parameters acquired from each sampling technique under the respective scenarios as an output distribution of travel time. While porosity and hydraulic conductivity usually exhibit some statistical dependency in the real world, any functional dependency between the two parameters has been ignored for the purposes of this example.

Inspection of Table IV will indicate the minimum and mean travel time realizations obtained from the normally distributed variables are very close to the same realizations obtained from the lognormally distributed parameters. The differences existing between the maximum travel time realizations are consistent with calculations based on parametric values obtained from the tailing end of a lognormal distribution. Table IV also indicates that while the mean travel time realization values for both normal and lognormally distributed parameters are similar, larger percentage differences exist between the output extremes. The variability in the endpoint travel time realizations helps to illustrate the importance of obtaining accurate description statistics for each input variable, something which is rarely possible or practical.

Table V illustrates the percentage difference in travel time between the two sampling techniques using the different input variable distribution assumptions. Examination of the table shows the mean realization obtained from the Latin Hypercube sampling mode is extremely close to the mean realization obtained from Monte Carlo sampling

of both normal and lognormally distributed inputs. Since these results are very similar, and the fact the Latin Hypercube sampling mode results were obtained twice as quickly, three minutes versus over six minutes for each simulation, Latin Hypercube sampling was used to obtain the stochastic platform realizations discussed in the following section.

TABLE V

Percentage Difference: Monte Carlo vs. Latin Hypercube Travel Time

<u>"Normal" Parametric Input Distributions</u>		
Minimum	Mean	Maximum
8.4	0.1	5.5
<u>"Lognormal" Parametric Input Distributions</u>		
Minimum	Mean	Maximum
20.1	-0.8	9.8

Fuzzy Platform Solution

It is well documented that many real world hydrogeological parameters are distributed in a lognormal fashion in the subsurface environment, and much effort and time has been spent with logarithmic transformed data [Cushman, 1983; Unlu et al., 1989]. Two questions which should be addressed before utilizing a fuzzy modeling platform are:

1. How does a lognormal distribution translate into a fuzzy number?,

2. What effects on fuzzy model output will be realized by using fuzzy numbers to represent lognormally distributed variables?

The answer to the first question is straightforward. In the simplest case a lognormal distribution can be represented via a skewed triangular membership graph just like a normal distribution can be well represented with an isosceles triangle. The defuzzification process of a fuzzy "lognormal" value is identical to the defuzzification of any other shaped membership function. For the purposes of this discussion the centroid of a fuzzy distribution will be used to represent the fuzzy number in a crisp fashion.

In a normal statistical distribution the distance between the minimum value and the most likely value is equal to the distance from the most likely value to the maximum value. In a lognormal distribution the log of each of these two distances is equal. Consequently, a very good approximation of a lognormal relationship can be achieved via forcing a triangular distribution to fit the following relationship [McGill, 1977]:

$$\frac{\text{Minimum Value}}{\text{Most Likely Value}} = \frac{\text{Most Likely Value}}{\text{Maximum Value}} \quad (11)$$

This relationship indicates that the square of the Most Likely Value must equal the Minimum Value multiplied by the Maximum Value. This relationship was used to develop the fuzzy lognormal triangular membership functions used in Table VI.

Table VI shows the fuzzy travel time realizations obtained by using both isosceles and skewed triangular membership functions to represent model input values of porosity and hydraulic conductivity. The isosceles triangular distribution represented a normally distributed parameter, while the skewed triangular distribution represented lognormally distributed variables.

Four different cases or scenarios were run, whereby each case represented a different level of support of the fuzzy parameter. Each case adjusted the absolute maximum and minimum value of the fuzzy number by a fixed percentage of the original centroid value; i.e. Case 1, 10%; Case 2, 20%; Case 3, 30%; and Case 4, 40%. The ten percent support case defines the minimum fuzzy endpoint as ninety percent of the centroid, and its maximum endpoint as one hundred and ten percent of its centroid. For example, the hydraulic conductivity in Case One has support values ranging from 18 md to 22 md because 18 md is 90% of the assumed centroid value 20 md, and 22 md is 110% of 20 md. Case Four on the other hand has hydraulic conductivity support ranging from 12 md to 28 md. These support ranges demonstrate that as the certainty of a fuzzy number becomes greater, the support becomes smaller, and conversely, as the uncertainty is greater, the support range becomes larger. This aspect of fuzzy modeling allows the incorporation of specialized knowledge into parameter selection. The fuzzy membership functions of both the input and output parameters shown in Table VI can be found in Appendices B and C.

TABLE VI
FUZZY MODELING PLATFORM PARAMETRIC DISTRIBUTIONS

	<u>Triangular Distribution Input</u>						<u>OUTPUT</u>		
	<u>Porosity (%)</u>			<u>Hydraulic Conductivity (ft/day)</u>			<u>Travel Time (days)</u>		
	Min.		Max.	Min.		Max.	Min.		Max.
	$\mu_F(t)=0$	$\mu_F(t)=1$	$\mu_F(t)=0$	$\mu_F(t)=0$	$\mu_F(t)=1$	$\mu_F(t)=0$	$\mu_F(t)=0$	$\mu_F(t)=1$	$\mu_F(t)=0$
Case 1	18	20	22	4.5	5.0	5.5	1,152	1,425	1,721
Case 2	16	20	24	4.0	5.0	6.0	939	1,477	2,112
Case 3	14	20	26	3.5	5.0	6.5	758	1,573	2,618
Case 4	12	20	28	3.0	5.0	7.0	604	1,725	3,289

	<u>Skewed Triangular Distribution Input</u>						<u>OUTPUT</u>		
	<u>Porosity (%)</u>			<u>Hydraulic Conductivity (ft/day)</u>			<u>Travel Time (days)</u>		
	Min.		Max.	Min.		Max.	Min.		Max.
	$\mu_F(t)=0$	$\mu_F(t)=1$	$\mu_F(t)=0$	$\mu_F(t)=0$	$\mu_F(t)=1$	$\mu_F(t)=0$	$\mu_F(t)=0$	$\mu_F(t)=1$	$\mu_F(t)=0$
Case 1	18	20	22.2	4.5	5.0	5.6	1,140	1,422	1,736
Case 2	16	20	25.0	4.0	5.0	6.3	901	1,488	2,197
Case 3	14	20	28.6	3.5	5.0	7.1	690	1,641	2,920
Case 4	12	20	33.3	3.0	5.0	8.3	509	1,866	3,872

Table VI shows the fuzzy numbers' endpoints and unity values along with the fuzzy travel time realization obtained by using fuzzy triangular membership functions to approximate lognormal distributions of the input parameters for the each case. In these cases only the maximum values of each parameter's fuzzy membership function was adjusted to force fit the membership function to maintain the value relationship shown in Equation 11.

Table VII indicates the travel time error created by utilizing a fuzzy number to represent a normal distribution through the use of an isosceles membership function instead of the more hydrogeologically correct lognormal triangular membership function is minimal.

TABLE VII
PERCENTAGE DIFFERENCE IN FUZZY PLATFORM
TRAVEL TIME REALIZATIONS

Triangular Input Distribution vs. Skewed Triangular Distribution

Support	$\mu_F(t)=0$	$\mu_F(t)=1$	$\mu_F(t)=0$
Case 1 (10%)	1.0	0.0	0.8
Case 2 (20%)	4.0	1.0	4.2
Case 3 (30%)	8.9	4.5	11.7
Case 4 (40%)	15.6	8.4	17.9

The differences are notably small in cases with supports of 10, 20, and 30 percent. While the differences in the minimum and maximum values in Case Four appear significant, the percentage difference in the $\mu_F(t)=1$ travel time is very reasonable

considering the magnitude of the difference between the underlying support values.

Figure 5a plots the fuzzy based platform travel time realization obtained from utilizing "normal" triangular distributions with the realization obtained from a stochastic platform solution utilizing identical triangular parametric distributions. This figure plainly shows the differences between the realizations obtained from a stochastic and a fuzzy modeling platform solution are quite small. The differences between the two methods are particularly diminutive in comparison to the great overall uncertainty inherent in accurately defining groundwater modeling parameters. The graph shows that the fuzzy solution expands its solution range faster than the stochastic model as doubt about the input is increased. Conversely, the range of a fuzzy realization contracts much faster than the stochastic solution as doubts regarding parametric input is reduced.

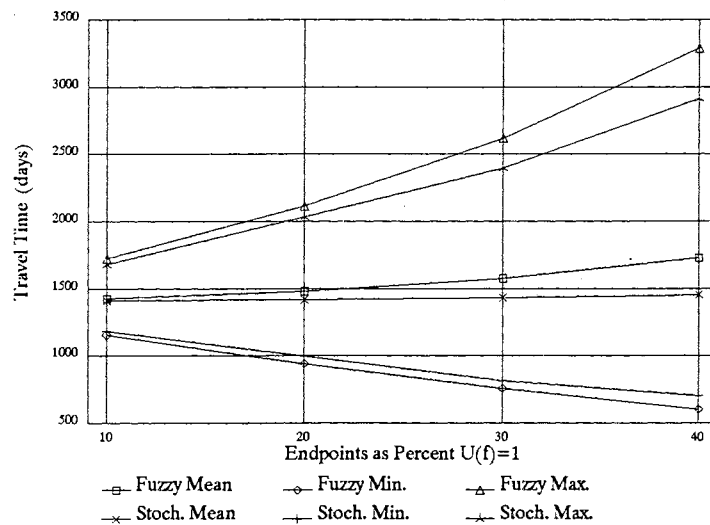


Figure 5a. "Normal" Fuzzy Distribution Travel Time vs Normal Stochastic Realization.

Note that the mean fuzzy travel times compare very well to the stochastic mean travel times, and both the fuzzy and stochastic means compare very well to the deterministic solution.

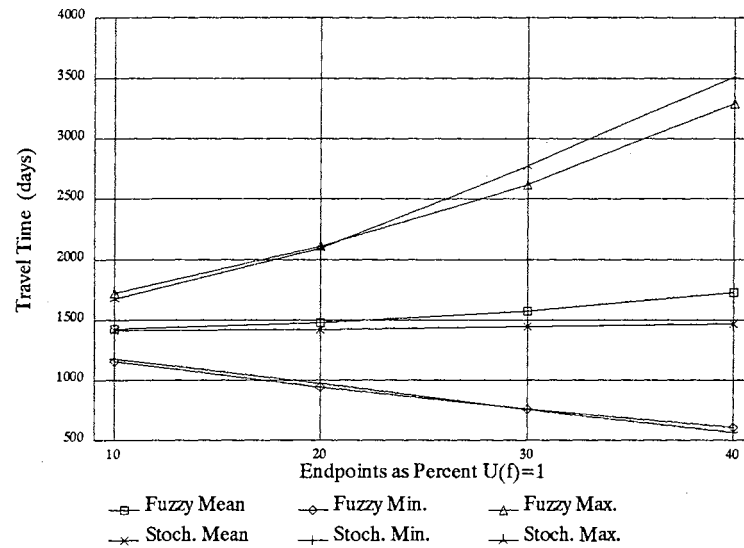


Figure 5b. "Normal" Fuzzy Distribution Travel Time vs Lognormal Stochastic Realization.

Figure 5b shows the same fuzzy solution data as Figure 5a with a stochastic solution utilizing lognormal input distributions. This graph has the same characteristics as Figure 5a, although the the fuzzy and stochastic solutions are somewhat tighter than before. This would indicate the fuzzy modeling platform incorporates some of the beneficial attributes of stochastic lognormal input distributions without the need for laborous calculations.

VI. GROUNDWATER VELOCITY APPLICATION

Connecticut Tobacco Field Crisp Parameters

Addressing a real world flow problem with the fuzzy modeling approach yields similarly encouraging results. Table VIII shows the hydrogeological parameters derived from eight samples of bedrock and six samples of overburden taken under a tobacco field in Connecticut [Pignatello, *et. al.*, 1990] The hydraulic conductivity of the overburden was obtained via the Hvorselev piezometer field method, while the bedrock's hydraulic conductivity was measured via packer testing.

TABLE VIII
CONNECTICUT TOBACCO FIELD: MEASURED
HYDROGEOLOGICAL PARAMETERS

Porosity			
Overburden	0.30		
Bedrock	0.10		
Hydraulic Conductivity (m/yr)			
	Mean	Range	
Overburden	1,200	79.9	- 5,290
Bedrock	246	24.5	- 327
Hydraulic Gradient (m/m)			
	Mean	Range	
Overburden	0.025	0.018	- 0.030
Bedrock	0.0134	0.0082	- 0.0148

Groundwater Velocity (m/yr)	
Overburden	100
Bedrock	33

The groundwater velocity shown in the table is the calculated velocity based on the mean hydrogeologic parameters and using the reported fixed porosity parametric values of 0.3 and 0.1 for the overburden and the bedrock respectively. The table shows that the ranges of measured hydraulic conductivity parameters vary by orders of magnitude for both sets of samples. This disparity is consistent with, and is often representative of, a very heterogenous spatial subsurface environment.

Variables exhibiting elemental distributions, such as those seen in Table VIII, indicate a very high degree of uncertainty, and the associated vagueness, exists in correctly describing the actual *in situ* environment. The nature of a media's heterogeneity has a direct impact on the type of modeling platform which should be utilized, as well as the application of the platform.

Recently, Paleologos et. al., showed that with respect to hydraulic conductivity, larger representative elementary volumes ("REV") should be used in groundwater modeling as media heterogeneity increases. Their work also suggests that how a modeling element should be treated in a modeling platform is largely dependent upon the size of the elemental block relative to the REV scale.

If we accept the reasonable supposition that the degree of precision in the characterization of any parameter decreases as the scale and heterogeneity of the parameter increases, we have variables which are ideal candidates for description and manipulation by a fuzzy modeling platform.

Connecticut Tobacco Field Fuzzy Parameters

Table IX shows fuzzified versions of the mean values found in Table VIII. These fuzzy values, as well as every fuzzy value used in this research, were obtained by using Fuzicalc v1.50 computer software. The endpoints of the normal triangular membership graph's support values were chosen to be plus or minus ten percent of the mean values shown in Table VIII.

TABLE IX
CONNECTICUT TOBACCO FIELD:
FUZZY VALUES

Hydraulic Conductivity			Hydraulic Gradient		
	$\mu K(t)=0$ - m/yr	$\mu K(t)=1$		$\mu I(t)=0$ - m/m	$\mu I(t)=1$
Overburden	1078.1 to 1320	1200		0.0225 to 0.0275	0.0249
Bedrock	221.4 to 271.7	246		0.01206 to 0.0147	0.0134

The hydraulic conductivity and the gradient values shown above were applied as fuzzy numbers with Darcy velocity Equation 8 to develop a fuzzy groundwater velocity.

Figures 6, 7, and 8 shown on the following pages are graphical representations of the data shown in Table IX regarding bedrock.

Figure 6 shows the hydraulic gradient of the bedrock expressed as a fuzzy parameter. The support of the fuzzy hydraulic gradient can be seen to exist between 0.012 and 0.01474. The centroid of the fuzzy number is 0.0134.

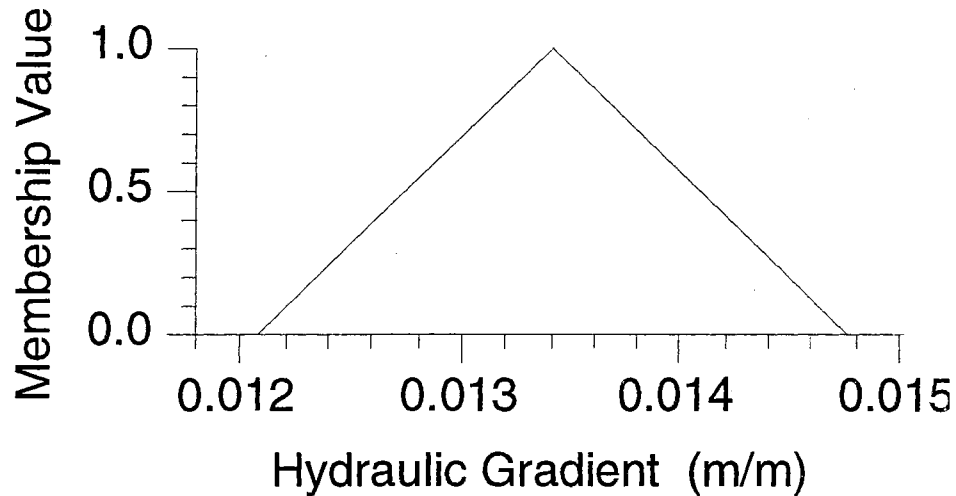


Figure 6. Fuzzy Hydraulic Gradient of Connecticut Bedrock

Figure 7 shows the hydraulic conductivity of the bedrock expressed as a fuzzy variable. The support of the fuzzy hydraulic conductivity can be seen to exist between 221.4 and 271.7. The centroid of the fuzzy hydraulic conductivity is 246.

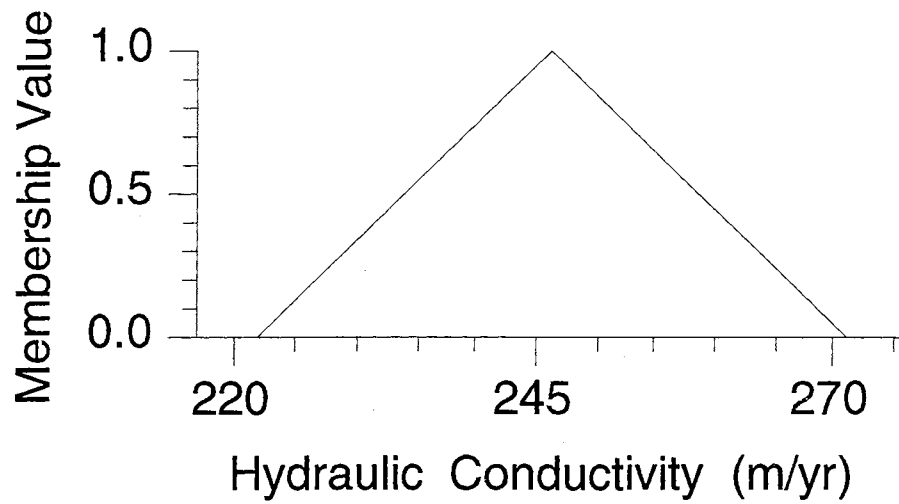


Figure 7. Fuzzy Hydraulic Conductivity of Connecticut Bedrock

Utilizing the fuzzy parameters represented in Figures 6 and Figure 7 with Equation 8 yields the fuzzy groundwater velocity represented below as Figure 8.

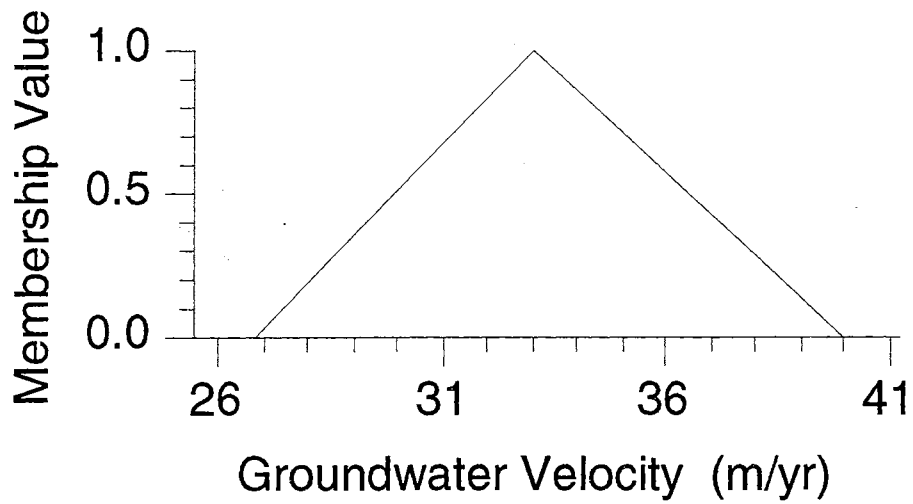


Figure 8. Fuzzy Groundwater Velocity in Connecticut Bedrock.

The figure could be interpreted as indicating the groundwater velocity in the bedrock definitely lies between the values 26.7 and 39.9 m/yr, and is believed to be 32.9 m/yr.

TABLE X
CONNECTICUT TOBACCO FIELD:
FUZZY REALIZATION

	Groundwater Velocity (m/yr)	
	$\mu V(t)=0$	$\mu V(t)=1$
Overburden	81.0 and 121.0	100
Bedrock	26.7 and 39.9	32.9

Connecticut Tobacco Field: Realization Comparison

A comparison of Tables VIII and X indicates the centroid of the calculated groundwater velocity to be within 1 percent of the mean groundwater velocity obtained from field measurements. The differences in two modeling platform approaches is small enough to suggest the fuzzy mathematical modeling platform captures the essence, if not the totality of accurate simulation in this real world example.

The two previous examples have demonstrated how a fuzzy modeling platform can be used to simulate groundwater flow and velocity. The following section will illustrate the use of a fuzzy groundwater modeling platform to simulate the transport of a unretarded contaminant in a homogenous groundwater flow media.

VII. ONE-DIMENSIONAL TRANSPORT APPLICATION

A soluble contaminant's rate of travel through an aquifer will be the same as the average linear velocity of the aquifer's groundwater if the contaminant is not retarded or reacted in some manner in the flow media matrix. Without retardation or reaction effects the rate of advective transport in an aquifer is usually estimated from some form of Darcy's law. In order for Darcy's Law to be applicable, the existence of steady state flow conditions, along with a saturated, homogenous, and isotropic porous flow media must be assumed.

Governing Equations

Equation 12 represents a one-dimensional flow state, and indicates that the average linear velocity of groundwater is proportional to the hydraulic gradient and the open pore volume in the flow matrix.

$$v_x = \frac{K}{n_e} \frac{dh}{dl} \quad (12)$$

Where: dh/dl = hydraulic gradient
 v_x = average linear velocity
 K = hydraulic conductivity
 n_e = effective porosity

As we know, physical flow and transport processes in the real world are rarely completely described by linear relationships like the one shown above. Even if an idealized aquifer could be found, an accurate description of the movement of any groundwater contamination would need to consider the mass transfer, or diffusion process, of the contamination into uncontaminated groundwater as an additional transport process.

The diffusion process itself involves the physical laws of the conservation of mass, and describes the molecular process of dissolved contaminant ions moving from areas of higher concentration into areas of lower concentration. Fick's First and Second Laws are generally applied to describe the diffusion of a solute into, and throughout, water. Inspection of Fick's First Law, shown below for a one-dimensional flow state as Equation 13, indicates the mass flux is proportional to both an empirically derived diffusion coefficient, and the solutes' concentration gradient.

$$F = -D \frac{dC}{dx} \quad (13)$$

Where:

F = mass flux of solute per unit area per unit time
D = diffusion coefficient (area/time)
C = solute concentration (mass/volume)
 dC/dx = concentration gradient (mass/volume/distance)

This law describes the mass flux of a non-retarded solute passing through a given cross sectional area per unit of time under steady state conditions. Fick's Second Law, shown for one dimensional flow as Equation 14, expands the First Law Equation to incorporate time into the diffusion phenomenon.

$$\frac{dC}{dt} = D \frac{d^2C}{dx^2} \quad (14)$$

Where: dC/dt = the change in solute concentration with time

The molecular diffusion process is a slow one, and a solute's diffusion in porous media cannot progress as rapidly as it can in open water due to blockage by the media itself. Both soluble and non-soluble aquifer contamination, like groundwater, can only flow through the open pathways in the media. In order to consider the actual flow pathways, an effective diffusion coefficient is commonly employed to modify the theoretical diffusion process in order to match reality. Diffusion coefficients have been derived empirically, and are documented to range from 0.01 to 0.5. The diffusion coefficient cannot be derived in the field and must be determined from laboratory data. One additional real world complication for describing the diffusion process is the fact the solute ions must maintain electrical neutrality as they diffuse.

The above factors combine to make the diffusion coefficient one of the most ill-defined and least understood parameters in groundwater modeling. As such, it is a

prime candidate for fuzzy estimation.

The reality of the flow environment is such that the effects of ionic diffusion and mechanical mixing combine to blend a contaminant with uncontaminated groundwater during transport in the flow media. Mechanical mixing, or dispersion, occurs even during the typically laminar flow conditions of groundwater transport. This phenomenon is mainly caused by the tortuous flow pathways the fluid must take.

Groundwater modeling usually does not consider either molecular dispersion or mechanical mixing as stand alone parameters, rather, the two different and distinct individual phenomena are combined into a single mathematical restriction referred to the dispersion coefficient. The dispersion coefficient attempts to describe both mechanical dispersion and molecular diffusion by a single expression. Equation 15 represents the coefficient of hydrodynamic dispersion for a one-dimensional flow system. This expression represents the mixing which occurs along the stream path of fluid flow and only accounts for longitudinal dispersion. Mixing which occurs in directions other than that of the x axis is accounted for with a lateral dispersion term which is usually taken as some percentage of the estimated longitudinal coefficient of diffusion.

The first term of the equation, $a_L v_x$ represents mechanical mixing, while the last term D^* represents the molecular diffusion process. Neither of these two parameters can

be measured directly in a field environment.

$$D_L = a_L v_x + D^* \quad (15)$$

Where:

- D_L = longitudinal coefficient of hydrodynamic dispersion
- a_L = dispersivity
- v_x = average linear groundwater velocity
- D^* = effective diffusion coefficient

The parameter D^* is required to account for the effects of actual *in situ* flow pathways, the conservation of mass, and electrical neutrality. As this coefficient cannot be derived in the field, it must be determined solely from laboratory data. The coefficient has been documented to range from 0.01 to 0.5. [Berner, 1971]

Combining the laws of the conservation of mass with the coefficient of dispersion yields the one-dimensional advective-dispersion transport equation for hydrodynamic dispersion for the $C(0,t) = C_0$ and $C(x,0) = 0$ boundary conditions shown as Equation 16. The first boundary condition requires a continuous source of contamination influx as the concentration of the contaminant at $X=0$ is equal to C_0 for all time. The second boundary condition requires that at all points of time equal to zero the initial contaminant concentration be zero. The first term of Equation 16 addresses dispersion effects while the second term addresses transport by simple advection.

$$D_L \frac{\partial^2 C}{\partial x^2} - v_x \frac{\partial C}{\partial x} = \frac{\partial C}{\partial t} \quad (16)$$

where: D_L = longitudinal dispersion coefficient
 C = solute concentration
 v_x = average groundwater velocity in the x direction
 t = time since start of solute invasion

Analytical Solution Form

Equation 17 is one common form of an analytical solution to Equation 16 [Ogata, 1970], where the initial boundary conditions require an initial concentration of zero contamination in the flow media and a continuous injection source of the contaminant. When molecular diffusion can be safely assumed to be small relative to mechanical dispersion, such as in high velocity, high permeability aquifers, the dispersion coefficient can be reduced to simply $\alpha_x v$ and yields Equation 17.

$$C = \frac{C_0}{2} \left[\operatorname{erfc} \left(\frac{X - v_x t}{2\sqrt{D_L t}} \right) + \exp \left(\frac{v_x X}{D_L} \right) \operatorname{erfc} \left(\frac{X + v_x t}{2\sqrt{D_L t}} \right) \right] \quad (17)$$

Where: C = Solute Concentration
 C_0 = Initial Solute Concentration
 X = Spatial Distance Along Flowpath
 t = Time
 D_L = Hydrodynamic Dispersion Coefficient
 V_x = Average Linear Groundwater Velocity
 erfc = Complementary error function

The analytical solution for Equation 17 requires the complementary error function to be considered in the solution. This function is well documented with tables and charts such as those found in the appendix of Freeze and Cherry's Groundwater. The chart values are derived from Equations 18 and 19.

$$\operatorname{erfc} x = 1 - \operatorname{erf} x \quad (18)$$

where:

$$\operatorname{erf} x = \frac{2}{\sqrt{\pi}} \int_0^x e^{-t^2} dt \quad (19)$$

Values of the error function x can also be approximated by using the Maclaurin series represented in a truncated form as Equation 20 shown below. For all practical purposes $C = C_0$ at small negative values of β and $C = 0$ at positive values of β greater than 2.

$$\operatorname{erf} x = \frac{2}{\sqrt{\pi}} \left(x - \frac{x^3}{1! \cdot 3} + \frac{x^5}{2! \cdot 5} - \frac{x^7}{3! \cdot 7} + \dots \right) \quad (20)$$

Brine Lagoon Example

As an illustration, consider an idealized one-dimensional example of a lagoon used to store brine water for the pressure maintenance of a propane storage well is leaking into a fresh water aquifer. We know the main constituent of brine, sodium chloride,

is highly miscible in fresh water, and is not retarded by most, if not all, aquifer matrix media. We wish to estimate what the concentration of a sodium chloride plume will be 18.75 meters down-gradient from a leak one year from now.

Analytical Platform Solution

If the leachate concentration is 906.25 mg/l; the average linear groundwater velocity in the freshwater aquifer is 3.3×10^{-7} m/sec, and the longitudinal dispersion coefficient is estimated to be $4.9 \times 10^{-7} \text{m}^2/\text{sec}$, crisp calculations using the above equations indicate the future concentration of sodium chloride plume in the freshwater aquifer will be 56.7 mg/l one year from now. This information is summarized in Table XI.

Fuzzy Platform Solution

In this simulation we will assume both the initial chloride concentration of the brine and the longitudinal dispersion coefficient to be fuzzy values which can be represented by the triangular membership function. These two variables were chosen to "fuzzify" because the initial concentration of a contaminant rarely is known, and dispersion has been shown to be a highly variable and non-linear parameter [Freyberg, 1986; Sudicky et al., 1983; Anderson, 1979].

The endpoint extremes for the fuzzy input values were chosen to be plus or minus five percent of the corresponding crisp values. The fuzzy dispersion coefficient was estimated to be a fuzzy number with the membership function having a centroid value

of 4.8×10^{-7} with endpoint values of 4.6×10^{-7} and 5.1×10^{-7} . The fuzzy initial concentration of the leachate was estimated to have a centroid value of 906.25 mg/l, with endpoint values of 861 and 951. The resulting fuzzy realization output yields a fuzzy number with a centroid value of 57.2 mg/l. This information is also summarized in Table XI.

Figures 9 and 10 show the realization membership functions for the crisp analytical simulation and the fuzzy analytical simulation, while Figures 11, and 12 show the membership functions for the two fuzzy input parameters initial chloride concentration and the longitudinal dispersion coefficient.

TABLE XI

SUMMARY: ONE-DIMENSIONAL TRANSPORT EXAMPLE (mg/L)

	Co(mg/l)	Vx(m/sec)	D _l (m ² /sec)	C _l (mg/l)
Crisp Calculations	906.25	3.3E-7	4.9E-7	56.7
Fuzzy Centroid	906.25	3.3E-7	4.8E-7	57.2
Fuzzy Endpoints	861 - 951	3.3E-7	4.6E-7 to 5.1E-7	11.3 to 105

Table XI shows both the crisp and fuzzy input parameters as well as the crisp and fuzzy out realization values (C_l). The two endpoint extremes for the fuzzy parameters are also shown.

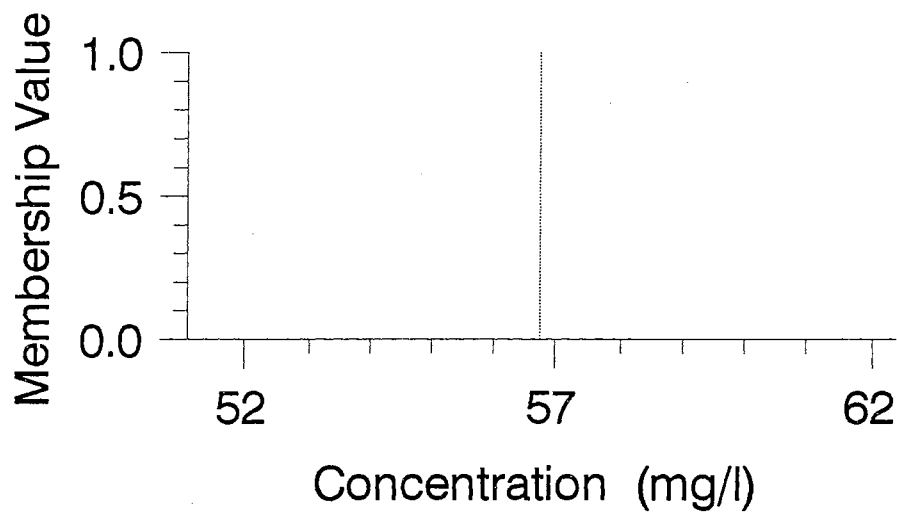


Figure 9. Membership Function of Crisp Analytical Solution

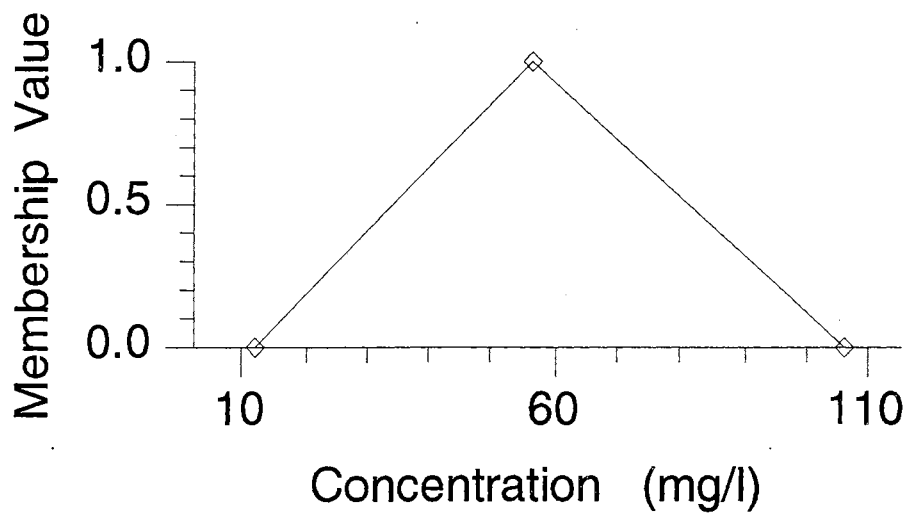


Figure 10. Membership Function of Fuzzy Analytical Realization

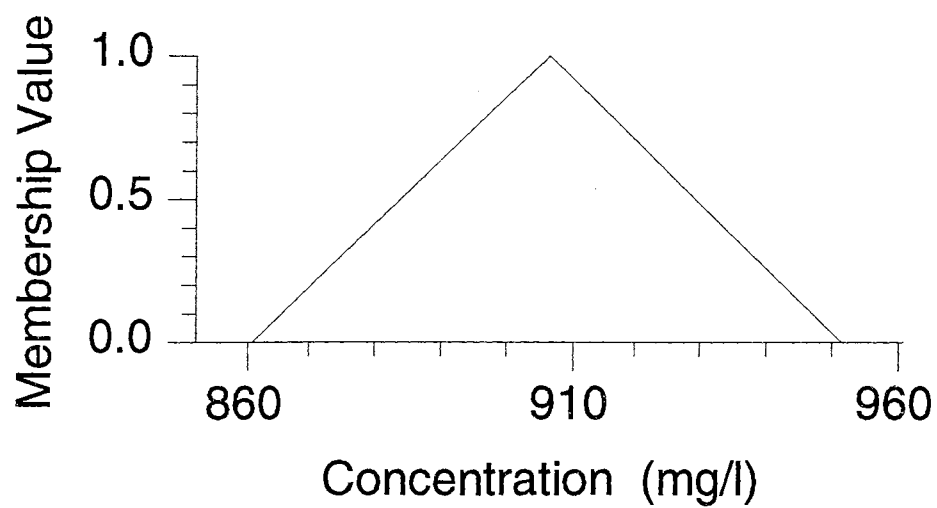


Figure 11. Membership Function of Initial Concentration

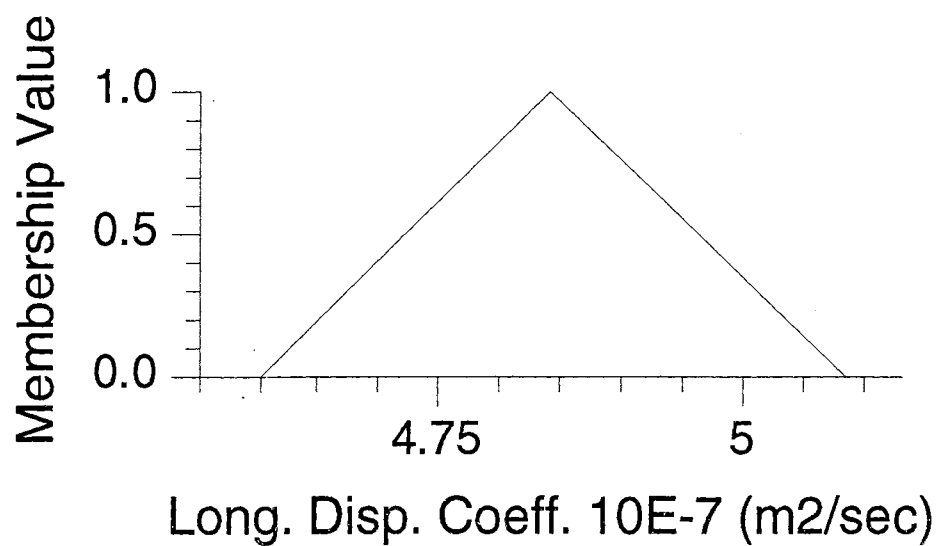


Figure 12. Membership Function of Fuzzy Longitudinal Dispersion Coefficient.

Comparison and Contrast of Results

The precise realization of predicted contaminant concentration of 56.7 mg/liter is derived by accepting the requisite assumptions and utilizing Equations 2.5, 2.6, 2.7, and 2.8 with crisp numbers. One significant weakness of this approach is the necessity of actually estimating the unknown longitudinal dispersion coefficient.

While this parameter may be back-calculated based on historical transport performance history, estimating a truly accurate site specific value based on *a priori* information is highly unlikely.

It makes much more sense to estimate the initial chloride plume concentration and the longitudinal dispersion coefficient with a fuzzy value and derive a fuzzy solution using fuzzy arithmetic. The difference between the predicted concentrations of 56.7 and 57.2 mg/l is meaningless when the overall basis for the two different platform calculations is considered.

VIII. BORDEN SITE EXPERIMENT

Much of the following discussion was gleaned from an extensive series of articles published at the conclusion of the experiment [MacKay *et. al.*, 1986; Freyberg, 1986; Roberts *et. al.*, 1986; Domenico and Schwartz, 1990; Curtis *et al.*, 1986; Sudicky, 1986]. The results of related investigations have also been published [Criddle *et al.*, 1986]. The research efforts contained in this paper focused upon developing a fuzzy analytical model of the site using data published in the above citations.

A long-term field experiment was designed and conducted in an unconfined sand aquifer underling an abandoned sand quarry located in Borden, Ontario. The experiment was designed primarily to generate a data base of information which could be used to advance the study of solute transportation in unconfined, saturated aquifers. Advection was the term used to describe the average motion of the solute plume during the experiment, while the term dispersion was used to describe the volume-averaged concentration deviations from concentrations predicted by the plume's average linear velocity.

Scope of the Borden Experiment

The Borden Experiment was designed to generate well documented initial conditions, as well as accurate and precise observational data regarding solute transport during a

three year period. The two major goals of this experimental effort could be described as: 1.) identify the fundamental processes controlling groundwater flow and transport at the Borden site, and, 2.) assemble a data base suitable for developing and testing various mathematical groundwater flow and transport models. The precise mathematical definitions used by the investigators MacKay et al. were: 1.) advection was defined to be the vector velocity of the center of mass of the solute plume, and 2.) dispersion was defined to be one half the time rate of change of the spatial variance of concentration about the center of mass [MacKay et. al. 1986]. Both definitions are consistent with the current theory of groundwater transport

A well defined initial slug of tracer solute was injected into an uncontaminated section of an easily accessible and relatively homogenous unconfined sand aquifer. An extensive monitoring well network with a 5,000 point sampling network was used to gather ground-water samples following the injection of the solute. The primary goal of the sampling and monitoring program was to accumulate detailed information regarding the tracer concentrations at specific points in space and time, and to minimize the disturbance of natural groundwater flow field. Although seven tracer compounds were injected into the aquifer, this work will only consider the efforts reported for two of the tracer elements: chloride and bromide. Chloride was the primary tracer element studied, while bromide was used mostly as a marker indicator.

An existing contaminant plume was known to lie in the basal section of the aquifer.

This plume contained a high concentration of chloride ions, but contained no concentration of bromide ions. This allowed bromide to be used as a marker tracer in the uncontaminated section of the aquifer to confirm which solute plume was being sampled. Both chloride and bromide are inorganic and are typically not reactive with aquifer matrix media. As these compounds have fundamentally identical transport characteristics, the chloride-bromide concentration ratio of a sample was used to determine which solute plume was being sampled.

The sampling data was used to monitor changes in the location and concentration of the chloride plume over time, as well as to estimate the location of center of mass of the solute plume. The results of the field sampling effort were supplemented with measurements of water levels, as well as laboratory studies of the physical, and chemical characteristics of the aquifer.

The resultant data base provides an unique opportunity to examine the in-situ movement of a tracer plume in great detail. While the aquifer at the experimental site had some unexpected spatial variability in its hydrogeologic properties, the variability was small enough so that the fundamental groundwater models remain valid descriptors of the physical behavior.

Site Description

A relatively homogenous sand aquifer extends 9 meters beneath the horizontal floor of

a sand quarry and lies on a deposit of thick silty clay. The pre-existing chloride contaminant plume originated from a nearby landfill and was confirmed to be confined to the bottom 2-3 meters of the sand aquifer at the time of study. As can be seen in Figure 13 the Borden experiment was carried out totally in the uncontaminated upper section of the saturated aquifer.

The average depth to the water table at the experimental site was about 1.0 m below the quarry floor. The physiography, climate, and general hydrogeology of the area has been well described elsewhere [MacFarlane *et al.*, 1983].

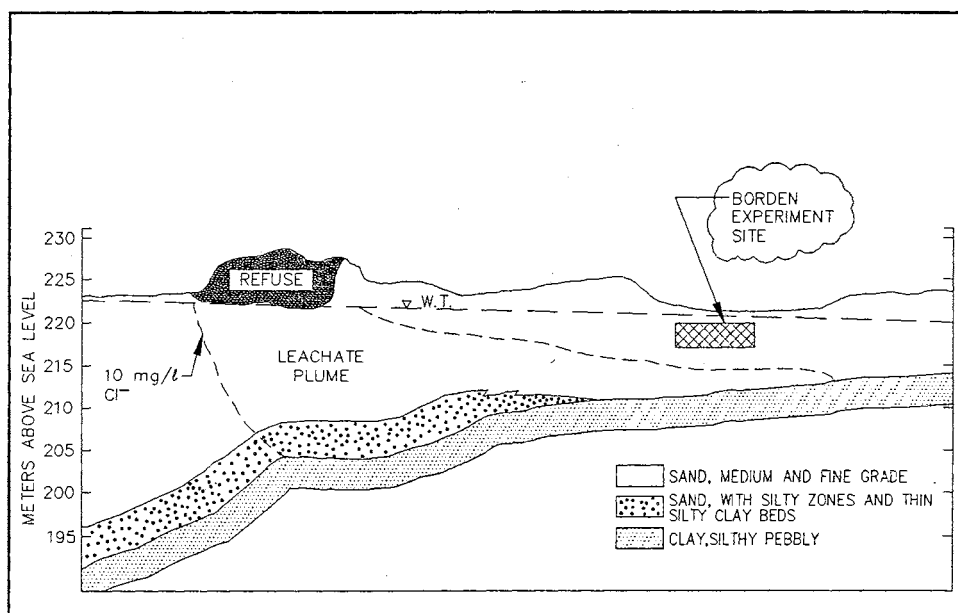


Figure 13. Borden Site Geological Cross Section

The mineralogy of aquifer material is summarized in Table XII [MacKay, 1986][Dance, 1981][O'Hannesin, 1981].

TABLE XII
BORDEN AQUIFER MINERALOGY

<u>Component</u>	<u>%</u>
Quartz	58
Feldspars	19
Carbonates	14
Amphiboles	7
Chlorite	2

The subject aquifer material can be described generally as non-fractured, relatively homogeneous, clean, well-sorted medium-to-fine grained sand, with grain roundness ranging from sub-angular to well-rounded. Table XII shows quartz and feldspars dominate the flow media along with a substantial mixture of carbonates and amphiboles.

The only clay mineral detected was chlorite although the clay content in the aquifer could almost be considered as zero as the detectible clay size fractions were extremely low. Seven hundred and thirty-nine of the 846 aquifer media samples (87%) had no measurable clay fractions at all. Of the 107 samples exhibiting clay content, only 8 samples showed clay fractions greater than 15% by weight.

While the aquifer could be considered relatively homogeneous, core sampling did reveal several distinct bedding features. The bedding features were predominately horizontal, although some cross-bedding sections were found. Spatial heterogeneity observed at the site consisted mostly of thin lenses (0.02 - 0.1 meters) with limited

lateral extent (2 - 5 meters). The lens were composed of the same materials shown in Table XII, but exhibited a greater contrast in particle size distributions and hydraulic conductivity [Sudicky, 1986]. Both finer-grained and coarser-grained lenses were observed, with the median grain sizes of the 846 samples (taken from 11 undisturbed cores samples) ranging from 0.070 to 0.69 mm [O'Hannesin, 1981].

Table XIII summarizes the chemical composition of the uncontaminated groundwater in the vicinity of the landfill [Nicholson *et al.*, 1983]

TABLE XIII
BORDEN BACKGROUND GROUNDWATER PARAMETERS

<u>Parameter</u>	<u>Range</u>
Ca ²⁺	50 - 110 mg/l
Mg ²⁺	2.4 - 6.1 mg/l
Na ⁺	0.9 - 2.0 mg/l
K ⁺	0.1 - 1.2 mg/l
Cl ⁻	1 - 3 mg/l
TDS	380 - 500 mg/l
DO	0 - 8.5 mg/l
pH	7.3 - 7.9

The table indicates the groundwater's total dissolved solids content is low, although the water could be considered to be moderately hard based on the calcium and magnesium content. The initial dissolved oxygen measurements indicated that the aquifer was aerobic in the experimental zone, although subsequent measurements showed that dissolved oxygen varied somewhat over the field of study.

Table XIV summarizes estimates of the key aquifer properties derived from field data obtained in the vicinity of the experimental site.

TABLE XIV
ESTIMATED BORDEN AQUIFER PROPERTIES

Horizontal Hydraulic Gradient	0.0043 m/m
Hydraulic Conductivity Geometric Mean	7.2×10^{-5} m/s
Porosity Mean Value	33%
Longitudinal Dispersivity	0.08 m
Horizontal Dispersivity	0.03 m

The hydraulic conductivity distribution in the aquifer at the experimental site was studied using several techniques. A total of 26 slug tests were interpreted using the Hvorslev method [Hvorslev, 1951], with the resulting estimates varying from 5×10^{-5} to 1×10^{-4} m/s, with an approximate mean value of 7×10^{-5} m/s.

Throughout the experiment, porosity was treated as a spatially uniform parameter having a value of 33 percent. Relatively little data was obtained to evaluate the spatial variability of media porosity because of the difficulty in obtaining undisturbed core samples from the aquifer. Data taken from two cores at 0.15 meter increments yielded an estimated coefficient of variation for porosity of 0.05. Based on this small value the field porosity was judged to be uniform within the upper section of the aquifer for the purposes of this experiment, although the porosity value of 33 percent

was considered in subsequent works as a mean value.

Experimental Methodology

The Borden experiment's transport study began with the injection of a known mass and volume of a chloride and bromide mixture. Both compounds were chosen due to their nonreactive tendencies with each other and typical aquifer media, as well as the reasons discussed previously.

A nine well injection system was installed and designed to create an instantaneous slug of tracer material in the upper section of the aquifer. The injection header system was designed to provide each of nine injection wells an equal amount and concentration of tracer material, as well as to cause minimal disturbance in the natural flow field. The amount of injected tracer volume was chosen to be large relative to the scales of heterogeneity believed to exist in the aquifer, as well as to ensure the plume could be reliably monitored over several years. The composition of the slug of the chloride and bromide tracer solution used in the experiment is shown in Table XV.

TABLE XV
INJECTED NON-REACTIVE TRACER COMPOSITION

	Average	Total Mass
<u>Tracer Material</u>	<u>Concentration (mg/l)</u>	<u>Injected (kg)</u>
Chloride (Cl ⁻)	892	10.7
Bromide (Br ⁻)	324	3.87

Movement of the tracer plume was governed solely by the natural processes occurring at the site, and the plume's position was monitored via a dense network of 3-D sampling points. More than 19,900 samples were collected during the course of the experiment, and all the evidence indicates neither the chloride or bromide reacted with each other or within the aquifer. The plumes were monitored for 1,038 days, and the maximum distance traveled exceeded 110 meters.

Observed Chloride Plume Development

As expected, the chloride plume's internal structure and shape changed as the plume traveled throughout the aquifer. As the plume moved down gradient, it spread significantly in the longitudinal direction, somewhat in the horizontal direction, and a small amount in the vertical direction. The most interesting and unexpected aspect of the plume's structural development began occurring during the first 85 days of the experiment, and the effects were still observable 1,038 days later. Specifically, the chloride plume developed a bimodal structure in the vertically averaged concentration profile even though the plume cloud never lost its structural continuity. This bimodal structure was apparently caused by the divergence of the plume into two separate areas of distinctly higher concentration chloride ions. Somewhat unexpectedly, the plume was able to maintain its integrity as a single coherent body of chloride ions; however, it should be noted the plume did not obtain a Gaussian distribution of chloride ions in any direction or orientation.

The separation, or bifurcation, of the plume was inferred to have been caused by a reduced horizontal permeability section located in the aquifer. The reduced hydraulic conductivity of the lower section of the aquifer allowed certain sampling wells to see both the upper and lower portion of the plume at the same time and thereby create a bimodal concentration distribution. Figure 14 is a plot of equal concentration contours of the vertically averaged chloride ion concentrations 462 days after injection.

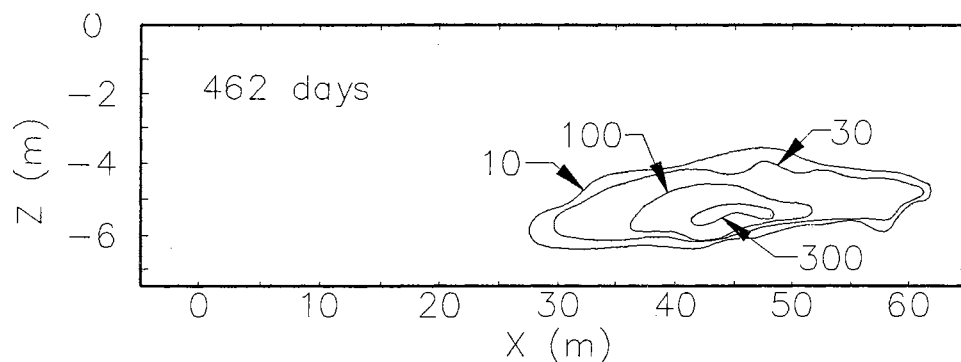


Figure 14. Chloride Concentration Contours: 462 Days. (MacKay et al. 1986)

Figure 14 was produced by hand contouring sampling data projected onto the plume's horizontal cross-section, and is reproduced here from another publication [MacKay *et al.* 1986]. The plot indicates the structural integrity of the plume held cohesively through 462 days of transport, and that the vertical spreading is very small relative to the horizontal elongation (note the different scales of the X and Y axis). The bimodal nature of the distribution is somewhat attenuated by the contouring, but can be seen in the qualitative sense as the kidney bean shape of the 300 mg/L center contour.

Observed Chloride Plume Trajectory

The spatial coordinates for the chloride plume's center of mass at the various sampling times were determined based on an established field coordinate system.

Figure 15 graphically presents the horizontal (X-Y) trajectory of the center of mass of the chloride plume, and indicates the plume followed a nearly linear horizontal trajectory in the aquifer throughout the course of the experiment.

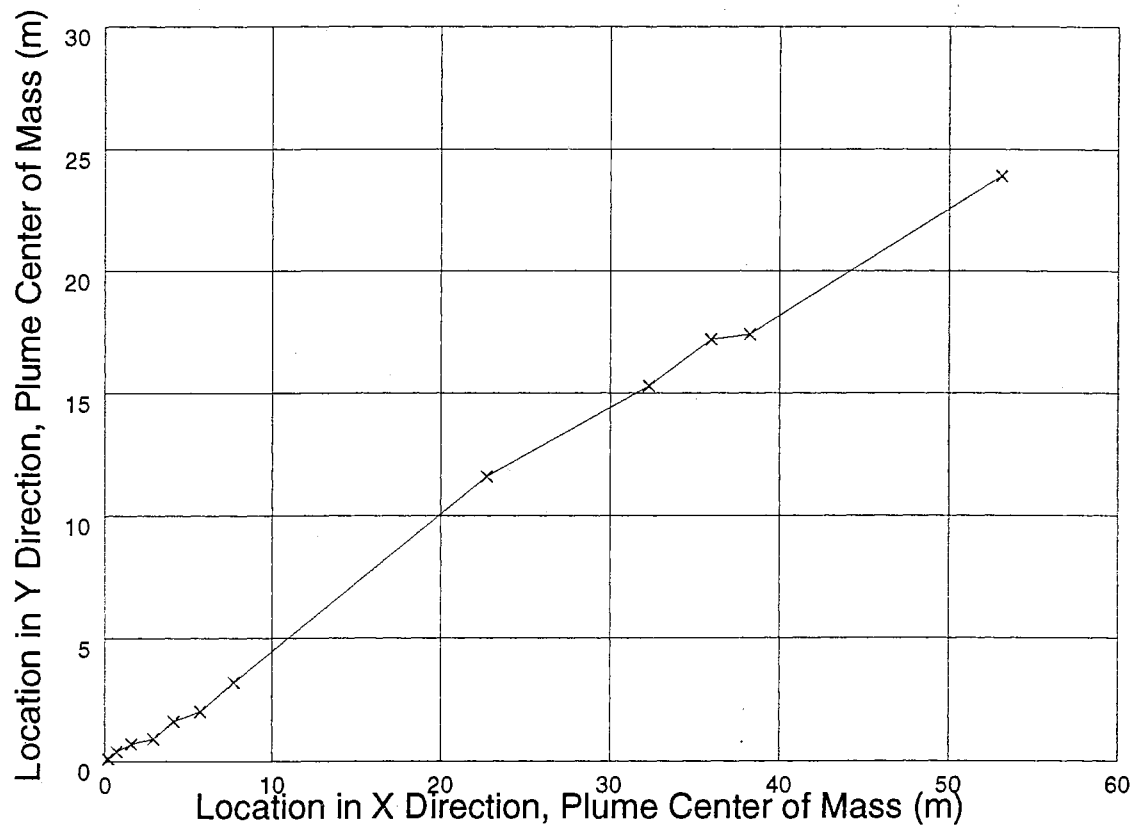


Figure 15. Chloride Plume Horizontal Trajectory

It should be noted that while the X-Y trajectory of the plume's center of mass shown in Figure 15 is nearly linear, the actual horizontal trajectory was approximately 25 degrees different than the forecasted trajectory, which was predicted based on local water table observations. All the spatially related data used in this work regarding the Borden site have been corrected to a common coordinate system. The corrected data are shown in the Appendix and was used as the basis for the development of Figures 15, 16, and 17.

Interpretation of the plume trajectory shown in Figure 15 is straightforward, and indicates the mean horizontal hydraulic conductivity in the aquifer was remarkably consistent along the direction of travel. This observation confirms a similar conclusion drawn from the analysis of 1,279 core samples taken from an area adjacent to the Borden Experiment site.[*Sudicky*, 1986] These facts indicate any horizontal anisotropy existing in the hydraulic conductivity field would have to be very small or negligible relative to the overall size of the plume.

The small irregularity in the horizontal (X-Y) trajectory which occurred at approximately $X=36$ and $Y=17$ corresponded with an observed seasonal change in the hydraulic gradient at the site around day 470 of the experiment. Figure 15 indicates the impacts of the variation in hydraulic gradient upon the chloride plume were minimal and temporary.

Observed Chloride Vertical Displacement

Figure 16 indicates that in contrast to the horizontal (X-Y) trajectory of the center of mass of the chloride plume, the vertical (X-Z) trajectory of the plume's center of mass was not uniform over time and space. The vast majority (79%) of the total vertical displacement occurred within the first 30 meters of horizontal displacement, and required approximately one year of transport time.



Figure 16. Chloride Plume Vertical Trajectory

The total vertical displacement of 2.85 meters over 1,038 days represents only 2.5 percent of the 110 meters of horizontal displacement. This value is small enough to indicate the vertical displacement can safely be considered a negligible component of the total displacement of the plume.

While the reasons for the nature and magnitude of the observed vertical movement shown in Figure 16 are not fully understood at present, it is likely that a number of mechanisms were jointly responsible. One researcher [Sudicky *et al.* 1986] attributed the vertical plume movement to hydraulic head differences and the specific gravity differences between the plume and the native groundwater. While not quantified in any way, local infiltration and recharge probably also played a role in the early vertical displacement of the plume.

Observed Chloride Plume Velocity

Assuming that the chloride ions were not affected by either retardation or ion exchange within the aquifer, the velocity of the center of mass of the tracer plume must equal the actual linear groundwater velocity. Figure 17 shows the velocity of the center of mass of the chloride plume was uniform throughout the course of the experiment.

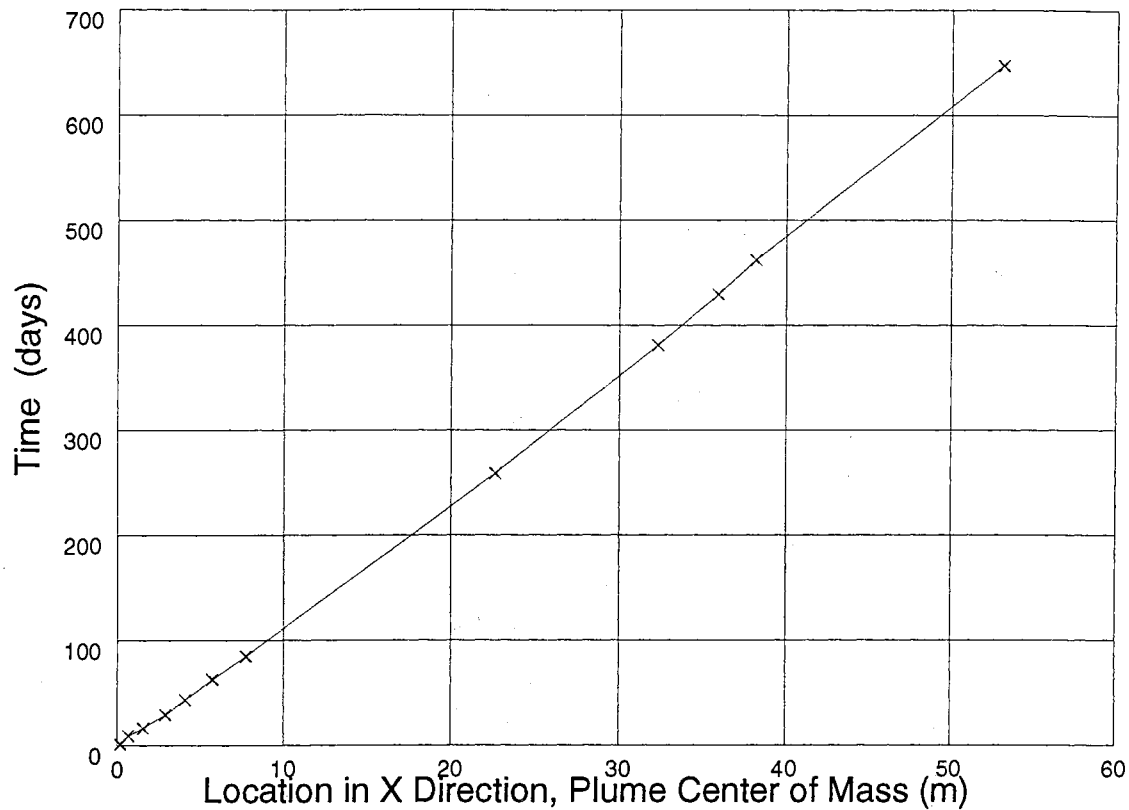


Figure 17. Chloride Plume Horizontal Displacement vs. Time

Figure 17 plots the horizontal displacement of the plume's center of mass as shown in Figure 15, against the travel time of the center of mass of the plume. The figure clearly indicates the horizontal velocity is linear, and has a magnitude of 0.091 meters/day. The velocity of 0.091 meters/day can easily be read directly from the graph at time $t=100$ days.

The figure shows the transport velocity during the first 650 days of the experiment is a linear function with time. The overall size of the plume appears to have been large

enough such that the local variation in the velocity field observed in Figure 15 at X=36 and Y=17 did not effect the average transport rate of the plume.

Estimates of groundwater velocity are usually derived indirectly from measurements of hydraulic gradient, hydraulic conductivity, and the porosity of the aquifer. Table XVI shows the results of field work conducted at the Borden site.

TABLE XVI
RESULTS OF METHODS OF ESTIMATING AVERAGE LINEAR
GROUNDWATER VELOCITY

<u>Method</u>	<u>Range</u>	<u>Mean</u>	<u>Calculated Value (m/d)</u>
Slug Test	5 - 10	7.0	0.078
Grain Size Analysis (11 cores)	0.03 - 76	7.1	0.079
Permeameter Analysis			
2 Core plugs	0.10 - 15	6.7	0.076
32 Cores plugs	0.04 - 15	7.2	0.081

The estimates of the site's groundwater velocity shown in Table XVI agree pretty well with the observed velocity of 0.091 meters/day. The estimated velocities range from 0.076 meters/day to 0.081 meters/day, or approximately 10-15% lower than the observed velocity of 0.091 meters/day. The differences among the indirect estimates of velocity are less than 3%, except for the one derived from permeameter analysis of the core data. All the differences in the estimates could be explained by possible errors made in either the sampling techniques or the methodology used to estimate the

hydrogeologic parameters. A fuzzy informational approach to determining velocity estimates may not be handicapped to the same extent as other techniques by parameter estimation errors.

Summary: Borden Experiment

The horizontal trajectory of the chloride plume was linear and aligned well with the naturally occurring hydraulic gradient. The total vertical displacement of the plume was relatively small and indicated the vertical component of the mean groundwater velocity vector was negligible. The observed mean plume velocity was 0.091 meters/day, and remained spatially and temporally uniform during the first 647 days of the experiment.

A heterogeneity in the aquifer led to the bifurcation of the plume's chloride concentration, and demonstrates some of the difficulties inherent in predictive groundwater modeling. The observed behavior of the chloride plume indicated an unexpected heterogeneity existed in the aquifer which was believed to be homogenous. Fuzzy information based modeling platforms may provide a more satisfactory quantitative and qualitative predictive methodology through their abilities to successfully deal with vaguely defined modeling parameters.

Transport Modeling Platform Comparison, Analytical vs. Fuzzy at the Borden Site

The following groundwater transport modeling application contrasts an analytical

platform solution with a fuzzy based transport realization based on the Borden site data. In the fuzzy transport model hydrodynamic dispersivity is considered to be a fuzzy number. While any, or all, of the groundwater modeling parameters could be considered as fuzzy variables under a fuzzy modeling platform, only dispersivity was chosen. This choice was made for two reasons: One involved the wish to isolate the differences between the two contrasting platforms' realizations to the impact of the effects of a single fuzzy parameter. Reason number two had to do with the history and nature of the dispersivity parameter itself.

Dispersivity is one of the most difficult parameters with which accurate groundwater modeling must manage. The classic model of hydrodynamic dispersion is developed at the scale of Representative Elementary Volume ("REV") and requires the diffusive, or Frickian model of transport be accepted. Unfortunately, a significant body of field work indicates dispersive spreading in an aquifer is non-Frickian in nature [*Anderson, 1979; Gelhar and Axness, 1981*].

Laboratory and theoretical studies have been used to develop both deterministic and stochastic modeling platforms which perform well under the right circumstances [*Matheron and DeMarsily, 1980; Guven, et. al., 1984*]. The right circumstances almost always include having an accurate characterization of the variability of all the aquifer parameters. When forced to generate predictive modeling realizations without an accurate and complete characterization of the aquifer, most modelers strongly

suggest the stochastic type modeling platform be invoked. The use of fuzzy informational modeling techniques in situations where the variability of any of the groundwater modeling parameters is high may be an equally valid, and possibly more robust, methodology as the prerequisite assumptions are less restrictive.

The true nature of the dispersivity phenomena is an area needing more real world observation and study. In an extensive review of literature regarding field-scale studies, [Gelhar *et. al.*, 1985] fifty-five different sites were identified where modeling dispersivity values were documented and reported. Only five of the fifty-five studies yielded dispersivity values which could be considered to be reliable, and only one of the five reliable studies involved solute transport under natural gradient conditions [Sudicky *et. al.*, 1983]. The dispersivity values generated by the Borden site experiment can be considered to be reliable; unfortunately, they must also be considered to be non-linear and scale dependent [Freyberg, 1986].

Borden Analytical Groundwater Model

Equation 17 can describe the concentration of a non-retarded slug of miscible tracer fluid anywhere along a single flowpath axis.

$$\frac{\partial C}{\partial t} = D \frac{\partial^2 C}{\partial x^2} \quad (17)$$

The analytical solution to Equation 17, shown as Equation 18 [Bear, 1972], was used to evaluate the plume concentration data generated from the Borden Site experiment.

$$C(x,t) = \frac{M/n}{\sqrt{(4\pi Dt)}} \exp \left[\frac{-x^2}{4Dt} \right] \quad (18)$$

Data Preparation

In order to use a one-dimensional transport model with the Borden site data the field data had to be represented in a one-dimensional format. Figure 14, the two-dimensional, hand contoured, X-Z plane concentration profile of the chloride plume was transformed into reduced one-dimensional point concentration data profile shown in Table XVII. The reduced 1-D data was generated by digitizing the hand contoured cross-section [MacKay, 1986] into a Sun Microsystem Workstation with a Summagraphics Microgrid III Digitizing Tablet and the corresponding Summagraphics software. The summation of each isopleth's average concentration value weighted by the component plume thicknesses at that spatial location determined the one-dimensional concentration value. Development details of the reduced 1-D data shown in Table XVII may be found in Appendix D.

Increments of 5 meters along the plume's idealized center line were chosen as locations to represent the compression points of concentration values. These data points effectively represent the compression of the two-dimensional plume chloride concentration onto a single directional axis after 462 days of transport.

Table XVII
PLUME CONCENTRATION DATA AND REALIZATIONS

Spatial X Coordinate (m)	Plume Thickness (m)	Reduced 1-D Concentration (mg/L)	Analytical Realization (mg/L)
30	1.2	31	27
35	2.1	147	170
40	2.3	395	430
45	2.5	450	434
50	2.2	231	174
55	1.6	72	28
60	0.8	22	2

An analytical solution to the transport model described by Equation 18 was applied with site specific hydrogeological parameters [McKay 1986; Freyberg 1986] and the reduced 1-D data by aligning the X axis parallel with, and superimposed upon the site's mean groundwater vector. Table XVII also shows the plume's thickness and the analytical solution of Equation 18 at identical spatial values of X.

The reduced 1-D concentration data and the analytical realization data shown in Table XVII are depicted graphically as Figures 18 and 19. Both figures illustrate the spreading of the injected chloride slug in both the leading and trailing directions of transport after 462 days of travel time in the aquifer.

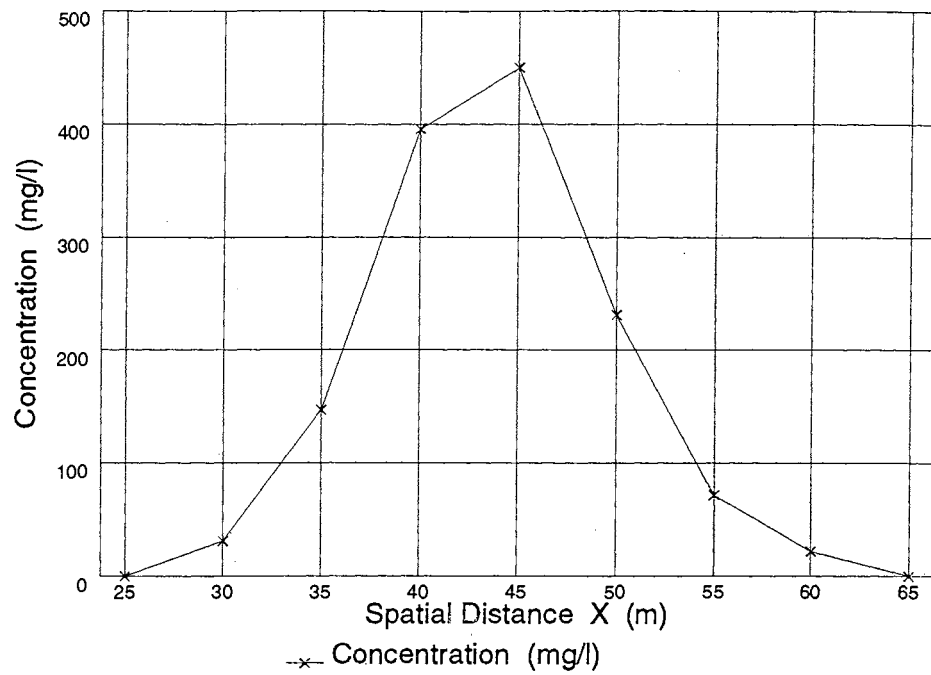


Figure 18. Profile of Reduced 1-D Concentration Data

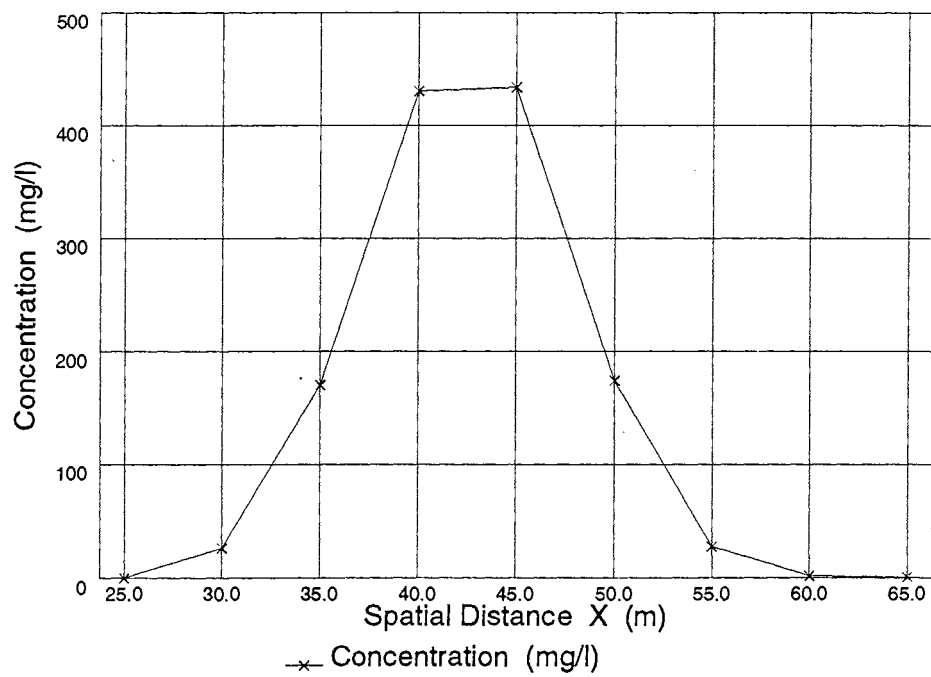


Figure 19. Profile of Analytical Realization

The observed peak concentration in Figure 18 occurs at $X=45$, and compares very favorably with the theoretical peak concentration location of $X=42$. The theoretical peak concentration location of $X=42$ is the expected distance traveled after 462 days of transport if the contaminant was moving at the mean groundwater velocity.

[Distance (meters) = Rate (meters/day) * Time (days); 42 meters = 0.091 meters/day * 462 days]

Inspection of Figure 19 and the data shown in Table XV shows the one-dimensional analytical platform solution generates a plume profile having the same general shape and characteristics as the reduced 1-D data concentration point profile shown in Figure 18. As expected for a miscible contaminant, the peak concentration values are again located in the area where the spatial distance X equals the product of the travel time and mean groundwater velocity.

Solving Equation 18 with the spatial distance X incremented in 1.25 meter segments instead of the 5 meter segments used to generate Figure 19, yields the normal distribution realization presented as Figure 20.

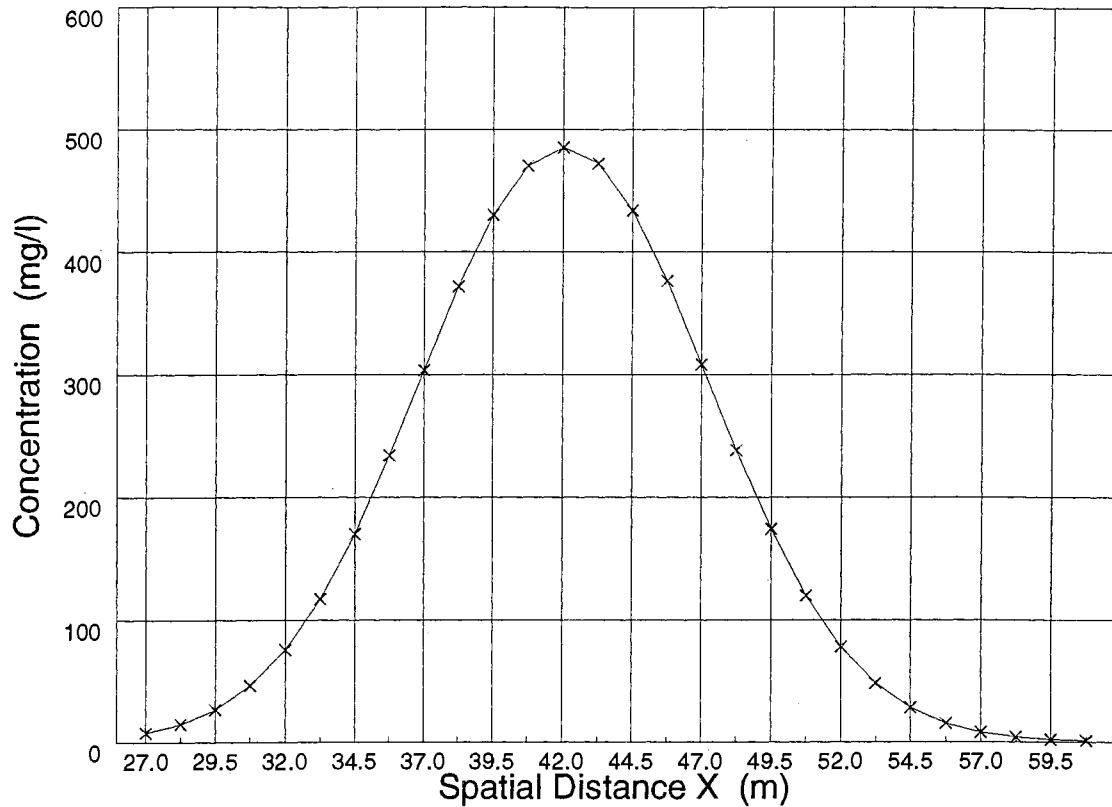


Figure 20. Analytical Solution at 1.25 meter Increments

Inspection of both Figure 20 indicates a point of inflection and the peak concentration value occurs at $X=42$ when the smaller spatial incrementalization is used. This graph validates the reduced 1-D data compression technique and highlights the fact care should be exercised near the center of mass so as to not underestimate the total concentration values.

In the case of the Borden Experiment, the cause of the bifurcation of the plume which occurred during transport also caused the analytical modeling platform to "miss the

mark" in terms of precise agreement with field data. There was; however, good overall agreement in the predicted plume concentration profile and the magnitude of the predicted concentration values.

Figures 21 shows the difference between the observed concentration data and the analytical realization, and clearly indicates the differences increase rapidly the further one moves away from the contaminate's centroid.

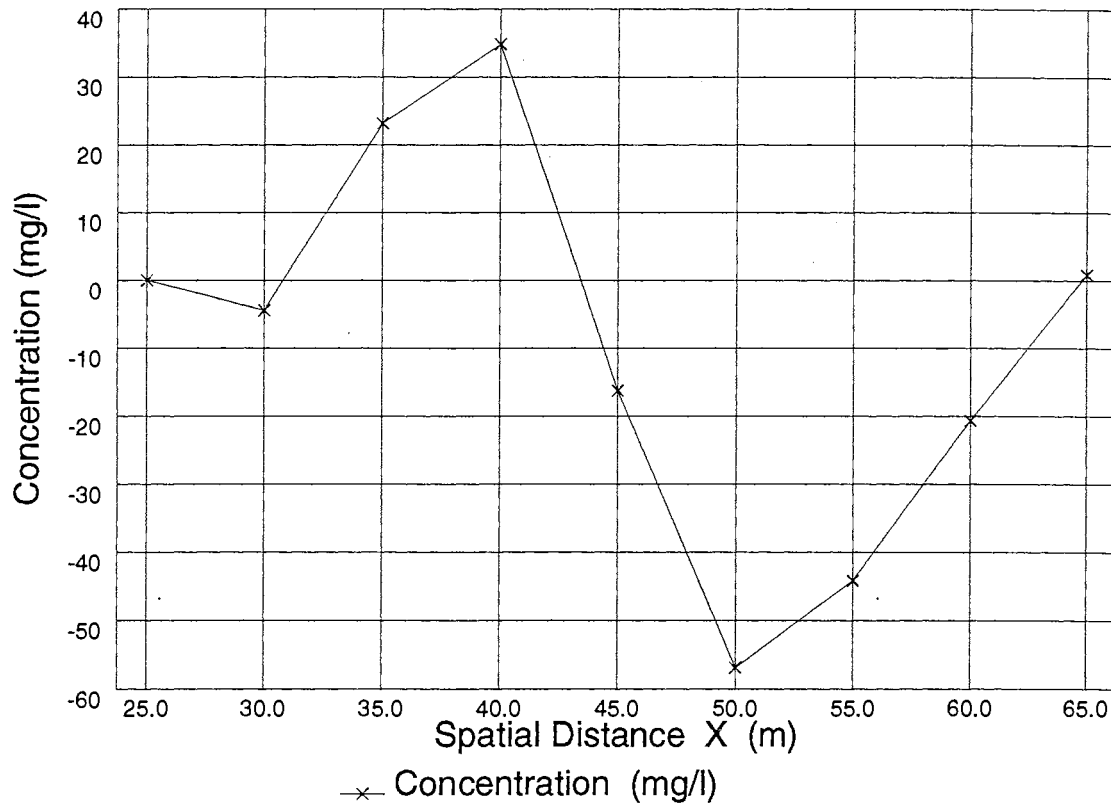


Figure 21. Difference Between the Observed Concentration Data and the Analytical Realization

Figure 21 indicates the differences between the observed data and the theoretical analytical solution along on the leading edge of the plume are almost twice those of the trailing section at corresponding values of X.

Mass Balance

An idealized slug of contaminant injected into a non-fractured, homogenous aquifer will spread in three dimensions with the predominate spreading occurring along the axis of groundwater flow. Consequently, the maximum total concentration of the contaminant will be seen in the spatial planes intersecting the centroid of the plume cloud. The centroid of the plume cloud can be determined from Equation 19 and will occur at the spatial location where $Z=0$; $Y=Z$; and $X=v(t)$ [Domenico and Schwartz, 1990]

$$C_{\max} = \frac{Mass}{8(\pi t)^{1.5} \sqrt{D_x D_y D_z}} \exp \left[-\frac{(X-Vt)^2}{4D_x t} - \frac{Y^2}{4D_y t} - \frac{Z^2}{4D_z t} \right] \quad (19)$$

The general shape of chloride plume cloud in the Borden experiment can be described as a general ellipsoid shape, such as the one shown in Figure 22. The volume of an ellipsoid can be defined with Equation 21, using the three principle axes described by Equations 20 a, b and c.

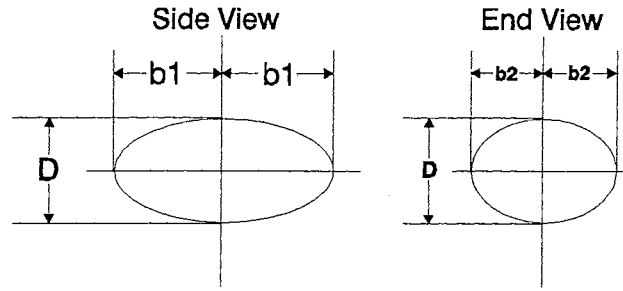


Figure 22. Ellipsoid Profile

Where: $D = 2(3\delta_z)$

$$b_1 = 2(3\delta_x)/D$$

$$b_2 = 2(3\delta_y)/D$$

and

$$\begin{array}{lll} 3\delta_x = 3(2D_x t)^{0.5} & 3\delta_y = 3(2D_y t)^{0.5} & 3\delta_z = 3(2D_z t)^{0.5} \end{array} \quad (20)$$

a. b. c.

At the Borden site the dispersivities after 462 days were determined [Freyberg, 1986] to be 0.323 for the longitudinal dispersivity α_x , and 0.028 for the transverse dispersivity α_y . Assuming α_z is an order of magnitude less than α_y , as is consistently found in both laboratory and field experiments, and using the site specific parameters with Equations 20 a, b, and c, an ellipsoid having the dimensions of $X=10.4$, $Y=6.1$ and $Z=1.9$ will, by definition, contain 3δ , or 99.7 percent of the chloride mass.

Equation 21 describes the volume of an ellipse.

$$V_e = \frac{\pi}{6} b_1 b_2 D^3 \quad (21)$$

Applying Equation 21 with the X, Y and Z axes calculated with Equations 20 a, b, and c, indicates that after 462 days the plume will occupy a 227 cubic meter volume in the aquifer.

If this is indeed the case, the initial 12 cubic meter volume of injected solution with an average chloride ion concentration of 892 mg/l, will have become a diluted volume of 227 cubic meters with an average chloride concentration of 47 mg/l. Equation 19 indicates the chloride concentration centroid of this diluted volume is 183 mg/l.

Multiplying 183 mg/l by the plume thickness of 2.5 meters at x=45 meters (the location of the peak reduced 1-D concentration) yields a composite plume concentration value of 457 mg/l. This point concentration value approximates the peak concentration value of the reduced data (450 mg/l) and the analytical solution's peak concentration value (434 mg/l). The similarity between these values helps to validate the legitimacy of the both concepts.

In an attempt to further validate the one-dimensional analytical solution and the concept of compressed reduced 1-D data, the data obtained from digitizing Figure 14 was combined with the known limits of the chloride plume to generate Figure 23.

This page intentionally left blank.

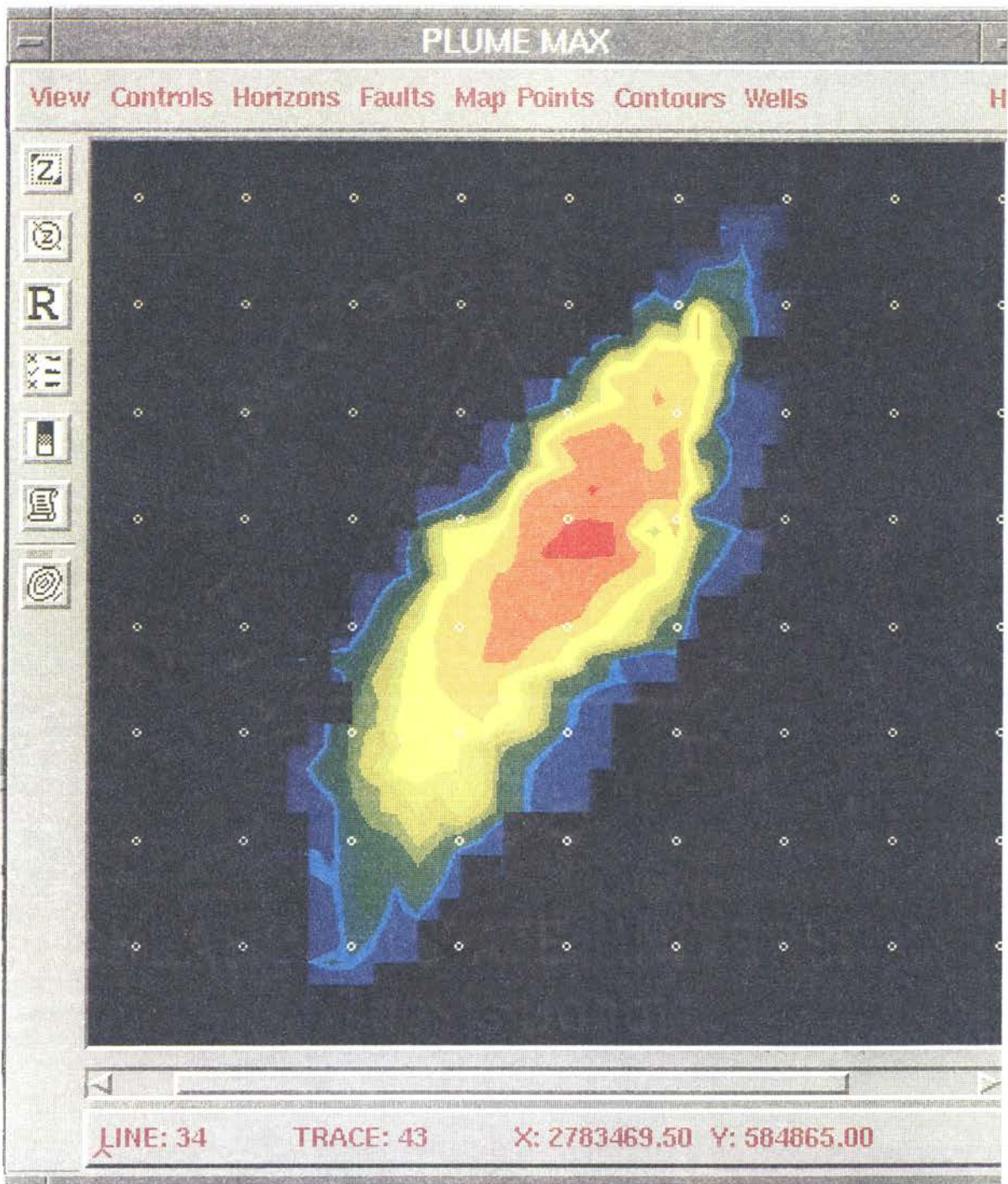


Figure 23. Digitized Chloride Plume Data

Figure 23 represents a top view of the chloride plume presented in the horizontal (X-Y) plane. The color shading indicates relative chloride concentration values with blue representing zero concentration and red representing the highest concentration. The scale of Figures 23, 24, 25, and 26 must be read from the body of the figure, with the dot pattern being on a 5 meter square. The color shading was developed by the software discussed below, and should only be considered in the relative, or qualitative, sense.

Figure 23, as well as Figures 24, 25, and 26, were developed with Landmark's Z-Map and SeisWorks/3D software running on a Sun Microsystem Workstation. These software packages are designed for the oil and gas exploration industry and are traditionally used to process raw seismic data. The software is extremely computationally powerful, and was deemed flexible enough to process the limited data set developed at Borden.

The SeisWorks/3D software was used to prepare the Borden data as input for the Z-Map software package. The SeisWorks/3D software has multiple splining and triangulation algorithms, and these algorithms allow the construction of three-dimensional objects with limited spatial input data.

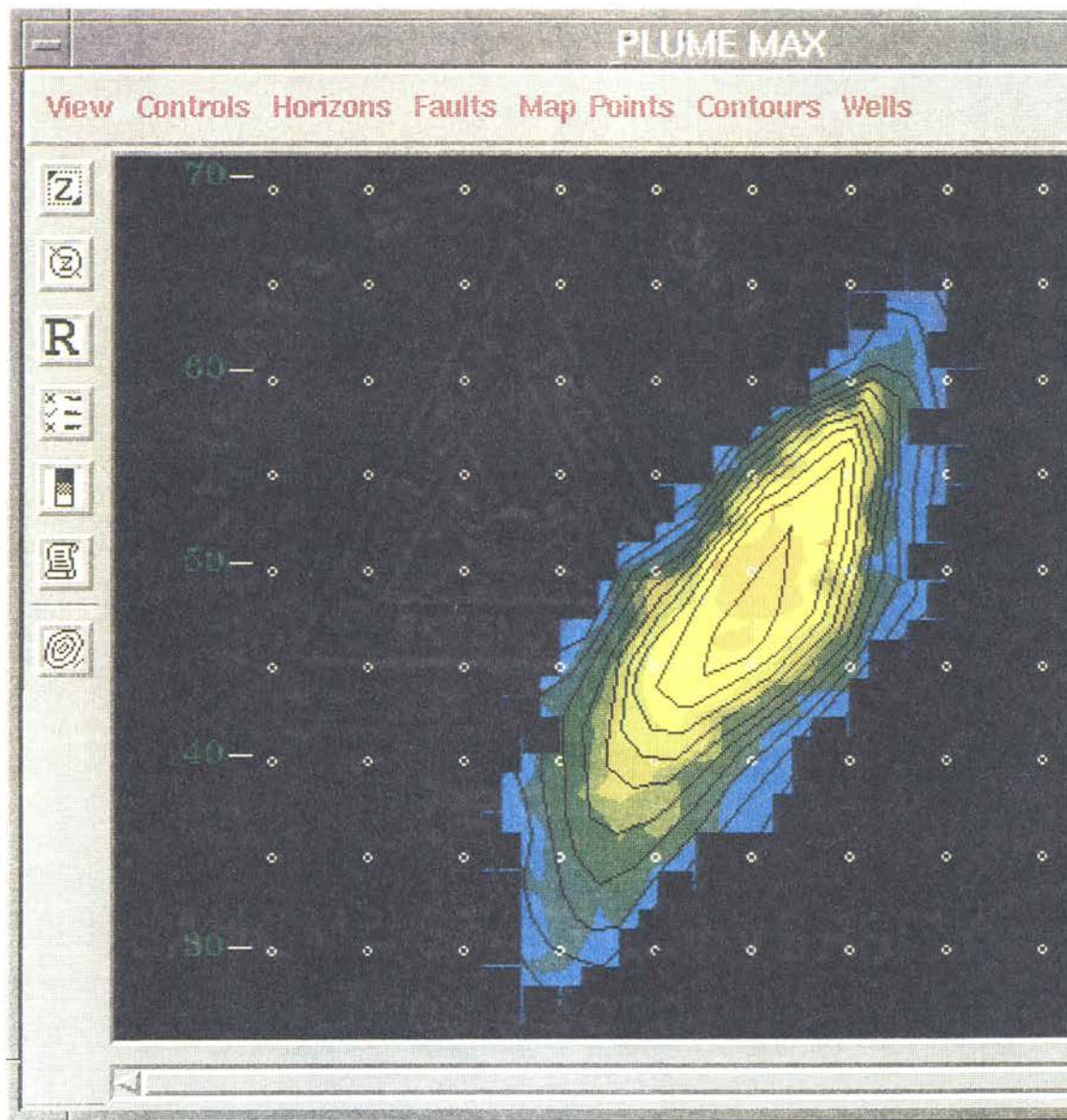


Figure 24. Digitized Chloride Plume Data with Isopleth Overlay

Figure 24 shows the color filled chloride plume of Figure 23 overlaid with concentration isopleth contours. These contours were generated by the software previously discussed and should only be considered in the qualitative sense.

Figure 24 was then used to provide the input data necessary to generate Figure 25.

Figure 25 shows a rear view of a rough three-dimensional model of the chloride plume viewed from a 33 degree angle to the direction of transport.

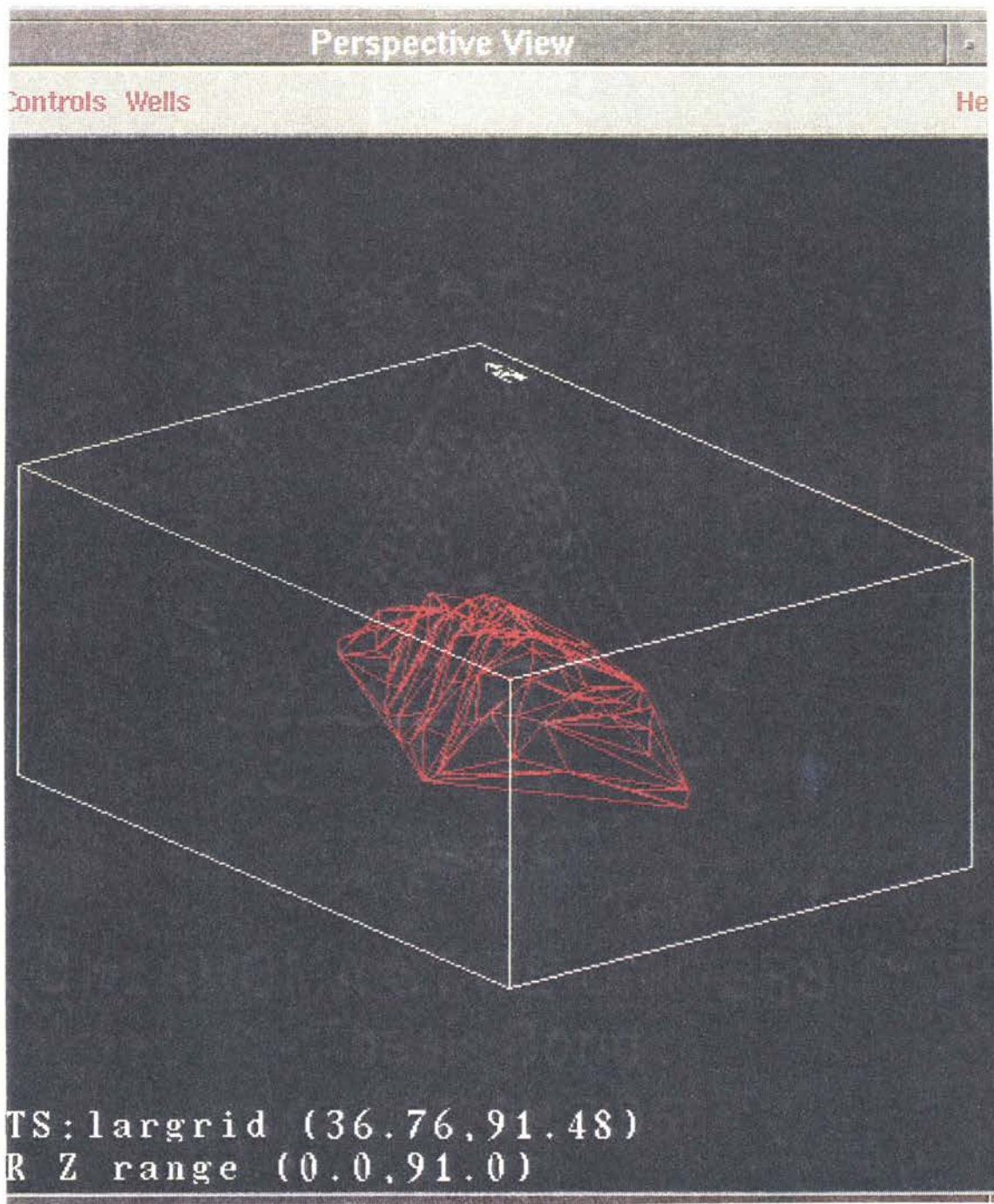


Figure 25. Rough Three-Dimensional Chloride Plume Structure

Like before, Figure 25 was used as input to generate Figure 26. Figure 26 was generated by a biharmonic flexing sub-routine whereby the surface planer structures seen in Figure 25 are bent as smoothly as possible from one inflection point to the other. The perspective shown in Figure 26 is identical to that of Figure 25. Close inspection of the two figures will show the plume in Figure 26 contains a greater number of planer surfaces than the plume in Figure 25.

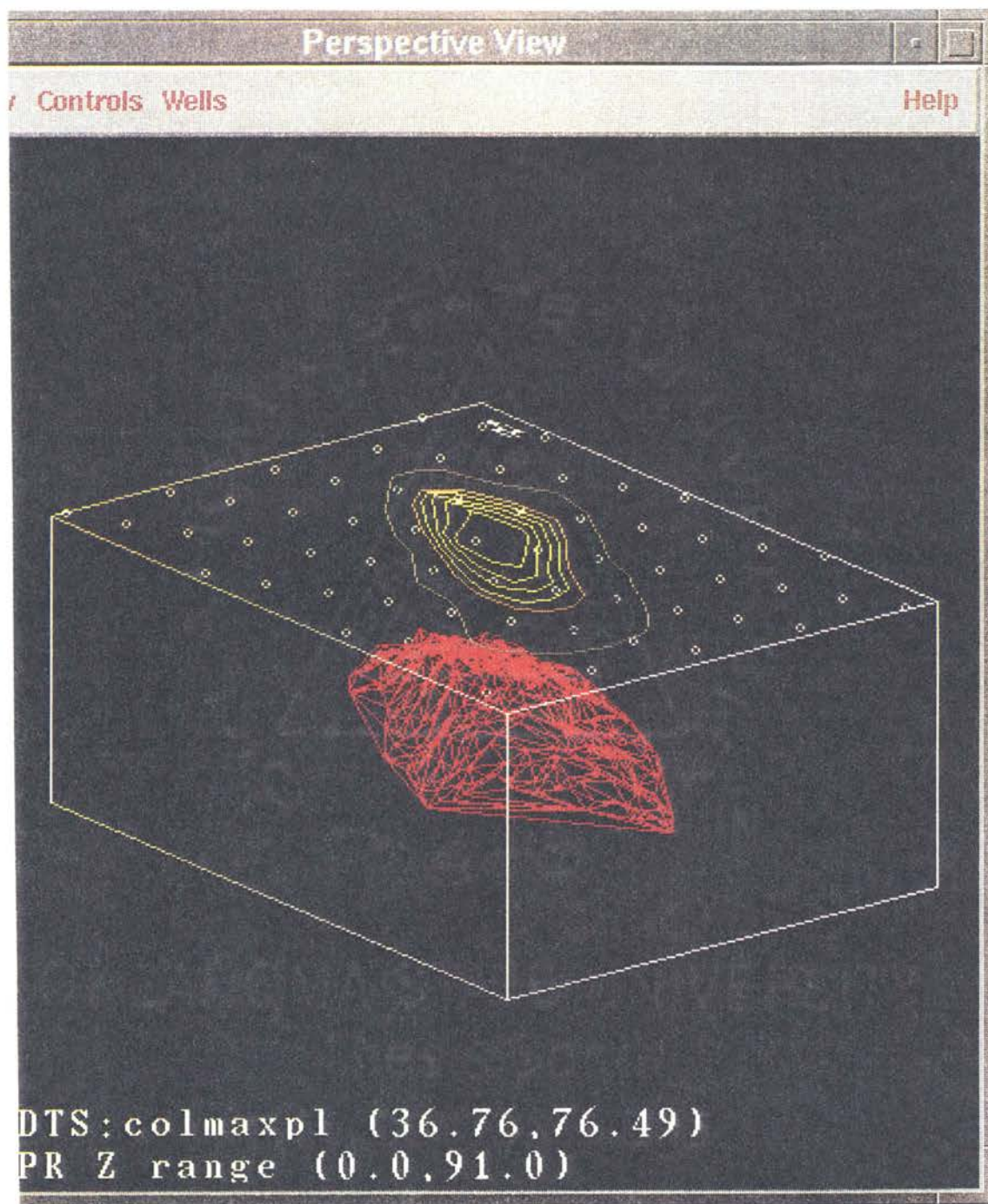


Figure 26. Smoothed Three-Dimensional Chloride Plume Structure

After the plume shown in Figure 26 was fully developed, the same software was utilized to calculate the plume's volume. The volume of the plume shown in Figure 26 was determined to be 256 cubic meters. Using this spatial volume with the total injected chloride mass yields a plume cloud having an average concentration of 42 mg/l. This average concentration value compares very favorably with the theoretical average plume concentration value of 47 mg/l calculated previously, and thereby validates both the analytical solution and the concept of the reduced 1-D data as legitimate.

Summary: Analytical Realization

Figure 27 overlays the field observed concentration profile with the analytical solution profile, and shows the difference between the two along the zero axis. As expected this figure indicates the analytical solution matches the observed plume concentration profile quite well.

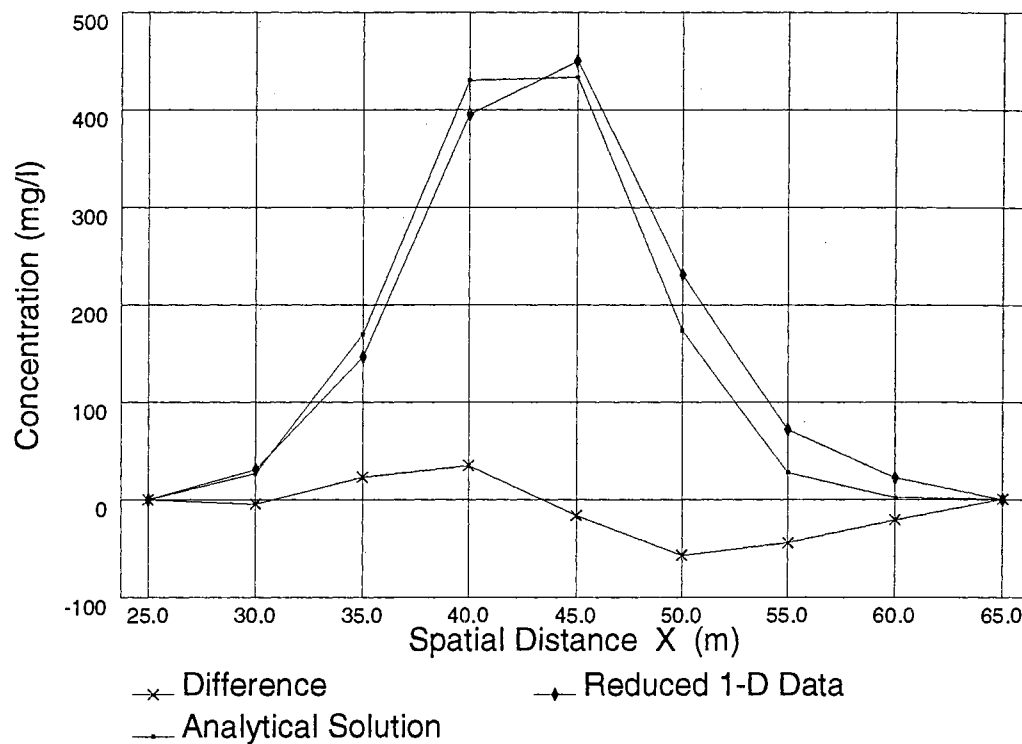


Figure 27. Reduced 1-D Concentration Data, Analytical Realization and the Difference Between the Two

While the profiles of the two data sets have the same general shape, there are significant differences. The differences between the observed reduced data and the analytical realization indicates the analytical model overestimates the observed concentration in the tailing portion of the plume, and underestimates the observed concentration in the leading portion of the plume along the axis of flow. The modeling realization and the observed data match exactly at the location where travel Distance = Rate * Time. As there is a high level of confidence in the consistency of the groundwater velocity, media homogeneity, and hydraulic conductivity, Figure 27 suggests either the dispersivity values along the line of advection used in the model do not completely describe the dispersion phenomenon, or the aquifer's heterogeneity effectively retarded the advance of the entire plume body. These observations come as no major surprises, as variations in aquifer and parameter heterogeneity are often unaccounted for in groundwater models. As Figure 17 indicates the velocity of the plume was not retarded during this time frame, it is likely the reported dispersivity value does not completely describe the dispersion events.

The effects of the two components of hydrodynamic dispersivity, molecular diffusion and mechanical dispersion, are reflected in both the observed field data and the reduced data at Borden. Some of these effects can easily be seen in Figure 27 in that the chloride/native groundwater interface is not an abrupt transition, but a gradual gradation from zero chloride concentration to the maximum chloride concentration. The variations in the solute concentration from zero values to a peak value can be

well represented by a fuzzy number. In fact the gradational change in chloride concentration values is very similar to the changes represented by fuzzy number triangular membership functions. The facts that dispersivity is one of the most studied, most important, and most variable parameters used in groundwater modeling make it a prime candidate for parametric description via fuzzy modeling techniques.

IX. BORDEN SITE FUZZY MODELING

Equation 18, the analytical solution to the partial differential transport equation shown as Equation 17, was used as the basis for the development of the following fuzzy modeling platform. The resultant fuzzy model was then used to calculate the expected chloride concentrations along a one-dimensional flowpath at the Borden site.

✓ The sole fuzzy input parameter was chosen to be dispersivity, and was generated by fuzzifying the crisp dispersivity value into an isosceles triangle membership function having endpoints defined as $\pm 10\%$ of the crisp dispersivity parameter's value.

Crisp and Fuzzy Realizations

Figure 28 shows both endpoints of the fuzzy model's concentration realization membership function at five meter increments along the flowpath axis, along with the crisp analytical realization's predictions. Figure 28 plainly shows that the crisp solution is bound by the upper and lower endpoints of the fuzzy realization's membership function. At the trailing edge of the chloride plume, the lower limits of the fuzzy realization are closer to the analytical realization profile than the upper values of the fuzzy realization's membership function. Conversely, at the leading edge of the chloride plume the upper values of the fuzzy realization better approximate the analytical realization's profile values.

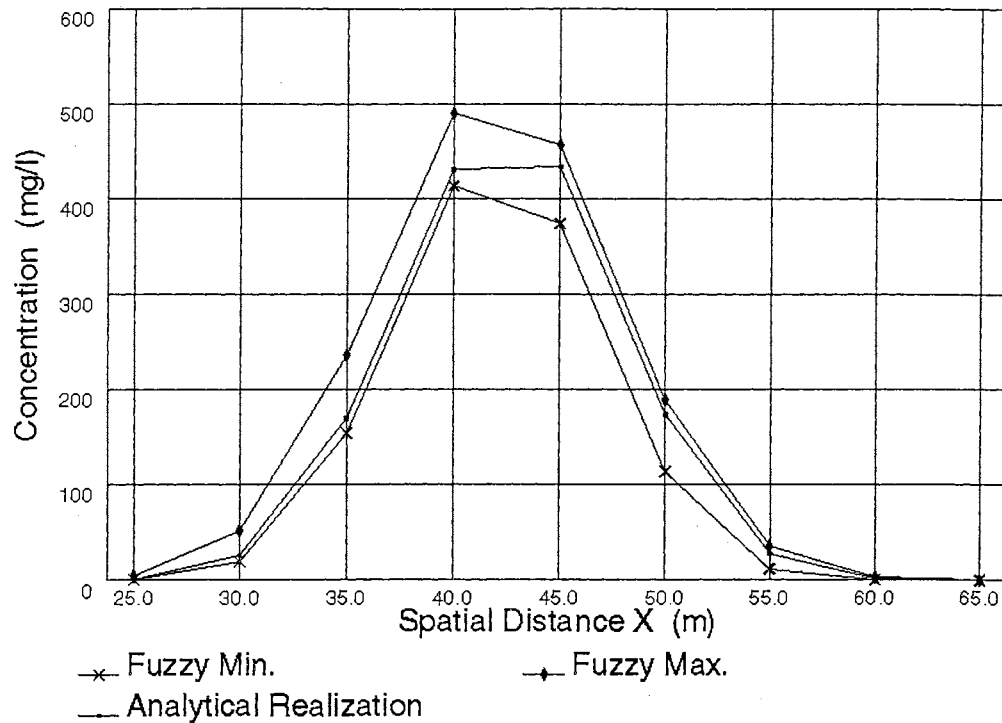


Figure 28. Crisp Analytical Realization and Fuzzy Endpoints
(+/- 10% dispersivity)

Figure 29 shows the differences between the analytical realization and the fuzzy endpoints at common spatial values. Both fuzzy endpoints were subtracted from the corresponding crisp analytical realization in order to easily visualize the behavior of the two endpoints. Note that the differences due to the fuzzy minimum endpoints will appear as a positive number in this scenario, while the maximum fuzzy endpoints will generate negative differences as the crisp realization is completely bound by the fuzzy realization. The general characteristics and shape of Figure 29 is revealing, and should be kept in mind when reviewing Figures 30, 31, 32, 33 and 34.

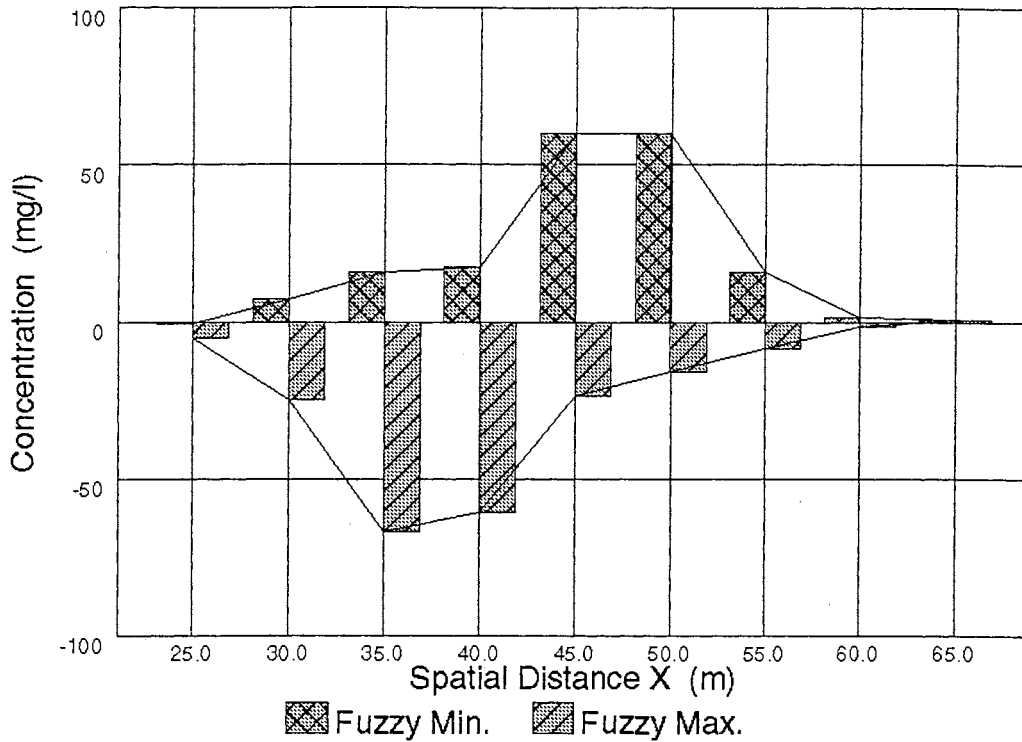


Figure 29. Crisp Realization Less Fuzzy Realization Endpoints
($\pm 10\%$ crisp dispersivity)

Figures 27 and 28 show this fuzzy realization yielded, in a general sense, concentration values which tended to overestimate the chloride concentration in the trailing section of the plume, and underestimate the chloride concentration in the leading portion of the plume. However, closer approximation to the crisp realization is achieved if one uses the lower membership endpoints at the trailing edge of the plume, and the upper membership endpoints at the plume's leading edge. Near the center of mass of the plume both the upper and lower membership endpoints approximate the crisp realization with a similar degree of accuracy.

Figure 30 shows the same information presented in Figure 28, with the addition of the observed reduced 1-D data being superimposed on the graph. This graph indicates the fuzzy realization generated with dispersivity endpoints defined as plus or minus 10% of the crisp dispersivity value did not completely bound the reduced data as they did the crisp analytical realization.

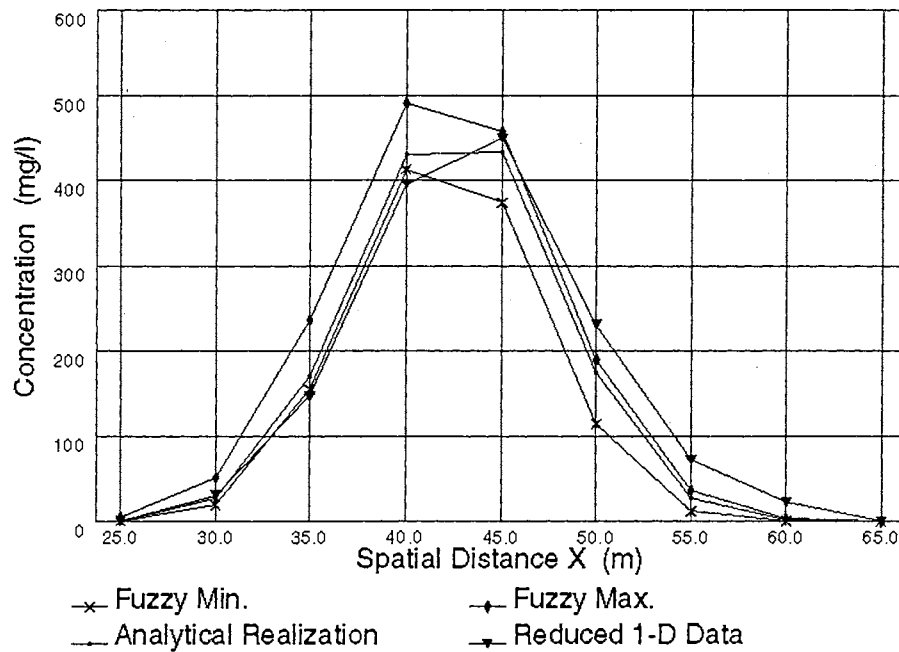


Figure 30. Reduced 1-D Data with Analytical and Fuzzy Realizations (+/- 10% of crisp dispersivity)

The observed reduced 1-D data can be seen to exceed the crisp realization projections in the leading section of the plume, as well as the upper endpoint of the fuzzy realization's membership graph. The extent the fuzzy realization's over and under estimation of the reduced data can be seen in Figure 31. Figure 31 was generated in

the same fashion as Figure 29, and graphically represents the difference between the observed reduced data and the fuzzy realization's membership function endpoints.

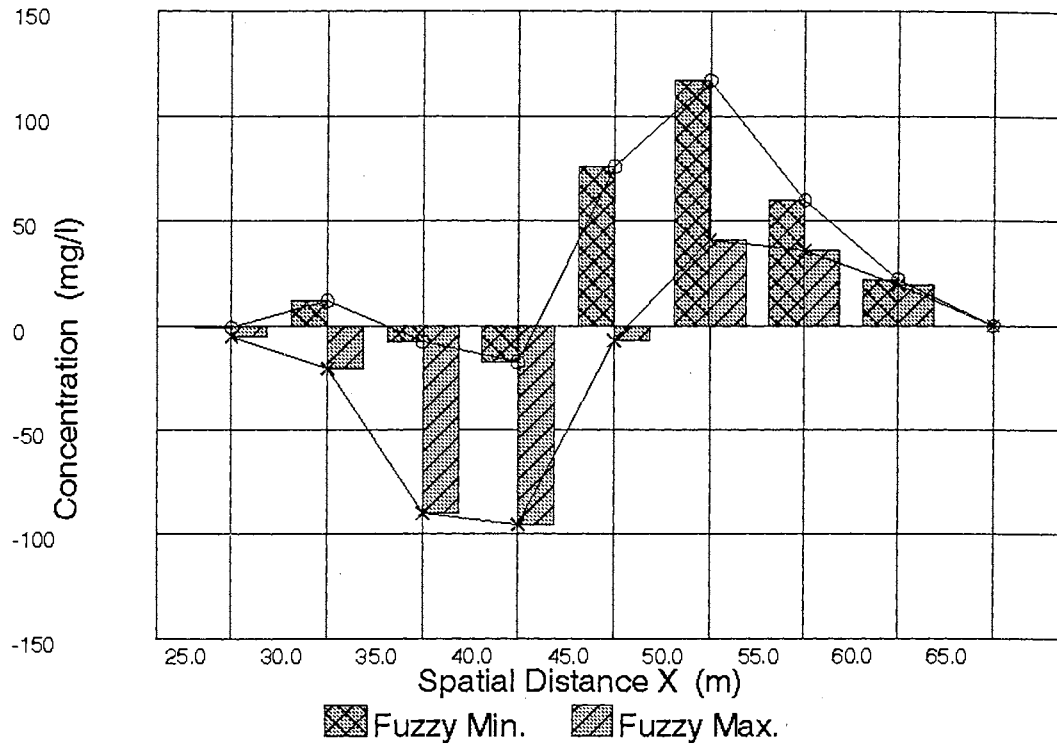


Figure 31. Reduced 1-D Data Less Fuzzy Realization Endpoints
($\pm 10\%$ crisp dispersivity)

The figure plainly indicates both the fuzzy endpoints overestimate the expected concentration of chloride ions in the trailing section of the plume and underestimate the concentration in the leading section. This suggests a dispersivity value with a support larger than the $\pm 10\%$ used above is necessary to match the observed behavior of the chloride plume.

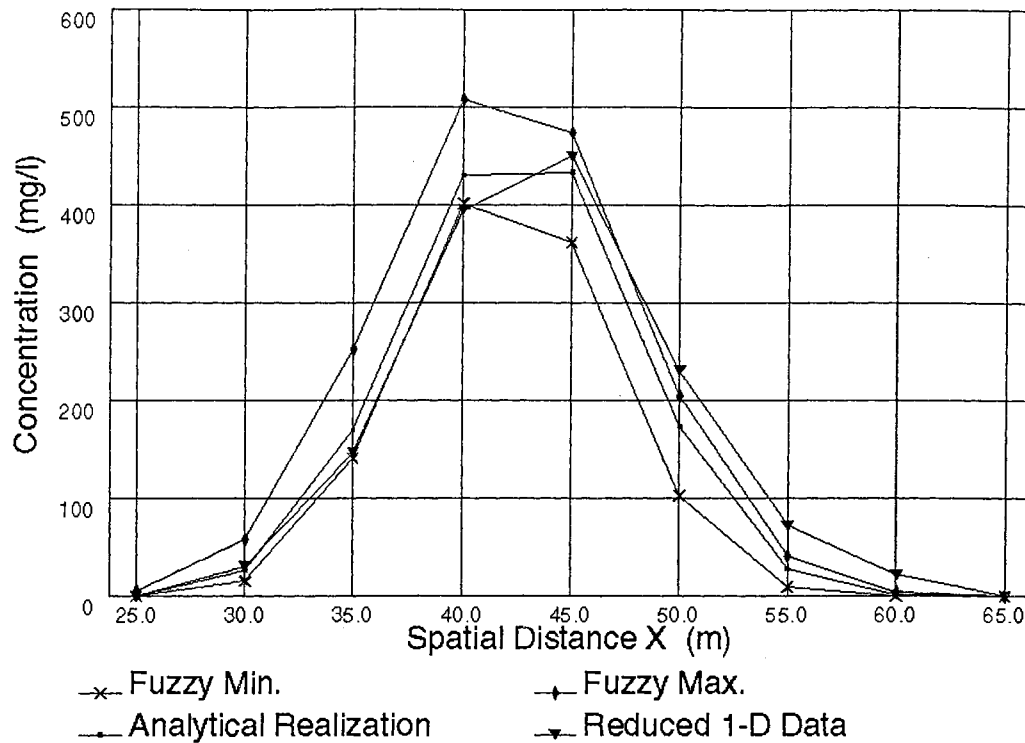


Figure 32. Reduced 1-D Data with Analytical and Fuzzy Realizations
($\pm 20\%$ crisp dispersivity)

Figure 32 was generated by fuzzifying the same crisp dispersivity value into an isosceles triangle membership function with defined endpoints of $\pm 20\%$ of the crisp dispersivity parameter's value. The resultant output is shown along with the observed data as well as the analytical solution. This figure, like Figure 30 shows the crisp solution to be bound by the upper and lower endpoints of the fuzzy realization's membership function. Also like Figure 30, the observed data concentration profile exceeds the maximum fuzzy endpoints at the leading portion of the plume.

Figure 33 shows the differences between the crisp analytical realization and the fuzzy realization obtained from using a dispersivity membership function derived as $\pm 20\%$ of the crisp parameter. Figure 33 shows the fuzzy realization obtained with the larger dispersivity value bounded the crisp realization very well; although the tendency to overestimate concentration in the tail and underestimate in leading section of the plume is still apparent.

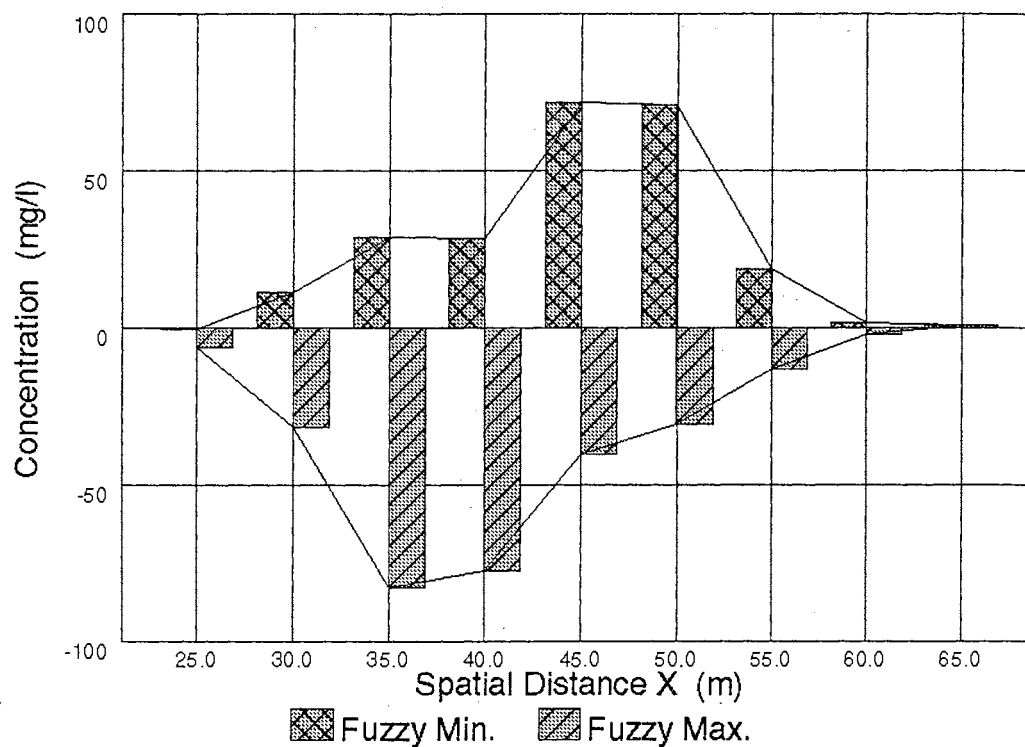


Figure 33. Crisp Analytical Realization Less Fuzzy Realization Endpoints ($\pm 20\%$ crisp dispersivity)

Figure 34 replicates Figure 31 except the fuzzy dispersivity value had its membership function endpoints increased to $\pm 20\%$ of the centroid's value.

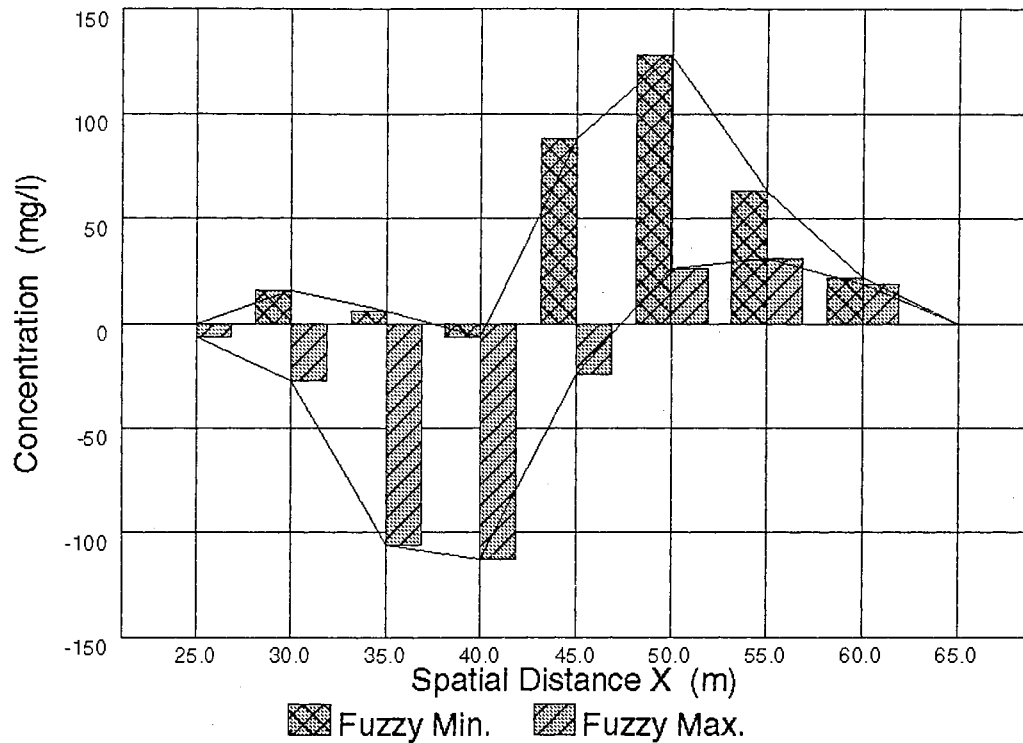


Figure 34. Reduced 1-D Data Less Fuzzy Realization Endpoints
($\pm 20\%$ crisp dispersivity)

The graph indicates some movement towards bounding the reduced data; however, the fuzzy solution, like the analytical realization, still overestimates concentration in the trailing plume section, and underestimates concentration in the leading section.

Discussion of Fuzzy Realizations

Figure 35 represents the percentage difference between the two different fuzzy realizations. The graph indicates a total increase of about 10% in the realizations bounds between $X=40$ and $X=45$ occurs if one uses the $\pm 20\%$ dispersivity end point values. The percentage difference increases dramatically as one moves away

from the center of the plume and toward plume edges. A total difference of about 50 percent can be observed at the plume extremes $X=25$ and $X=60$.

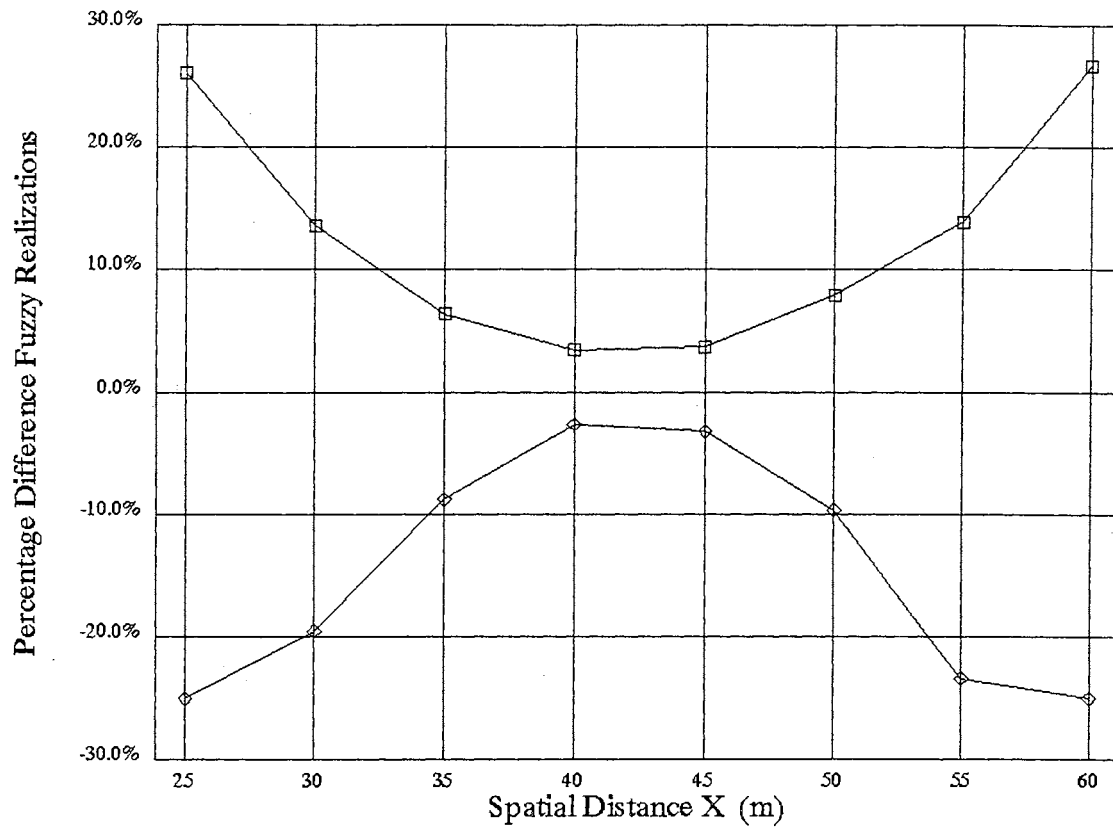


Figure 35. Percentage Difference Between the Two Fuzzy Realizations

The figure indicates an increase in the support of a fuzzy dispersivity value will have a more pronounced impact on the predicted concentration values at the extremes of the plume than near the center of mass.

Conclusion: Borden Experiment

In the example of chloride ion transport in the Borden Experiment using a fuzzy dispersivity parameter, the upper values of the resultant membership function better approximated observed plume behavior at the leading edge of the plume. Conversely, at the trailing edge of the chloride plume, lower values of the resultant membership function better replicate observed behavior. These same tendencies were also observed regarding the comparison of analytically derived data to the fuzzy realizations. Increasing the base of the fuzzified variable from 10% to 20% of the centroid's mean value increased the interval of the fuzzy realization; however, it did not change the tendencies of over and under-estimation at the leading and trailing edges of the plume. The fact a doubling of the fuzzy dispersivity membership endpoints on a percentage basis did not change the basic relationship of the fuzzy realizations to the observed data and analytical solution indicate the robustness of the fuzzy platform.

X. FRACTURED MEDIA TRANSPORT APPLICATION

The last decade has seen a resurgence in interest in modeling fluid transport in fractured aquifers. Much of this interest has been inspired by concerns relating to the underground storage of nuclear waste material, while another, and somewhat ironic factor, is the revived exploration economics of the oil and gas industry. It is intriguing to note that while the oil and gas industry is seeking underground formations which allow the rapid release of fluids entrained in rock reservoirs, the waste disposal industry is interested in rock formations which will readily accept, then retain, waste fluids injected in the formation material.

The study and exploitation of fractured media by both of these industries has increased the knowledge and understanding regarding fluid behavior in fractured formations. As with any naturally occurring phenomenon, accepted modeling practices evolve over time as research and understanding of the field is increased. Early models are traditionally qualitative in nature, and often rapidly fall out of favor as quantitative models are developed. Unfortunately, the seductive nature of quantitative models can overwhelm an industry, and pull participants away from the fundamental understandings and basic workings of the field of study. (One example would be the over dependence of "Wall Street" on computer hedging programs during

1986 and 1987.) The best aspects of both qualitative and quantitative modeling can be achieved with the utilization of a fuzzy modeling platform.

Characteristics of Fractured Media

Fracturing is usually defined by geologists as "the rupture and separation into discrete parts along a planar surface not parallel to bedding planes" [Stearns and Friedman, 1972] The fracturing of a rock media causes several morphological changes in the matrix of the rock, which in turn, impact the ability of fluid to move through the media. These morphological changes effect the more common modeling parameters used in the mathematical simulation of groundwater flow and transport. In particular the orientation, density, aperture size, and connectivity of the fractures, as well as the roughness along the open fracture walls, and the amount of fill material in "healed" fractures have dramatic effects on fluid movement. Unfortunately, these properties are high variable, and like most heterogenous parameters, very difficult to measure or predict with any degree of accuracy.

While not all fractures are created equally, some fractures are created more equally than others. Fractures generated from tectonic movements such as local folding or fault straining are more uniform in nature than stratigraphically controlled fracturing. Stratigraphically controlled fractures are developed from processes such as thermal contraction, diagenetic shrinkage, or surface weathering [Nelson, 1979], and are more isotropic in their properties than tectonic induced fractures. In particular, fractures

resulting from these types of processes are usually very heterogenous in the vertical direction, and have lesser connectivity than tectonic related fractures.

Many studies of groundwater flow and transport in fractured media emphasize the influence of fractures on the permeability of the matrix media. This is logical as the permeability of the fracture network is often substantially greater than that of the matrix media, and thereby offers the least hydraulic resistance to flow. For good or bad, fractures have been shown to have great potential to be very effective flow pathways [Gale, 1979; Nelson and Handin, 1977; Wilson and Witherspoon, 1970].

When these pathways exist in a rock matrix, the transport of contaminant through the media matrix by advection is usually negligible in comparison to the transport occurring in the fracture. This is mainly due to the relatively low hydraulic conductivity of the rock compared to the hydraulic conductivity of the fracture [Sudicky and Frind, 1982]. Yet, matrix porosity existing between fractures can provide significant storage space and time for contaminant solutes [Sudicky and Frind, 1982].

Most groundwater modeling platforms combine the processes of diffusion and dispersion into the single modeling parameter known as hydrodynamic dispersion. This can often pose somewhat of a unique challenge for groundwater modeling in fractured media. The longitudinal dispersion component of transport in a fracture is usually assumed to be negligible, or have a linear relationship with the average fluid

velocity in the fracture. However, it has been shown [*Dronfield and Sillman*, 1993; *Tang et al.* 1981] these assumptions are often not always completely valid.

Porosity in the matrix media connected to the major fractures is commonly referred to as the matrix porosity [*Grisak and Pickens*, 1980] and can play a significant role in determining the amount of solute which can make its way into the rock matrix. The effects of matrix diffusion in the aquifer are well known, and have been shown to provide significant retardation of contaminant transport in fractures [*Davison et al.*, 1980]. The molecular diffusion of a solute from the fracture into the porous matrix retards the advance of the solute by removing, then returning, contaminant mass to and from the fracture flow channel. Acting thusly, matrix diffusion can be considered to be a dynamic and reversible storage mechanism for solute contaminants within the matrix media.

Conceptual Modeling in Fractured Media

Modeling of solute flow in fractured media has been the focus of an impressive amount of work in the recent years. While novel approaches to the problem, such as fractal network analysis [*Acuna and Yortos*, 1995], are being explored, two basic concepts remain as the foundation for most models.

One approach views the entire flow system as a single continuum and treats both the

fracture and the rock matrix as a single equivalent porous medium [*Huyakorn et al.*, 1983; *Warren and Root*, 1963; *Barenblatt et al.*, 1960] The other approach views the fractures and the matrix media discretely, and requires explicit knowledge of all the fractures in the rock [*Shapiro and Andersson*, 1983]. The requirement of exact and detailed knowledge regarding the fractures effectively restricts the applications of the discrete methodology to arenas primarily devoted to basic research regarding flow and transport behavior.

Both of the two basic approaches have their own limitations, not the least of which is defining the mass transfer function which occurs at the fracture wall/interface [*Chen and Douglas*, 1990; *Douglas and Arbogast*, 1990; *Maloszewski and Zuber*, 1990; *Arbogast*, 1989; *Quintard and Whitaker*, 1988; *Gilman*, 1986; *Kazemi and Gilman*, 1983; *Carbonell and Whitaker*, 1983].

The sheer magnitude of this field of study requires this research to limit itself to a single aspect of modeling solute transport in fractured media. This aspect will be to incorporate uncertainty, in the functional form of fuzzy numbers, into an analytical solution for the transport of a single solute in a single fracture. The fuzzy analytical solution will then be compared to three non-fuzzy solutions: one analytical, and two numerical solutions of the same problem. The conceptual physical system which will be investigated is shown as Figure 36. The figure will also help to illustrate the conditions under which equations 22 and 23, described below, are valid.

Assume groundwater is moving at a constant velocity in the X direction along a planer fracture having a half aperture width of "b". A contaminant solute is introduced into the fracture at $X=0$, and is transported in the fracture solely by advection. Solute movement into the matrix occurs by diffusion normal to the flowpath of the fracture, and the contaminant is assumed to be in equilibrium at the fracture/media wall interface.

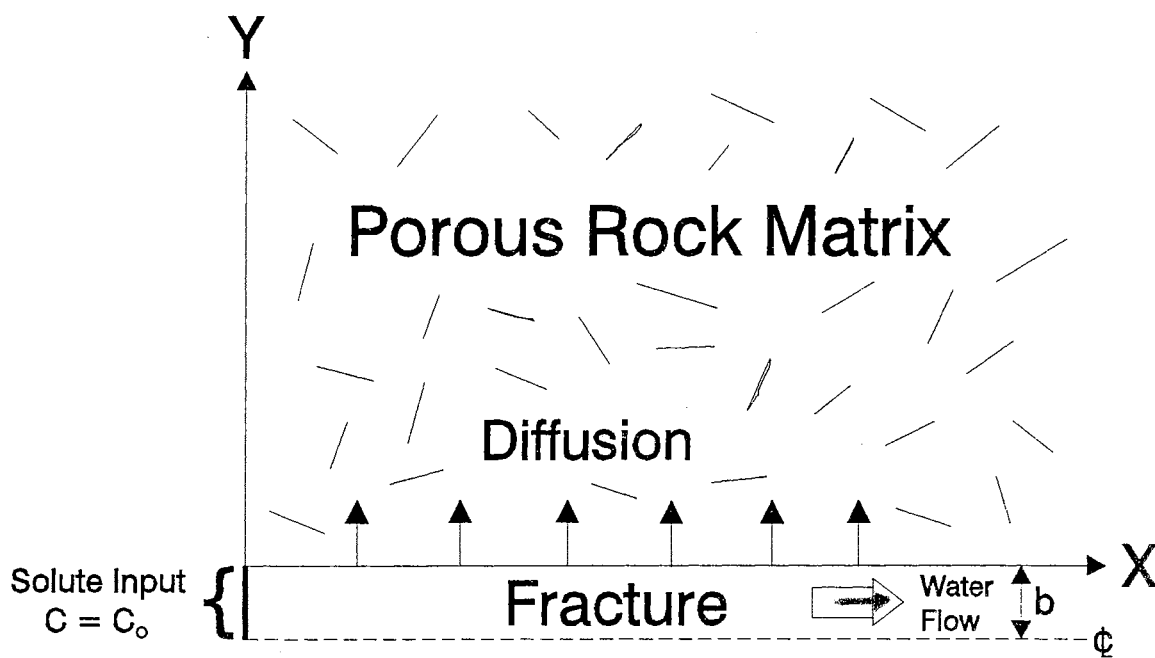


Figure 36. Physical Basis of Analytical Solution for Solute Transport in Fractured Media.

Governing Equations

The basic problem to be addressed via the fuzzy modeling platform is the incorporation of uncertainty into an analytical solution platform. In this instance we will investigate the situation where a non-reactive solute is transported in a fracture, and diffuses from the fracture into the adjacent matrix. The governing conditions include one-dimensional advective transport in the fracture and one-dimension diffusive transport into the matrix normal to the fracture. The flux of solute from a fracture into the media matrix is controlled primarily by the porosity of the matrix, the molecular diffusion coefficient, and the concentration gradient of the solute in the matrix. The differential equations governing solute transport in the fracture and the matrix, are respectively [Grisak and Pickens, 1981]:

In the fracture:

$$b\left(\frac{\partial C_f}{\partial t} + V\frac{\partial C_f}{\partial x}\right) = \theta_m D \frac{\partial C_m}{\partial y} \quad (22)$$

In the matrix media:

$$\frac{\partial C_m}{\partial t} = D \frac{\partial^2 C_m}{\partial y^2} \quad (23)$$

Given the boundary conditions of:

$$\begin{aligned} C_f(x,y) &= C_m(x,y)=0, & t=0 \\ C_f(0,0) &= C_m(0,0)=C_0, & t>0 \\ C_f(x,0) &= C_m(x,0) & x>0; t>0 \end{aligned}$$

Where:

V	Groundwater velocity (L/t)
b	Aperture width (L)
θ_m	Porosity (%)
D	Diffusion coefficient (L ² /t)
x	Distance along fracture (L)
y	Distance in matrix normal to fracture (L)

The boundary conditions indicate the initial concentration of a solute in the fracture and matrix is zero. Water and solute enter the fracture at $X=0$, and the matrix is assumed to extend to infinity normal to the fracture. The following solution assumes non-reactive transport in both the fracture and the matrix, and concentrations of the contaminant in the fracture and at the fracture/media interface are equal. Equations 24 and 25 are analytical solutions to equations 22 and 23, and were developed for determining solute concentrations in the fracture and in the matrix media [*Grisak and Pickens*, 1981].

For the matrix media:

$$\frac{C_m}{C_o} = \operatorname{erfc} \left(\frac{\frac{\theta_m D}{Vb} x + y}{2[D(t - \frac{x}{V})]^{0.5}} \right) \quad (24)$$

where: $t > x/V$; and 0 where $t < x/V$

For the fracture:

$$\frac{C_f}{C_o} = \operatorname{erfc} \left(\frac{\frac{\theta_m D}{Vb} x}{2[D(t - \frac{x}{V})]^{0.5}} \right) \quad (25)$$

where: $t > x/V$; and 0 where $t < x/V$

and:

V	Groundwater velocity (L/t)
b	Aperture width (L)
θ_m	Porosity (%)
D	Diffusion coefficient (L ² /t)
x	Distance along fracture (L)
y	Distance in matrix normal to fracture (L)

Due to the basic and fundamental similarity between equations 24 and 25, and the author's personal interest, only equation 25 will be analyzed for suitability with fuzzy modeling. If equation 25 is proved to be viable for modeling with fuzzy parameters, there is no reason to believe equation 24 would not be suitable for the same.

Laboratory Trial

Before a fuzzy model is developed from equation 25, it is worth testing the basic viability of the equation with some real world data. A laboratory experiment was carried out [Grisak and Pickens, 1981] to test equation 25 against physically observed data and a numerical platform solution to fractured flow. The experiment utilized a chloride tracer fluid and a large column of fractured till. Two sets of vertical

fractures were reported to exist in the till approximately 4 centimeters apart in the test media. The experiment forced the tracer fluid through the till, and the fluid breakthrough time and volume data was recorded. A relative concentration curve for the experiment was subsequently developed.

The actual numerical breakthrough data for the chloride tracer shown in Figure 37 was obtained by digitizing a graphical representation of the results of the experiment. The same Sun Microsystem Workstation and digitizing tablet used to develop Figures 23, 24, 25, and 26 were used to develop the data shown in Figure 37 and Appendix G.

Figure 37 shows the numerical results of the experiment along with an analytical modeling platform solution for the data. The digitized information is shown as point data in the figure, while the solution to the analytical equation 25 is shown as a line.

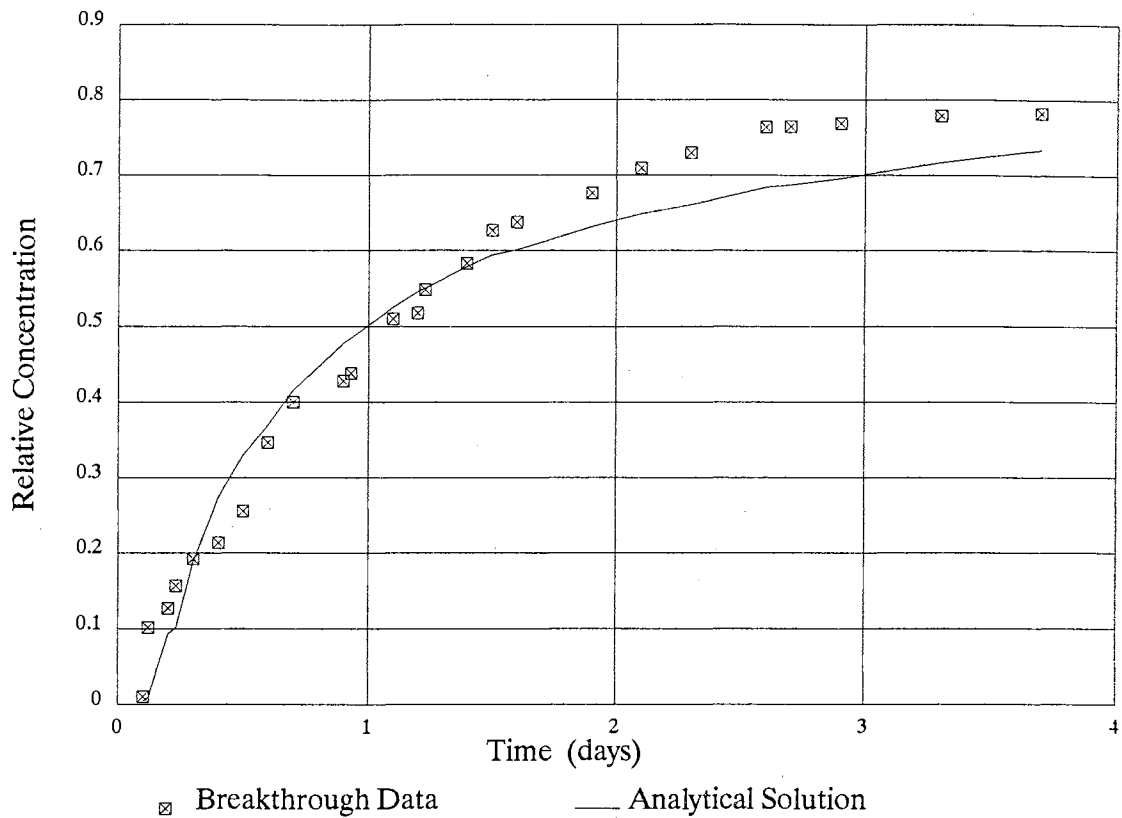


Figure 37. Experimental Chloride Breakthrough Data and an Analytical Solution.

The analytical solution shown in Figure 37 was prepared by using equation 25, along with an approximation of the complementary error function. The complementary error function was approximated with an elaborate equation based on a Chebyshev fitting of a functional form of the error function. The equation estimates the complementary error to within 1.2×10^{-7} , and can be found in Appendix F. The figure shows a relatively good fit between the analytical solution and the observed data, and thereby helps to validate the usefulness of equation 25.

Fuzzy Analytical Model

This research developed a fuzzy analytical model based on Equation 25, and compared the fuzzy solution to published solutions (one analytical and two numerical) for the same well known problem. The problem [Tang *et al.*, 1981] and the numerical solutions were obtained from the finite element code "Transport in Fractured Porous Media with Water Table Boundary Conditions" commonly referred to as "TRAFRAP." This code was developed by HydroGeoLogic, Inc., and the International Ground Water Modeling Center of Holcomb Research Institute. TRAFRAP approaches groundwater modeling in fractured media via either a dual porosity approach or the discrete fracture approach. In the situations discussed below both methodologies yielded similar results.

Table XVIII shows the results obtained from TRAFRAP for the discrete and dual porosity finite element numerical solutions. The table also shows the results obtained from an analytical solution based upon Equation 25 which was applied to the same problem. As can be readily seen from Table XVIII and Figure 38, there is an extremely good agreement between the three different solutions.

TABLE XVIII

RELATIVE CONCENTRATION DATA
at time = 995

Distance X	Discrete Solution	Dual Porosity Solution	Analytical Solution
0.0	1.0000	1.0000	1.0000
0.1	0.8710	0.8807	0.8941
0.3	0.7156	0.7055	0.7072
0.6	0.4755	0.4748	0.4848
1.0	0.2705	0.2694	0.2729
1.5	0.1186	0.1209	0.1309
2.2	0.0305	0.0381	0.0399
3.0	0.0041	0.0090	0.0087
4.0	-0.0001	0.0015	0.0010
5.0	0.0000	0.0002	0.0000
6.0	0.0000	-0.0000	0.0000

The realizations shown in Figure 38 for the discrete and dual porosity numerical models are represented as points, whereas the analytical solution realization is presented as values along the line. The graph shows the realization outputs from the three different models are so close to each other they are difficult to distinguish in the figure. The goodness of fit between the three different solutions should be obvious to the casual observer, and indicates any one of the three models could be used as a proxy for any of the others in this situation.

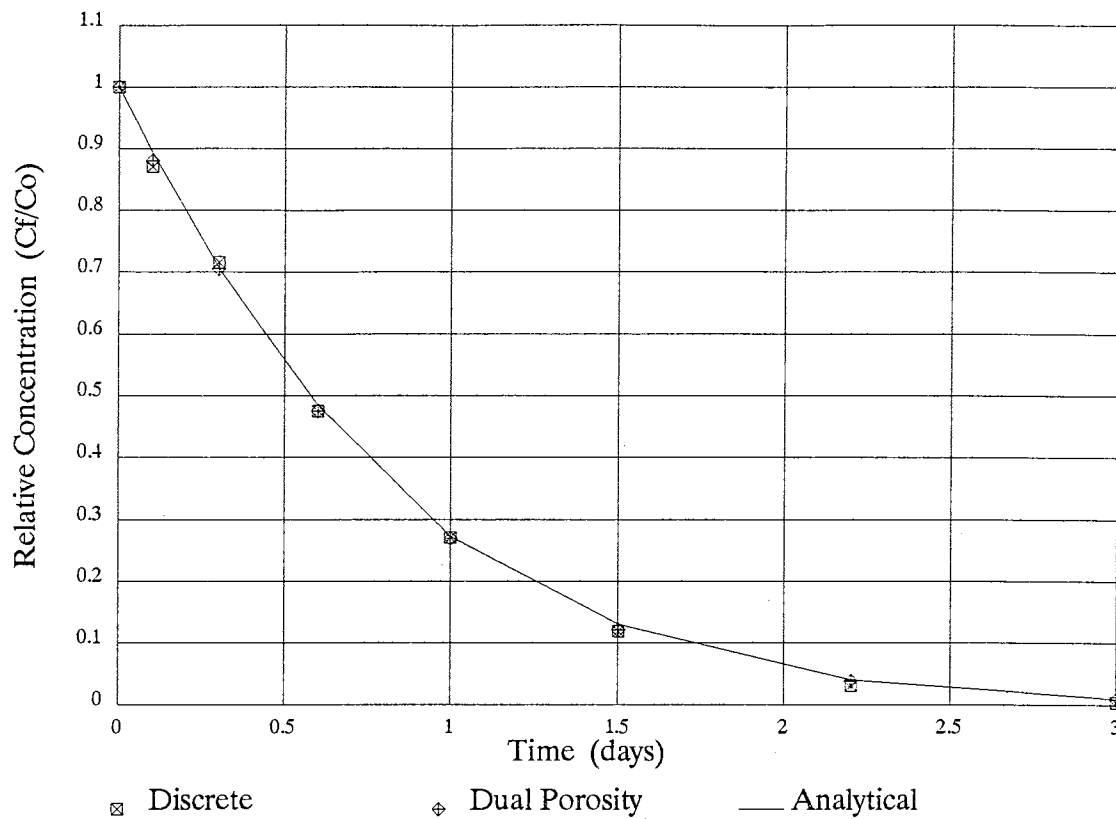


Figure 38. TRAFRAP Solution Comparison

This paper utilized equation 25 in an analytical solution as a vehicle by which to test the fuzzy number modeling concept against the two numerical modeling platform solutions. This was done by fuzzifying the molecular diffusion coefficient "D". While any or all of equation's parameters could have been fuzzified, only the molecular diffusion coefficient was chosen. This choice was made for many of the same reasons dispersion was fuzzified in the fuzzy models developed regarding flow and transport in non-fractured alluvium.

The centroid of the molecular diffusion coefficient, 1.38×10^{-4} was chosen to match a previously used crisp value [Tang. *et al.*, 1981] of "D", while the endpoints of 1.24×10^{-4} and 1.52×10^{-4} were chosen as plus or minus 10 percent of the centroid's value. As before an isosceles triangle was chosen to represent the shape of the membership function as this shape best approximates the statistical normal distribution. Table XIX shows the centroid and the endpoints of the resultant fuzzy relative concentration values obtained at various distances along the fracture after 995 days of transport.

TABLE XIX
"NORMAL" FUZZY MODEL REALIZATIONS:
RELATIVE CONCENTRATIONS

at time = 995

Distance X(m)	Low Endpoint	Centroid	High Endpoint
0.0	1.00000	1.00000	1.00000
0.1	0.88672	0.91113	0.93503
0.3	0.68070	0.73553	0.78944
0.6	0.41733	0.49358	0.56978
1.0	0.17274	0.24610	0.32307
1.5	0.03613	0.07677	0.12437
2.2	0.00135	0.00818	0.01834
3.0	1.450E-4	2.30E-4	0.00068
4.0	2.98E-11	2.88E-7	9.68E-7

Figure 39 shows the results of the fuzzy platform solution along with the crisp

calculation of the analytical solution. The graph indicates the fuzzy endpoints effectively bound the analytical solution until lower values of the relative concentration are reached. These lower values of relative concentration effectively represent the leading edge of the contaminant plume. This behavior is reminiscent of the numerical behavior shown in Figure 30, whereby the fuzzy solution's lower endpoints better approximated the analytical solution in the trailing section of the plume. Also, like Figure 30, the analytical solution and the fuzzy solution centroid values become identical near the middle of the plume.

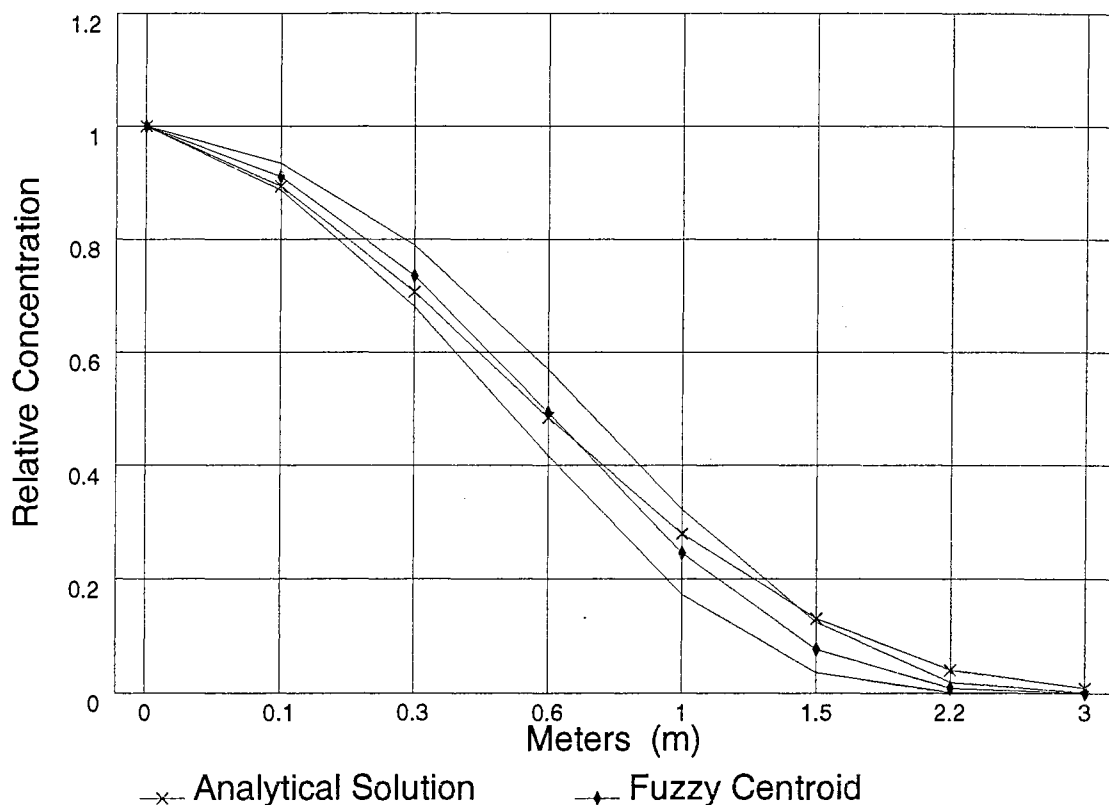


Figure 39. Analytical Solution and "Normal" Fuzzy Solution

After the midpoint is exceeded the analytical solution drifts towards the upper limit of the fuzzy solution. This observation suggests the fuzzy equivalent to a lognormal distribution for the input parameter should be investigated.

The same fuzzy analytical modeling platform was utilized along with a lognormal equivalent distribution of the fuzzy coefficient "D." Lognormalcy was achieved in the triangular distribution by maintaining the relationship shown as equation 3 in Chapter IV. Table XX shows the relative concentration results predicted by utilizing the fuzzy lognormal equivalent triangular distribution to represent the input parameter "D."

TABLE XX
"LOGNORMAL" FUZZY MODEL REALIZATIONS:
RELATIVE CONCENTRATIONS
at time =995

Distance X(m)	Low Endpoint	Centroid	High Endpoint
0.0	1.00000	1.00000	1.00000
0.1	0.88446	0.91149	0.93640
0.3	0.67551	0.73617	0.79230
0.6	0.41011	0.49361	0.57357
1.0	0.16642	0.24355	0.32701
1.5	0.03348	0.07182	0.12725
2.2	0.00115	0.00583	0.01921
3.0	0.00006	0.00007	0.00074
4.0	2.98E-11	3.02E-7	9.94E-7

Figure 40 shows the differences between the centroid values of the two realizations obtained in the fuzzy analytical solution using the two different triangular input

membership functions. It is evident from Figure 40 the differences between the centroids of the fuzzy analytical solutions obtained with the normal distribution equivalent of a triangular membership function, and a lognormal equivalent of a triangular membership function for the parameter "D," are minimal.

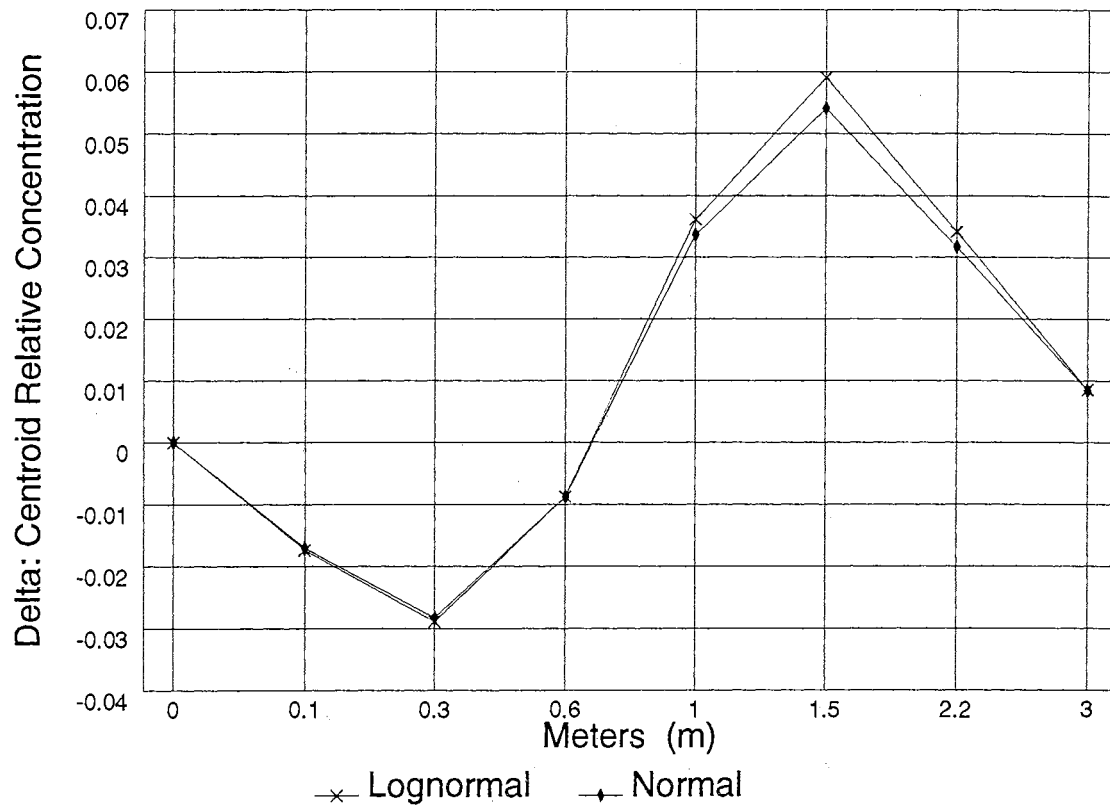


Figure 40. Differences Between Centroids Obtained with Normal and Lognormal Input.

The data shown in Table XX is plotted in Figure 41 along with the analytical solution data shown in Table XVIII.

As suggested by Figure 40, this figure indicates the fuzzy lognormal endpoints of the solution bound the analytical solution in a similar fashion as the non-lognormal fuzzy solution.

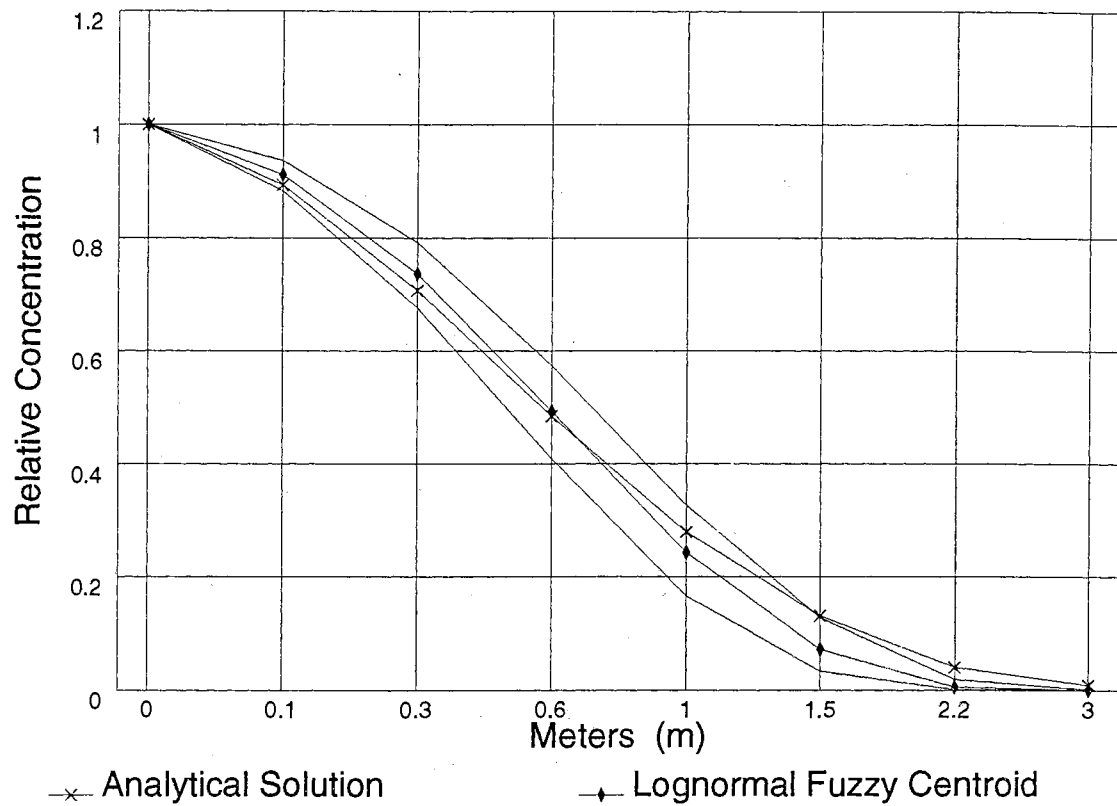


Figure 41. Analytical Solution and Lognormal Fuzzy Solution

Figures 39 and 41 indicate analytical modeling with fuzzy numbers is a viable tool in modeling non-reactive transport in fractured media. The realizations obtained via fuzzy numbers have been shown to approximate real world flow and transport behavior as well as analytical, and by proxy, numerical models of the same. The

centroid of the fuzzy solution has been shown to overestimate an analytical solution's crisp realization in the trailing section of the plume, and underestimate the same in the leading section. Near the middle of the plume, the fuzzy and crisp solutions are identical.

These are important results as they show fuzzy analytical solutions can be used to incorporate specialized knowledge into parameter value selection, and to estimate solute concentration and breakthrough when one is unsure about the accuracy of the dispersion parameter. As dispersion has been shown to be a scale dependent and non-linear parameter, this is probably more often the case than not.

XI. SUMMARY AND CONCLUSIONS

Summary

Reflection on the alluvial and fractured groundwater systems discussed in this work should indicate the *in situ* flow and transport process is a very complex one which can be described mathematically. If a system can be described mathematically, it can be modeled with fuzzy algorithms. Fuzzy analytical groundwater flow and transport models were developed in this paper by linking analytical solutions with fuzzy number representations. Published data regarding both alluvial and fractured aquifers was utilized in the fuzzy models to obtain fuzzy realizations. The resultant fuzzy realizations were found to compare very favorably to published realizations derived via other modeling techniques. The use of fuzzy numbers in analytical modeling simulations allowed the incorporation of uncertainty and imprecision directly into the model in a non-statistical framework, and did not require the generation of a large number of realizations.

This work has shown the fuzzy modeling platform can provide a robust and practical alternative to traditional methods of modeling complex nonlinear systems. This is possible primarily because fuzzy modeling platforms do an excellent job of trading off between realization significance and precision. While the fuzzy approach limits the precision in the description of a groundwater system, the approach increases the

practicality of the solution form by reducing the severity of the underlying assumptions. This characteristic of fuzziness may best be expressed by an early pioneer of fuzzy research, Lotfi Zadeh, in his Law of Incompatibility, "As the complexity of a system increases, our ability to make precise yet significant statements about its behavior diminishes until a threshold is reached beyond which precision and significance (or relevance) becomes almost mutually exclusive characteristics." [Zadeh, 1973]

Conclusions

From a groundwater modeling perspective, deterministic platform models are very useful when sufficient data is available regarding the necessary input parameters. When a system's definition or data is insufficient for deterministic modeling, stochastic models can provide realizations within certain degrees of statistical uncertainty. Unfortunately, these models require detailed information regarding the probability distributions of the ill-defined parameters. If there is a dearth of probability distribution information available, the use of a fuzzy modeling platform should be investigated as the informational requirements of a fuzzy platform are less.

Stochastic, deterministic, and fuzziness do not have to be viewed as mutually contradictory modeling concepts. Fuzziness should simply be viewed as a systematic way to process ambiguous information, and as such, can be used to represent data which possesses non-statistical uncertainty. This paper has shown:

- a. Fuzzy models can operate effectively with reduced informational requirements than either stochastic or deterministic modeling platforms.
- b. A fuzzy modeling platform can perform equally as well as deterministic and stochastic modeling platforms in alluvial aquifers, as well as fractured media.
- c. The fuzzy model's realization was not very sensitive to the type of triangular membership function used to represent the fuzzified variables in this work.
- d. The fuzzy platform performed very favorably compared to discrete numerical models of the same fracture system. Although this research was limited to relatively short distances along a fracture, there is no reason to believe a fuzzy approach would not perform equally as well when longer transport distances are considered.

Groundwater modeling in fractured media more often than not must be conducted under a high degree of uncertainty. The significant advantages of using a fuzzy platform becomes apparent in situations where the acquisition of precise data is impossible, too costly to obtain, or when the required calculations are computationally extensive. The relaxed formal informational requirements of fuzzy mathematics allow fuzzy modeling to be utilized in situations where uncertainty may have been previously unrecognized, or worse, ignored.

REFERENCES

- Acuna, J., and Y. Yortos, Application of fractal geometry to the study of networks of fractures and their transient, *Water Resour. Res.*, 31(3), 527-540, 1995.
- Anderson, M.P., Using models to simulate the movement of contaminants through groundwater flow systems, *CRC Crit. Rev. Environ. Control*, 9,97-156, 1979.
- Bardossy, A. and M. Disse, Fuzzy rule-based models for infiltration, *Water Resour. Res.*, 29(2), 373-382, 1993.
- Bardossy, A., and L. Duckstein, Fuzzy Rule-Based Modeling with Applications to Geophysical, Biological and Engineering Systems, New York, CRC Press, 1995, 216 pp.
- Barenblatt, G., I. Zheltov, and I. Kochina, Basic concepts in the theory of seepage of homogeneous liquids in fissured rocks, *Jrnl. Appl. Math. Mech.*, Vol. 24, 1286-1303, 1960.
- Bear, J., Dynamics of Fluids in Porous Media, New York American Elsevier Publishing Co., 1972, 764 pp.
- Beckie, R., A. Aldama, and E. Wood, The universal structure of the groundwater flow equations, *Water Resour. Res.*, 30(5) 1407-1419, 1994.
- Berkowitz, B., and I. Balberg, Percolation theory and its applications to groundwater hydrology, *Water Resour. Res.*, 29, 775-794, 1993.
- Berkowitz, B., J. Bear, and C. Braester, Continuum models for contaminant transport in fractured porous formations, *Water Resour. Res.*, 24(8), 1225-1232, 1988.
- Berner, R.A., Principles of Chemical Sedimentology, New York: McGraw-Hill, 1971, 240 pp.
- Bosch, P.P., A.C. Klauw, Modeling, Identification and Simulation of Dynamical Systems, New York, CRC Press, 1994, 195 pp.

- Chen, Z. and J. Douglas, Modeling of Compositional Flow in Naturally Fractured Reservoirs: Mathematical, Computational, and Statistical Analysis, IMA Volumes in Mathematics and its Applications, Springer-Verlag, Berlin, 1992, 289 pp.
- Criddle, C.S., P.L. McCarty, M.C. Elliott, and J.F. Barker, Reduction of hexachloroethane to tetrachloroethylene in groundwater, *Contam. Hydrol.*, (1), 133-142, 1986.
- Curtis, G.P., M. Reinhard, and P.V. Roberts, A natural gradient experiment on solute transport in a sand aquifer, 4, Sorption of organic solutes and its influence on mobility, *Water Resour. Res.*, 22, 2045-2071, 1986.
- Cushman, J.H., Comment on Three-dimensional stochastic analysis of macrodispersion in aquifers, *Water Resour. Res.*, 19, 1641-1642, 1983.
- Davison, C.C., Physical hydrogeologic measurements in fractured crystalline rock, Summary of FY 1979 research programs at WNRE and CRNL, Atomic Energy of Canada Limited Report, Technical Record Series, 1980.
- Dance, J.T., Evaluation of reactive solute transport in a shallow unconfined sandy aquifer, M.S. thesis, 93 pp., Univ. of Waterloo, Waterloo, Ont., 1980.
- Domenico, P.A., and F. Schwartz, Physical and Chemical Hydrogeology, John Wiley & Sons, 1990, 824 pp.
- Douglas, J. T. Arbogast, Dynamics of Fluids in Hierarchical Porous Media, London, Academic Press, 1990, 177-221 pp.
- Dou, C., W. Woldt, M. Dahab, and I. Bogardi, Transient ground-water flow simulation using a fuzzy set approach, *Ground Water*, Vol. 35, No. 2, 205-215, March-April 1997.
- Dronfield, D. M., and S. Silliman, Velocity dependence of dispersion for transport through a single fracture of variable roughness, *Water Resour. Res.*, 29(10), 3477-3483, 1993.
- Dubois, D., and H. Prade, Possibility Theory, New York, Plenum Press, 1988, 263 pp.
- Dverstorp, B., J. Andersson, and W. Nordqvist, Discrete fracture network interpretation of field tracer migration in sparsely fractured rock, *Water Resour. Res.*, 28(9), 2327-2343, 1992.

- Ewing, R., and D.B. Jaynes, Issues in single-fracture transport modeling: scales, algorithms, and grid types, *Water Resour. Res.*, 31(2), 303-312, 1995.
- Freyberg, D., A natural gradient experiment on solute transport in a sand aquifer, 2. Spatial moments and the advection and dispersion of nonreactive tracers, *Water Resour. Res.*, 29(11), 2031-2046, 1993.
- Fetter, C.W., Applied Hydrogeology, 1988, pp 592.
- Fourar, M., S. Bories, R. Lenormand, and P. Persoff, Two-phase flow in smooth and rough fractures: measurement and correlation by porous-medium and pipe flow models, *Water Resour. Res.*, 29(11), 3699-3708, 1993.
- Freeze, R.A., and J. Cherry, Groundwater, Prentice-Hall Inc. 1979, 604 pp.
- FuziWare, Inc., FuziCalc User's Guide, 1994, 308 pp.
- Gale, J.E., Comparison of coupled fracture deformation and fluid flow models with direct measurements of fracture pore structure and stress-flow Properties, Proc. U.S. 28th Symp. Rock Mech., Tucson, Ariz., pp. 1213-1222, 1987.
- Gillman, J., An efficient finite-difference method for simulating phase segregation in the matrix block in double-porosity reservoirs, *Soc. Petrm. Engrg.*, (26) 403-423, 1986.
- Grisak, G., and J. Pickens, An analytical solution for solute transport through fractured media with matrix diffusion, *Jrnl. of Hydrology*, Vol. 52, 47-57, 1981.
- Haack, S., Do we need fuzzy logic, *Int. Jrnl. of Man-Machine, Stud.*, Vol. 11, 437-445, 1979.
- Hoeksma, R.J. and P.K. Kitandis, Analysis of the spatial structure of properties of selected aquifers, *Water Resour. Res.*, 21(4), 563-572, 1985.
- Hull, L., J. Miller, and T. Clemon, Laboratory and simulation studies of solute transport in fracture networks, *Water Resour. Res.*, 23(8), 1505-1513, 1987.
- Huyakorn, P., B. Lester, and J. Mercer, An efficient finite element techniques for modeling transport in fractured porous media, 1. Single species transport, *Water Resour. Res.*, 19(3), 841-854, 1983.

- Huyakorn, P., B. Lester, and C. Faust, Finite element techniques for modeling groundwater flow in fractured aquifers, *Water Resour. Res.*, 19(4), 1019-1035, 1983.
- Huyakorn, P., H. White, T. Wadsworth, A Two-Dimensional Finite Element Code for Simulating Fluid Flow and Transport of Radionuclides in Fractured Porous Media with Water Table Boundary Condition, International Ground Water Modeling Center, 1991, 151 pp.
- Hvorslev, M.J., Time lag and soil permeability in groundwater observations, *Bull.* 36, U.S. Army Corps. Eng. Waterw. Exp. Sta., Vicksburg, Miss., 1951.
- Javandel, I., C. Doughty, and C.F. Tsang, Groundwater Transport: Handbook of mathematical models: *AGU Water Resour. Mono.* No. 10, American Geophysical Union, Washington DC, 1984,
- Johnson, P., and B.M. Ayyub, Modeling Uncertainty in prediction of pier scour, *Jrnl. of Hydraulic Eng.*, 122(2), 1996.
- Kaufmann, A., and M.M. Gupta, Introduction to Fuzzy Arithmetic: Theory and Applications, New York, Van Nostrand Reinhold 1985, 351 pp.
- Kazemi, H., and J. Gilman, Improvements in simulation of naturally fractured reservoirs, *Soc. Petroleum Engrg. Jrl.* (23) 695-707, 1983,
- Klir, G. *Generalized Information Theory*, Fuzzy Sets and Systems, 40, 127-142, 1991.
- Li, D., D. Liu, A Fuzzy Prolog Database System, Singapore, Research Studies Press Ltd., 1994, 424 pp.
- MacFarlane, D.S., J.A. Cherry, R.W. Gillham, and E. A. Sudicky, Migration of contaminants in groundwater at a landfill: A case study, 1. Groundwater flow and plume delineation, *J. Hydrol.*, 63, 1-29, 1983.
- Maloszewski, P., and A. Zuber, Mathematical modeling of tracer behavior in short-term experiments in fissured rocks, *Water Resour. Res.*, 26 (7), 1517-1528, 1990.
- Mauldon, A.D., K. Karasaki, S.J. Martel, J.C.S. Long, M. Landsfeld, and A. Mensch, An inverse technique for developing models for fluid flow in fracture systems using simulated annealing, *Water Resour. Res.*, 29(11) 3775-3789, 1993.

- McKay, L.D., J.A. Cherry, and R.W. Gillham, Field experiments in a fractured clay till, 1, Hydraulic conductivity and fracture aperture, *Water Resour. Res.* 29(4), 1149-1162, 1993.
- MacKay, D.M., D.L. Freyberg, P.V. Roberts, and J.A. Cherry, A Natural Gradient Experiment on Solute Transport in a Sand Aquifer, 1. Approach and Overview of Plume Movement, *Water Resour. Res.* 22(13), 2017-2029, 1986.
- McGill, R., An Introduction to Risk Analysis, Petroleum Publishing Company, 1977 118 pp.
- Mizumoto, M., and H.J. Zimmermann, Comparison of fuzzy reasoning methods, *Fuzzy Set Systems*, (8), 253-283, 1982.
- Nelson, R.A., Natural fracture systems: descriptions and classification, *Amer. Assoc. Petr. Geol. Bull.*, (63), 2214-2221, 1979.
- Neuman, S., Eulerian-Lagrangian theory of transport in space-time nonstationary velocity fields: Exact nonlocal formalism by conditional moments and weak approximation, *Water Resour. Res.*, 29(3), 633-645, 1993.
- Ogata, A., Theory of Dispersion in a Granular Medium, *U.S.G.S., Prof. Paper* 411-I 1970.
- Ogata, A., and R.B. Banks, A solution of the Differential Equation of Longitudinal Dispersion in Porous Media, *U.S.G.S. Prof. Paper* 411-A, 1961.
- O'Hannesin, S.F., Spatial variability of grain-size parameters and hydraulic conductivity at a dispersion test site, Bachelor of Environmental Studies *Honors Report*, 46 pp, Univ. of Waterloo, Waterloo, Ont., 1981.
- Palisades Corporation, Risk Analysis and Simulation Add-In, 1995, 124 pp.
- Paleologos, E., S.P. Neuman, and D. Tartakovsky, Effective hydraulic conductivity of bounded, strongly heterogeneous porous media, *Water Resour. Res.*, 32(5), 1333-1341, 1996.
- Persoff, P., and K. Pruess, Two-phase flow visualization and relative permeability measurement in natural rough-walled rock fractures, *Water Resour. Res.*, 31(5), 1175-1186, 1995.
- Quintard, M., and S. Whitaker, Transport in Porous Media, 1988, 357-413 pp.

- Rifai, M.N.E., W.J. Kaufman, and D.K. Todd, Dispersion Phenomena in Laminar Flow Through Porous Media, Report No.3, I.E.R. Series 90 Sanitary Engineering Research Lab., Univ. Calif., Berkeley, 1956, 143 pp.
- Raven, K., K. Novakowski, and P. Lapcevic, Interpretation of field tracer tests of a single fracture using a transient solute storage model, *Water Resour. Res.*, 24 (12), 2019-2032, 1988.
- Remson, I., G.M. Hornberger, and F.J. Molz, Numerical Methods in Subsurface Hydrology, New York, John Wiley & Sons, 1971.
- Roberts P.V., M.N. Goltz, and D.M. MacKay, 3. A Natural Gradient Experiment on Solute Transport in a Sand Aquifer, 3. Retardation Estimates and Mass Balances for Organic Solutes, *Water Resour. Res.* 22(13), 2047-2058, 1986.
- Shapiro, A.M., and J. Andersson, Steady state fluid response in fractured rock: A boundary element solution for a coupled, discrete fracture continuum model, *Water Resour. Res.*, 19(4), 959-978, 1983.
- Serrano, S., Analytical solutions of the non-linear groundwater flow equation in unconfined aquifers and the effects of heterogeneity, *Water Resour. Res.* 31(11), 2733-2742, 1995a.
- Serrano, S., Hydrologic theory of dispersion in heterogeneous aquifers, *Jrl. of Hydrologic Engineering*, 1(4) 144-151, 1996.
- Stearns, D.W., and Friedman, M., Reservoirs in fractured rock, *Amer. Assoc. Petr. Geol. Bull.*, 81-106, 1972.
- Sudicky, E.A., A natural gradient experiment on solute transport in a sand aquifer: Spatial variability of hydraulic conductivity and its role in the dispersion process, *Water Resour. Res.*, 22(13), 2074-2099, 1986.
- Sudicky, E. and E. Frind, Contaminant transport in fractured porous media: Analytical solutions for a system of parallel fractures, *Water Resour. Res.*, 18(6), 1634-1642, 1982.
- Tang, D., E. Frind, and E. Sudicky, Contaminant transport in fractured porous media: Analytical solution for a single fracture, *Water Resour. Res.*, 17(3), 555-564, 1981.
- Terano, T., K. Asai, M. Sugeno, Fuzzy Systems and Theory, Tokyo, Japan, Academic Press, Inc., 1992, 258 pp.

- Thoma, S., D. Gallegos, and D. Smith, Impact of fracture coatings on fracture/matrix flow interactions in unsaturated, porous media, *Water Resour. Res.*, 28(5), 1357-1367, 1992.
- Unger, A. and C.W. Mase, Numerical study of the hydromechanical behavior of two rough fracture surfaces in contact, *Water Resources Research*, 29(7), 2101-2114, 1993.
- Unlu, K., M.L. Kavvas, and D.R. Nielsen, Stochastic analysis of field measured unsaturated hydraulic conductivity, *Water Resour. Res.*, 25(12), 1989.
- Valliappan, S., and T.D. Pham, Fuzzy finite element analysis of a foundation on an elastic soil medium, *Int. Jr. for Numerical and Analytical Methods in Geomechanics*, (17), 771-789, 1993.
- Warrick, A., D.E. Myers, and D.R. Nielsen, Geostatistical methods applied to soil science, Physical and Mineralogical Methods, 2nd Ed., *ASA Mono. No.9*, American Society of Agronomy, Madison, WI., 53-82, 1986.
- Wilson, C.R., and P.A. Witherspoon, An investigation of laminar flow in fractured porous rocks, University of California, Berkeley, Dept. of Civil Eng., *Pub. 70-6*, 1976.
- White, D. and H.M. Gehman, Methods of estimating oil and gas resources, *AAPG Bulletin*, (6), 2183-2192, 1979.
- Yager, R., D. Filev, Essentials of Fuzzy Modeling and Control, New York, John Wiley & Sons, 1994, 388 pp.
- Zadeh, L., Fuzzy sets, *Information Control*, 8, 338-353, 1965.
- Zadeh, L., Outline of a New Approach to the Analysis of Complex Systems and Decision Processes, *IEEE Transactions of Systems, Man, and Cybernetics*, SMC- 3(1), Jan 1973, pp. 28-44.
- Zimmermann, H., Fuzzy Set Theory and its Applications, Boston MA, Kluwer Publishing, 1985, 363 pp.

Appendix A

The following examples illustrates the detail of four basic mathematical operations using two fuzzy numbers. All of the fuzzy numbers used in the following examples will be assumed to have a normal triangular membership function.

Fuzzy Addition

$$Y = X + Z$$

$$Y = (a_x, b_x) + (a_z, b_z)$$

$$Y = [(a_x + a_z), (b_x + b_z)]$$

Fuzzy Subtraction

$$Y = X - Z$$

$$Y = (a_x, b_x) - (a_z, b_z)$$

$$Y = [(a_x - b_z), (b_x - a_z)]$$

Fuzzy Multiplication

$$Y = (X) \times (Z)$$

$$Y = (a_x, b_x) \times (a_z, b_z)$$

$$Y = [(a_x \times a_z), (b_x \times b_z)]$$

Fuzzy Division

$$Y = (X) \div (Z)$$

$$Y = (a_x, b_x) \div (a_z, b_z)$$

$$Y = [(a_x \div a_z), (b_x \div b_z)]$$

Fuzzy Operations at an α -level

An α -level set of A, denoted as A_α , consists of all components of X whose membership grade is greater than or equal to α . Mathematically this is defined as:

$$A_\alpha = \{x / \mu_\alpha(x) \geq \alpha\}$$

Fuzzy Addition

Adding two fuzzy intervals at an α -level in R:

$$\begin{aligned} A_\alpha (+) B_\alpha &= [a_1, a_2] (+) [b_1, b_2] \\ &= [(a_1 + b_1), (a_2 + b_2)] \end{aligned}$$

Fuzzy Subtraction

Subtracting two fuzzy intervals at an α -level in R:

$$\begin{aligned} A_\alpha (-) B_\alpha &= [a_1, a_2] (-) [b_1, b_2] \\ &= [(a_1 - b_1), (a_2 - b_2)] \end{aligned}$$

Fuzzy Multiplication

Multiplication of two fuzzy intervals at an α -level in R:

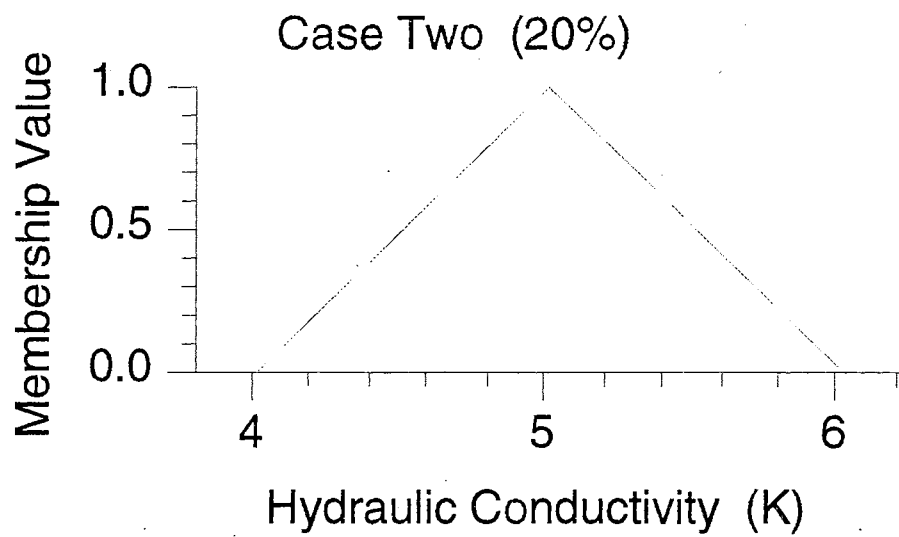
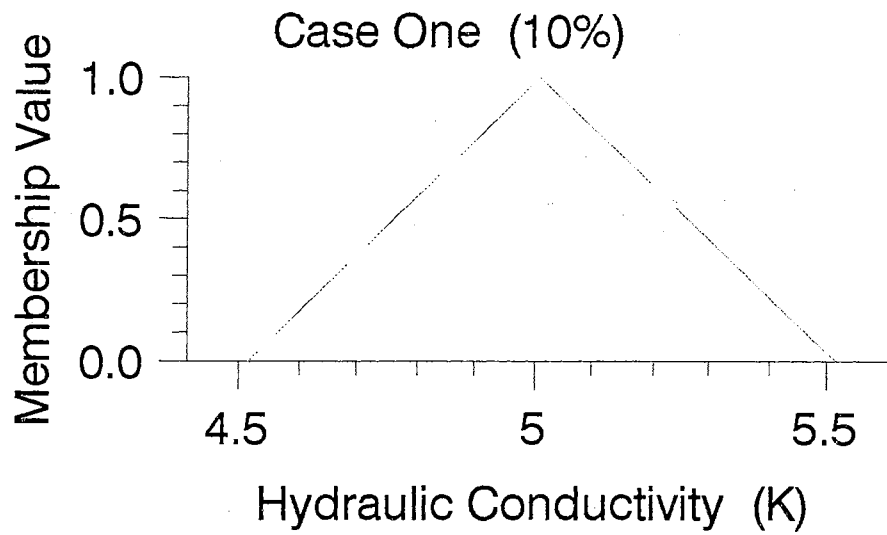
$$\begin{aligned} A_\alpha (x) B_\alpha &= [a_1, a_2] (x) [b_1, b_2] \\ &= [(a_1 \times b_1), (a_2 \times b_2)] \end{aligned}$$

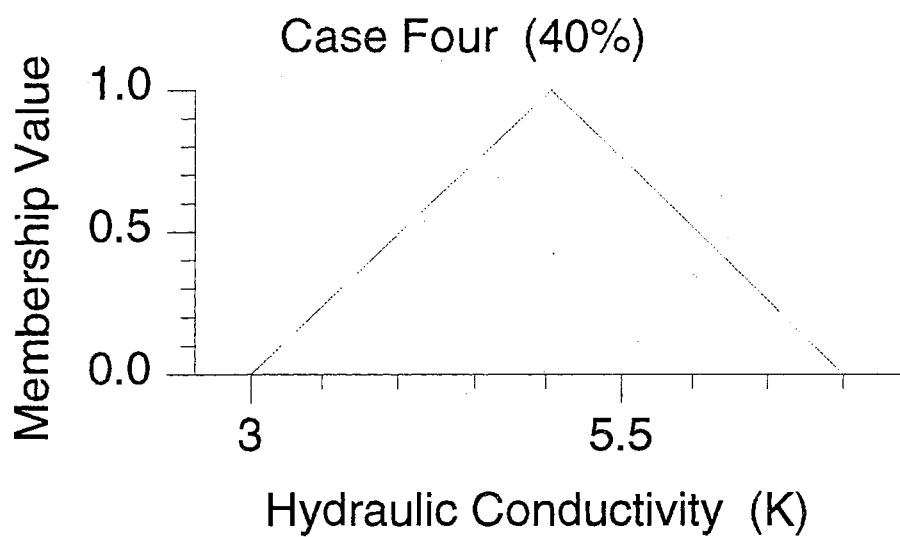
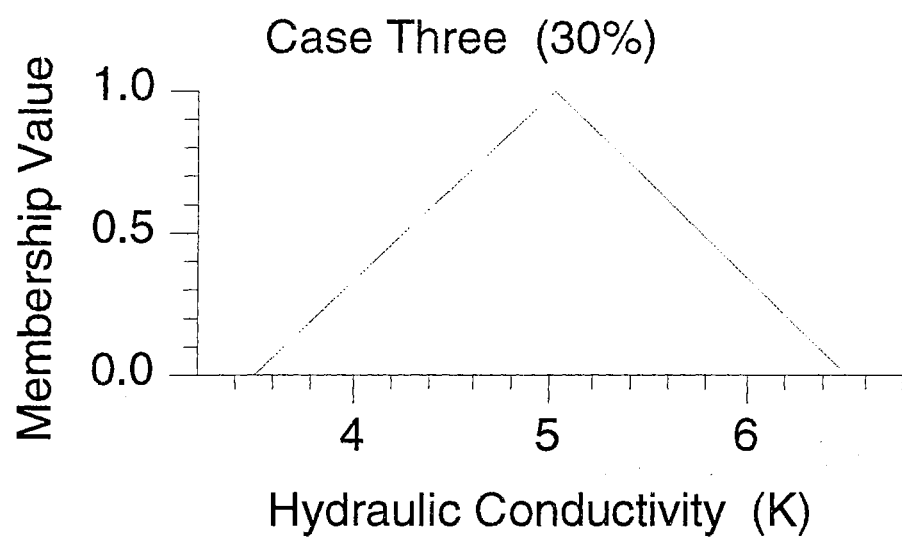
Fuzzy Division

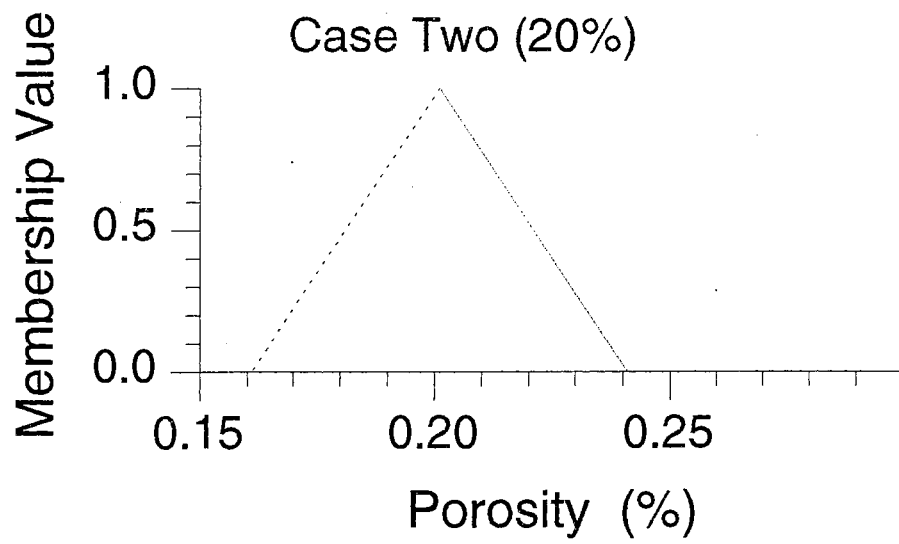
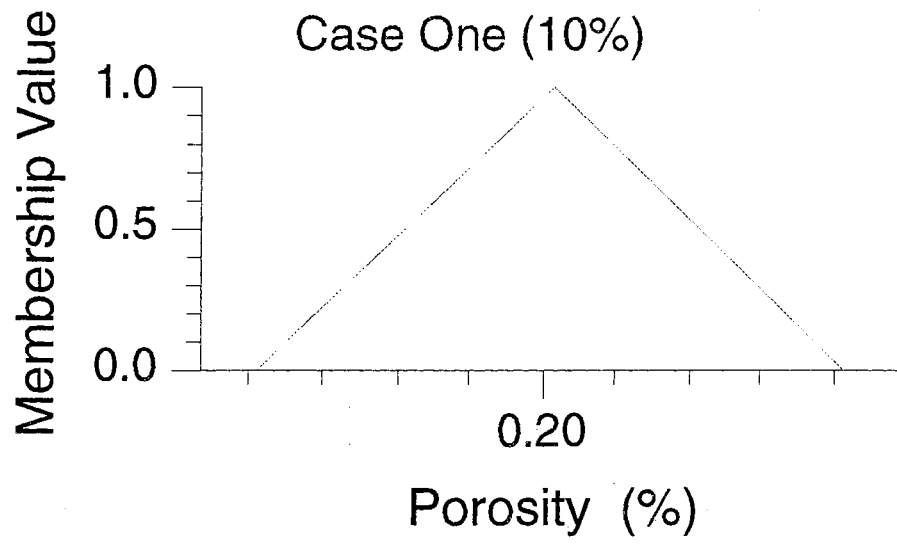
Division of two fuzzy intervals at an α -level in R:

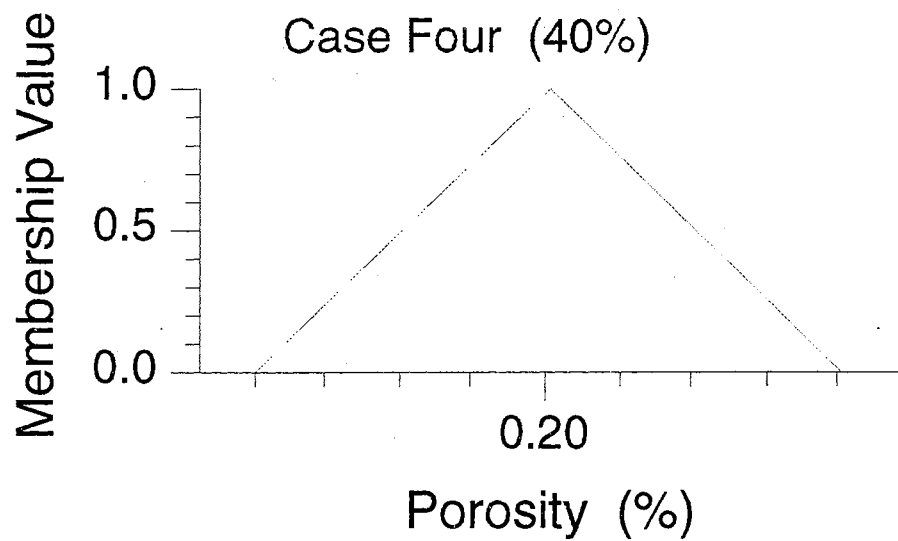
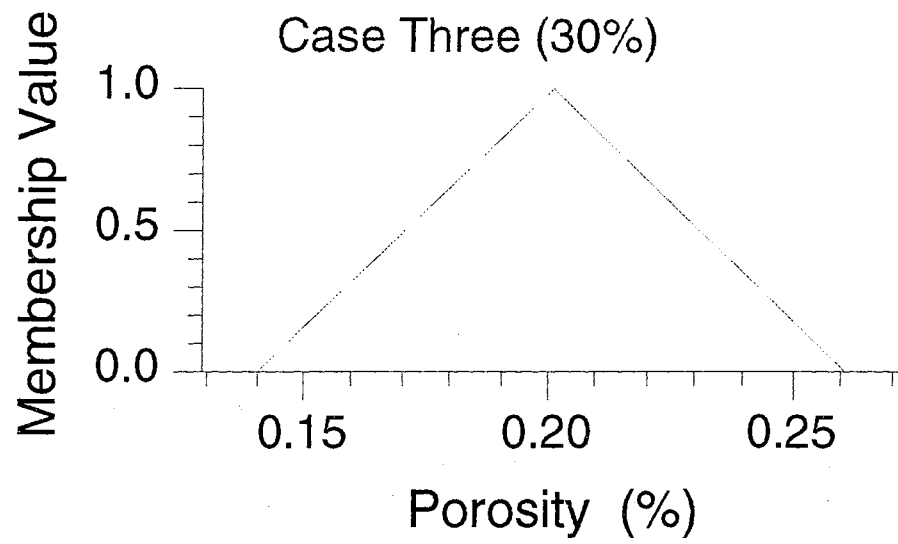
$$\begin{aligned} A_\alpha (\div) B_\alpha &= [a_1, a_2] (\div) [b_1, b_2] \\ &= [(a_1 \div b_1), (a_2 \div b_2)] \end{aligned}$$

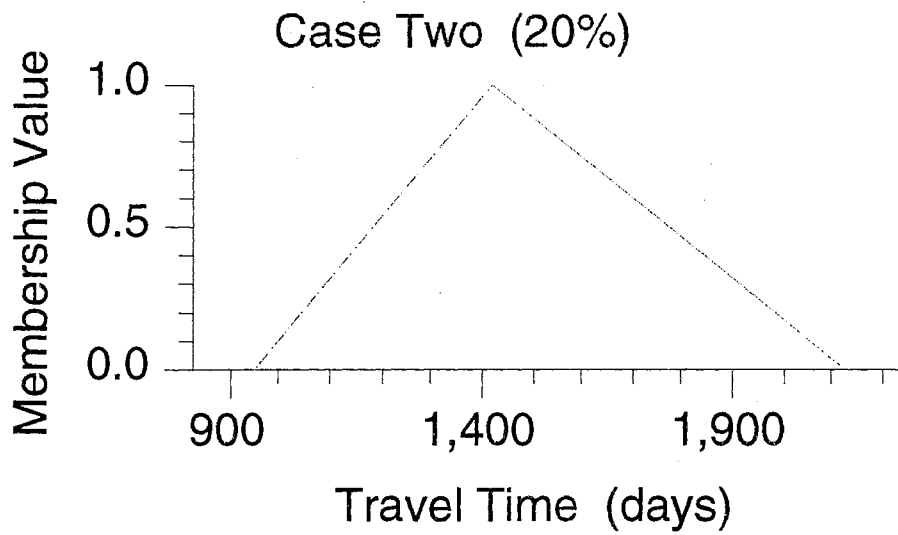
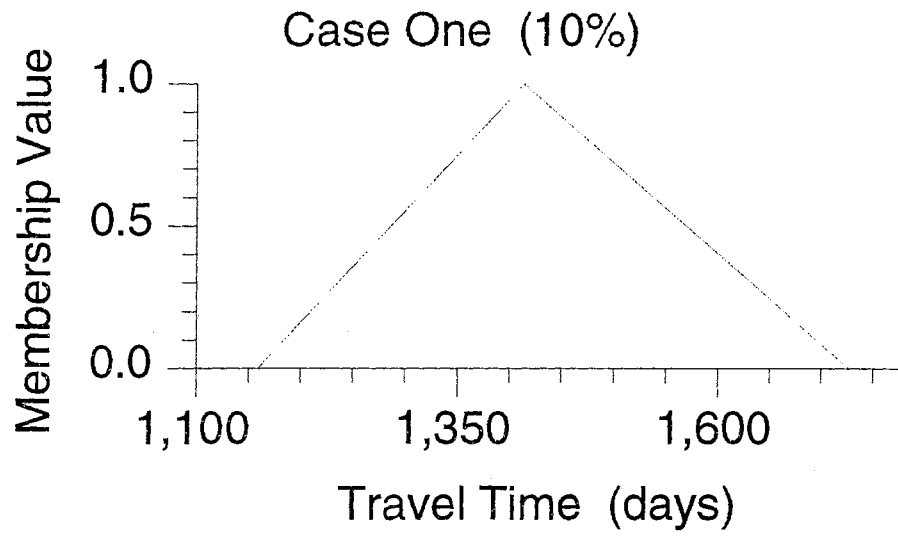
Appendix B

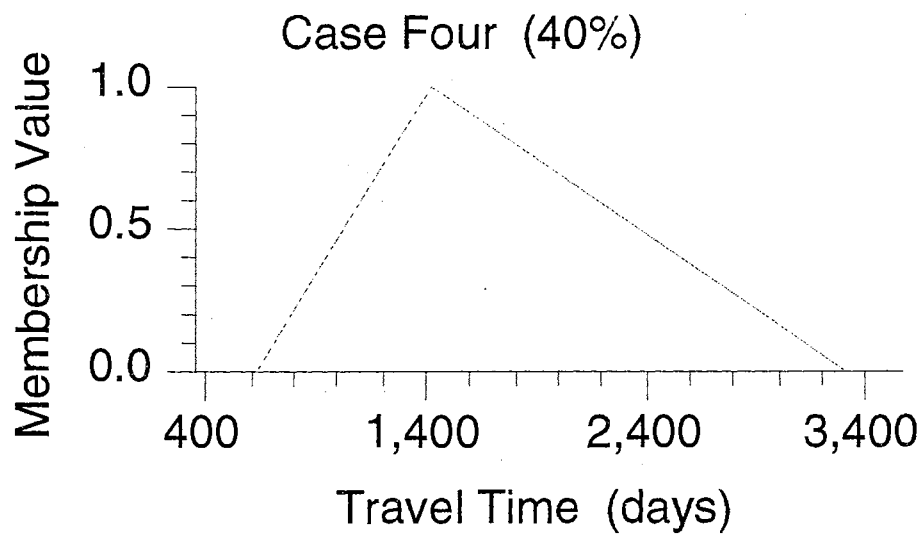
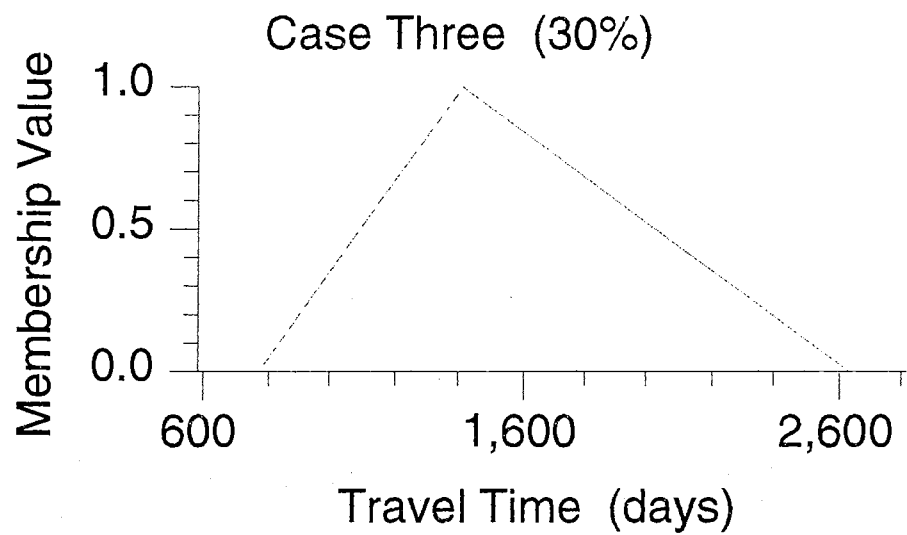




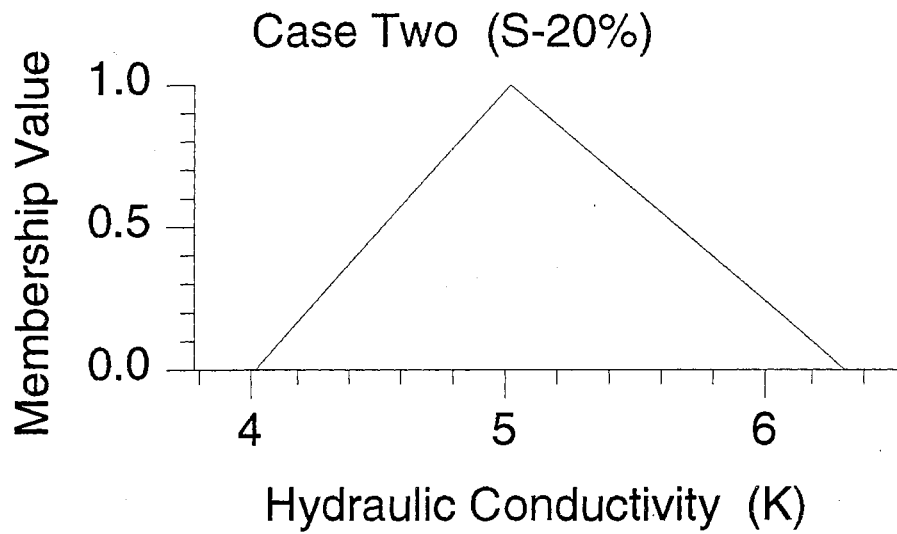
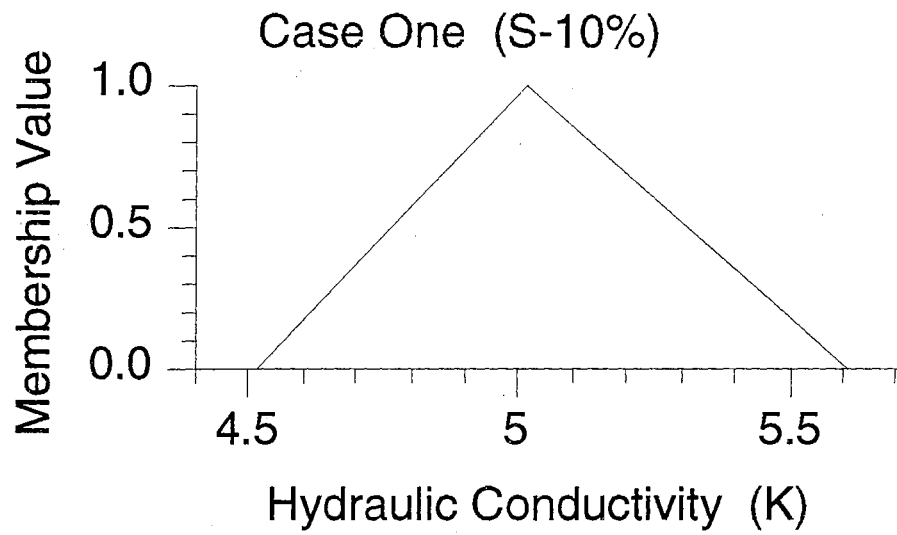


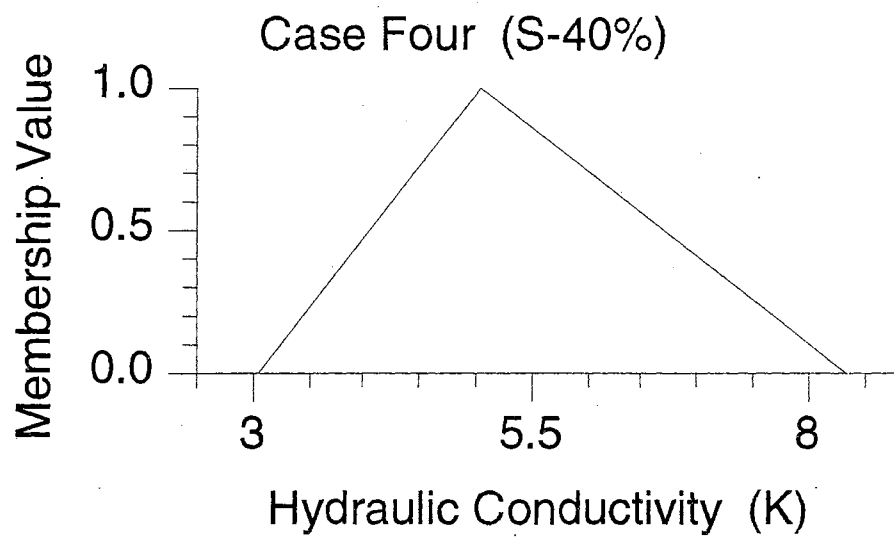
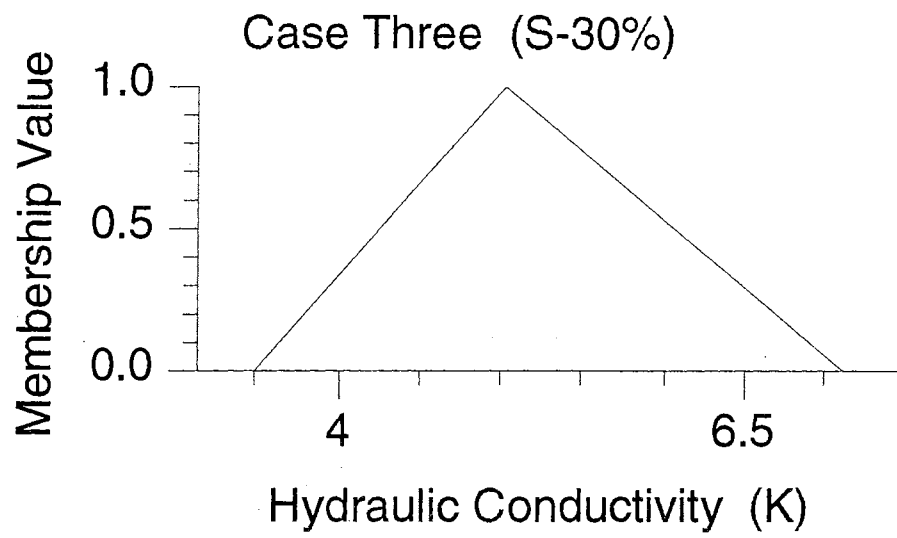


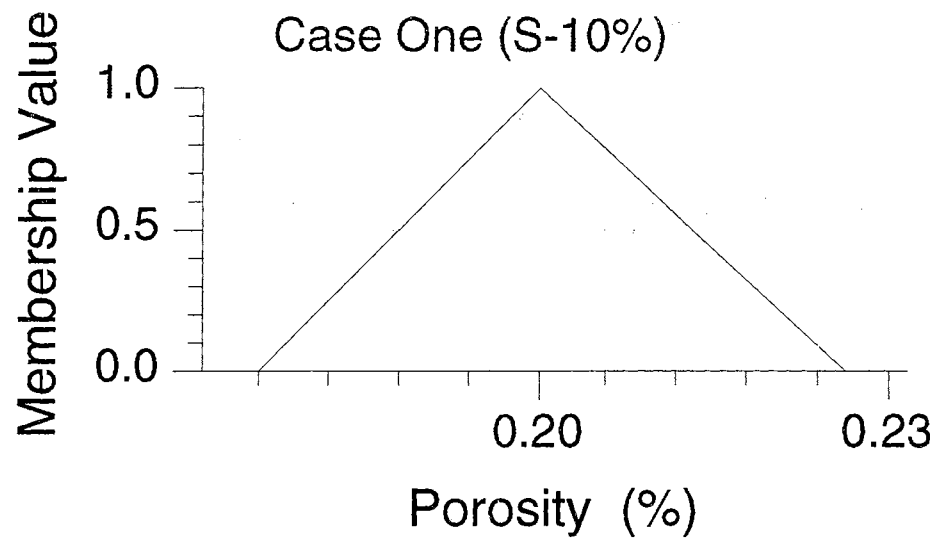


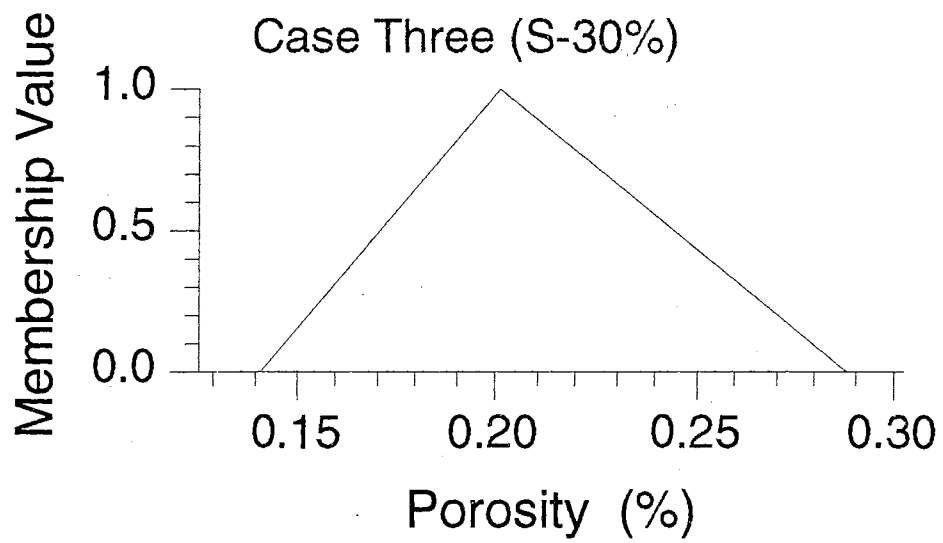
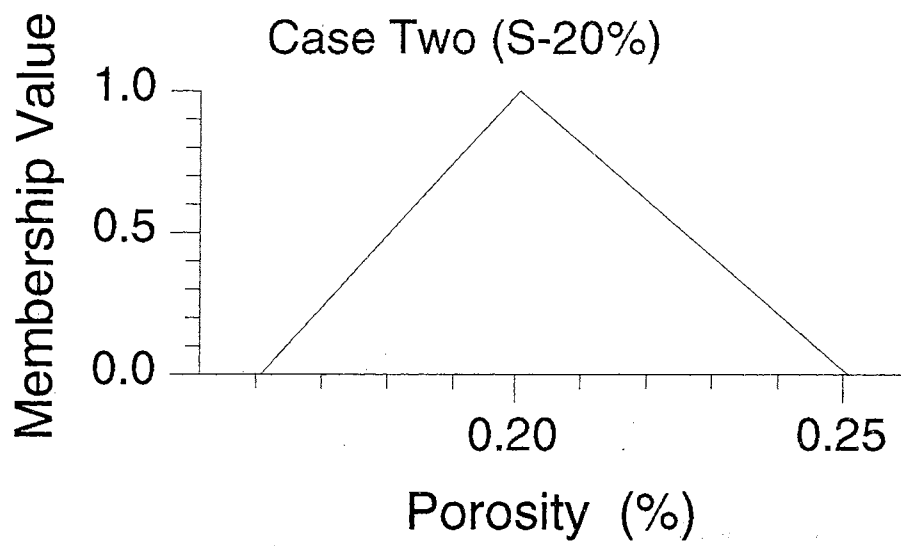


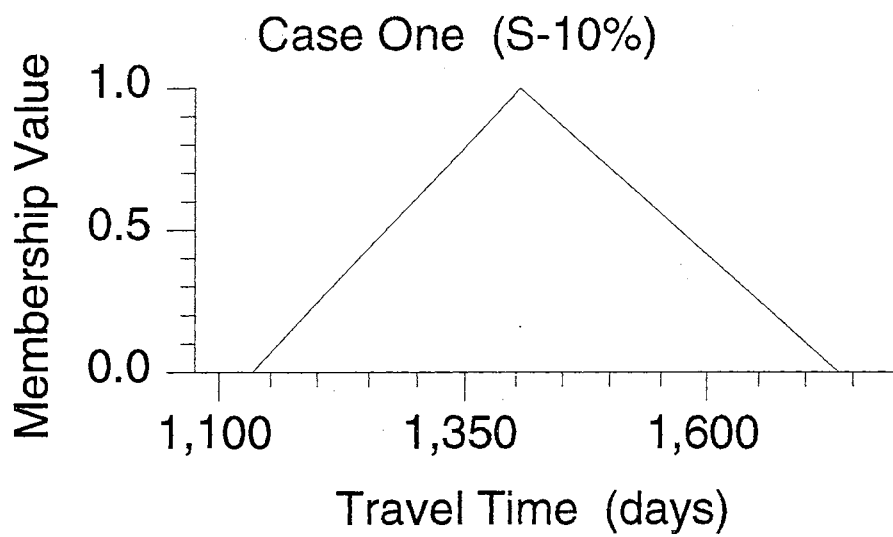
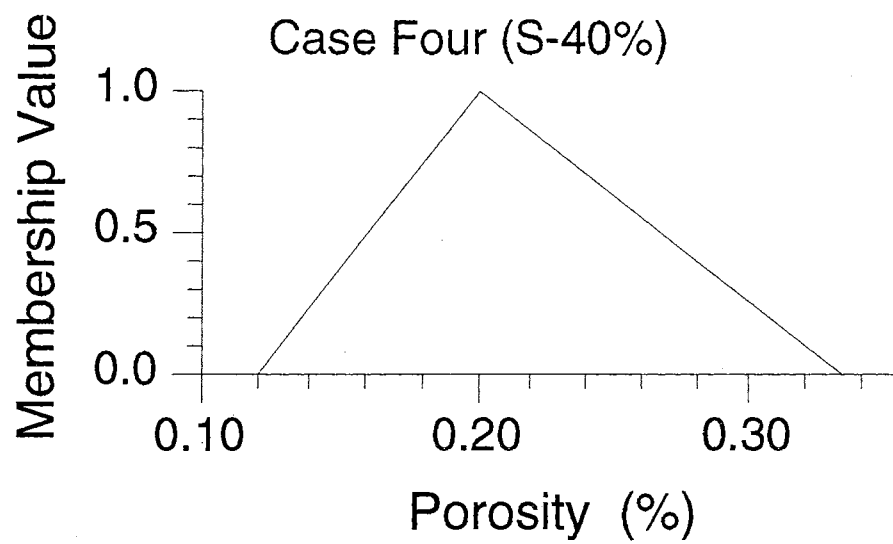
APPENDIX C

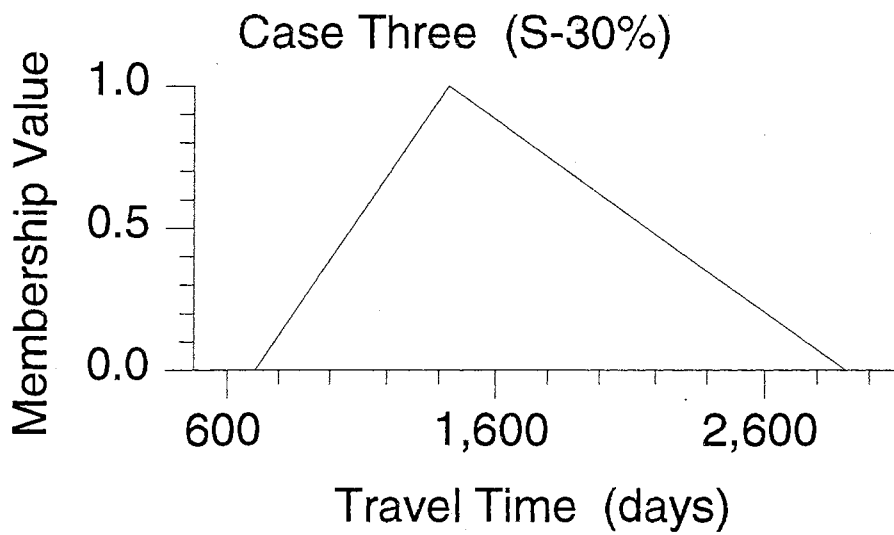
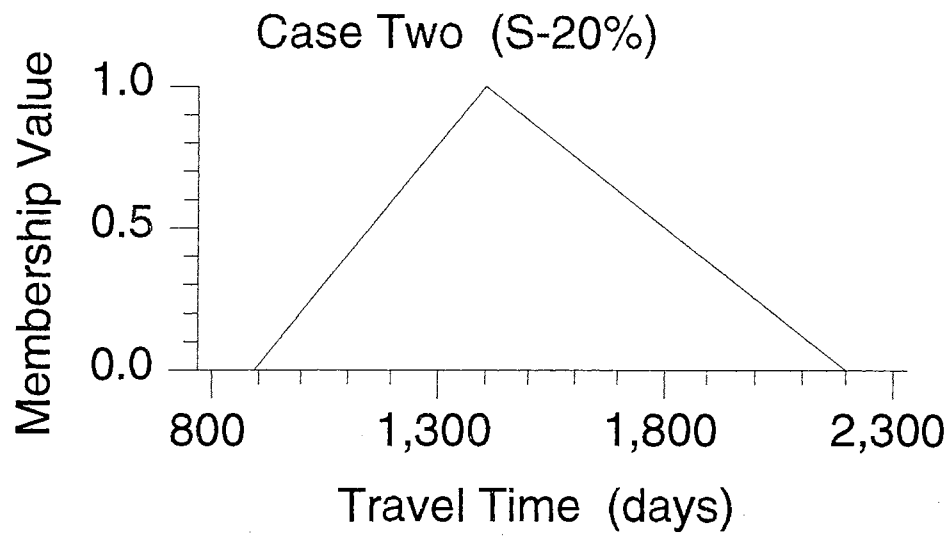


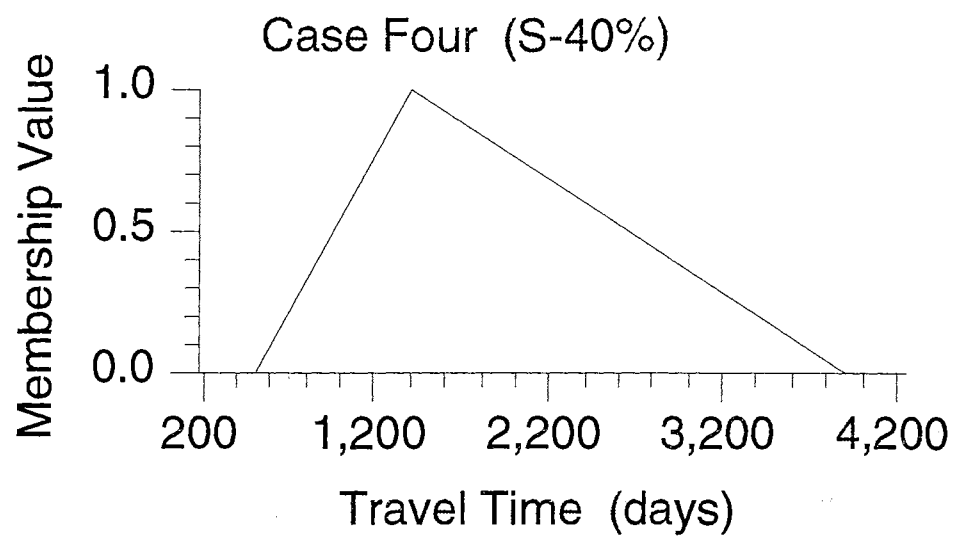












APPENDIX D

Each component section utilized in the determination of the point concentration data at spatial coordinate X can be found below. Each average isopleth value is weighted by the plumes' corresponding thickness value.

Spatial X Coordinate (m)	Total Plume Thickness (m)	$m(\text{mg/l}) + m(\text{mg/l}) + m(\text{mg/l}) + m(\text{mg/l})$	= Conc.
25	0.0	0.0(0)	=0.0
30	1.2	1.2(26)	=31.0
35	2.1	0.3(23) + 1.0(44) + 0.6(31)	=69.5
40	2.3	0.4(23) + 1.0(112) + 1.0(44)	=164.7
45	2.5	0.2(12) + 1.0(116) + 1.0(58) + 0.3(13)	=180.3
50	2.2	0.7(88) + 1.0(40) + 0.3(11)	=104.9
55	1.6	0.5(27) + 1.0(32)	=45.5
60	0.8	0.8(33)	=26.4
65	0.0	0.0(0)	=0.0

APPENDIX E

Elapsed Time (days)	Mass in Solution (Kg)	Center of Mass Location (m)		
		Xc	Yc	Zc
1	6.7	0.2	0.1	2.78
9	9.2	0.7	0.4	3.02
16	9.2	1.6	0.7	3.06
29	11.5	2.9	0.9	3.27
43	11.3	4.1	1.6	3.34
63	9.0	5.7	2.0	3.50
85	11.2	7.7	3.2	3.75
259	11.5	22.7	11.6	4.52
381	9.6	32.3	15.3	5.18
429	9.2	35.9	17.2	5.25
462	8.2	38.2	17.4	5.33
647	9.1	53.1	23.9	5.55

Appendix F

The following equation is taken from Numerical Recipes in C, 2nd edition, Cambridge Press, 1992, pg 221.

This equation is based on a Chebyshev fitting of the complementary error function $\text{erfc}(x)$, and returns answers with fractional errors everywhere less than 1.2×10^{-7} .

```
float t,z, ans;  
  
z=fabs(x)  
t=1.0/(1.0+0.5*z)  
ans=t*exp(-z*z-1.26551223+t*(1.00002368+t*(0.37409196+t*(0.09678418+  
    t*(- 0.18628806+t*(0.27886807+ t*(-1.13520398+t*(1.48851587  
    +t*(- 0.82215223+t*0.17087277))))))))))
```

Appendix G

FIGURE 37 DIGITIZED DATA
(from Grisak & Pickens)

<u>Relative Concentration</u>	<u>Time (days)</u>
0.102	0.12
0.157	0.23
0.192	0.30
0.214	0.40
0.256	0.50
0.346	0.60
0.400	0.70
0.428	0.90
0.438	0.93
0.510	1.10
0.518	1.20
0.549	1.23
0.584	1.40
0.627	1.50
0.638	1.60
0.676	1.90
0.709	2.10
0.729	2.30
0.763	2.60
0.764	2.70
0.769	2.90
0.779	3.30
0.872	3.70

Appendix H

DATA: FIGURES 5a and 5b

FuzziCalc Results

	Min. Endpoint	Centroid	Max. Endpoint
Case 10%	1,152	1,425	1,721
Case 20%	939	1,477	2,112
Case 30%	758	1,573	2,618
Case 40%	604	1,725	3,289

Results Using A Stochastic Normal Distribution

	Min. Endpoint	Centroid	Max. Endpoint
Case 10%	1,181	1,409	1,677
Case 20%	994	1,415	2,031
Case 30%	815	1,429	2,398
Case 40%	702	1,425	2,912

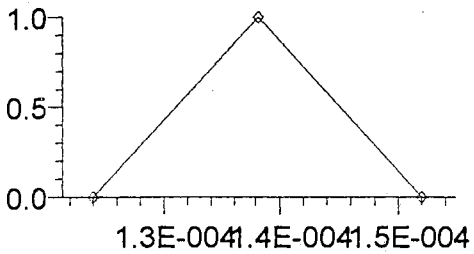
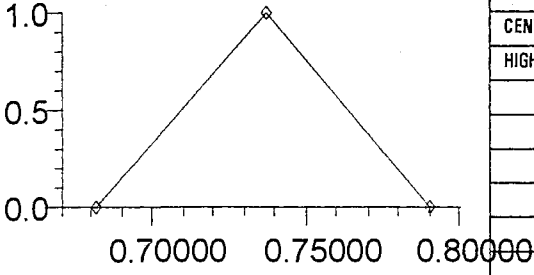
Results Using A Stochastic Lognormal Distribution

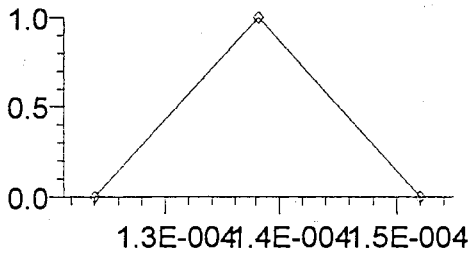
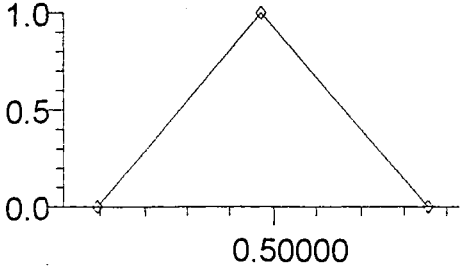
	Min. Endpoint	Centroid	Max. Endpoint
Case 10%	1,175	1,411	1,676
Case 20%	971	1,420	2,096
Case 30%	756	1,445	2,771
Case 40%	562	1,466	3,514

Appendix I

The following pages detail the concentration calculations produced by the FuziCalc software for transport at various distances along the fracture. The fuzzy concentration shown in the bottom graph corresponds to the depth of investigation shown in the upper left hand corner of each page.

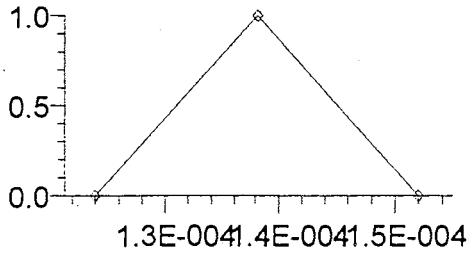
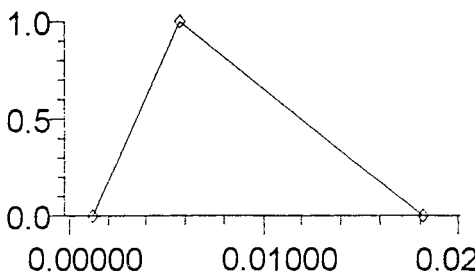
frac-trans	X = .1 METERS						
					$((\text{Por.} \cdot D) / (V \cdot b)) \cdot X$		
INPUT PARAMETERS		erfc					
0.01	= V (m/day)				$2[D \cdot (t-x/v)]^{0.5}$		
1.00E-004	= b(m)						
0.1	= X (m)	erfc			5.80E-004		
4.2E-005	= Porosity				7.37E-001		
1.38E-004	= D (m ² /day)						
995	= t (days)	erfc = >			0.0790208		
COMPLEMENTARY ERROR FUNCTION APPROXIMATION							
	0.07902	= beta					
	0.96201	= t = 1/(1+.5* beta)					
	-0.65777	a1					
	0.85573	a2	erfc(beta) =		0.91113		
	-0.31197	a3	erf(beta) =		0.08887		
	-0.02128	a4					
	-0.20679	a5					
	-0.10219	a6					
	0.27575	a7					
	1.26534	a8					
FUZZY "D "							
				LOW	0.000124		
				CENTROID	0.000138		
				HIGH	0.000152		
FUZZY RELATIVE CONCENTRATION ALONG FRACTURE							
				LOW	0.88672		
				CENTROID	0.91113		
				HIGH	0.93503		

frac-trans	X=0.3 METERS					
				$((\text{Por.} * D) / (V * b)) * X$		
INPUT PARAMETERS		erfc			
0.01	= V (m/day)			$2[D * (t-x/v)]^{0.5}$		
1.00E-004	= b(m)					
0.3	= X (m)	erfc	➤	1.74E-003		
4.2E-005	= Porosity		➤	7.29E-001		
➤ 1.38E-004	= D (m ² /day)					
995	= t (days)	erfc = >	➤	0.239506		
COMPLEMENTARY ERROR FUNCTION APPROXIMATION						
➤ 0.23951	= beta					
➤ 0.89319	= t = 1/(1+.5* beta)					
➤ -0.66953	a1					
➤ 0.89048	a2	erfc(beta)=	➤	0.73553		
➤ -0.33974	a3	erf(beta)=	➤	0.26447		
➤ -0.02478	a4					
➤ -0.20864	a5					
➤ -0.08977	a6					
➤ 0.29371	a7					
➤ 1.26256	a8					
FUZZY "D"						
				LOW	0.000124	
				CENTROID	0.000138	
				HIGH	0.000152	
FUZZY RELATIVE CONCENTRATION ALONG FRACTURE						
					C _f /C _o	
				LOW	0.6807	
				CENTROID	0.73553	
				HIGH	0.78944	

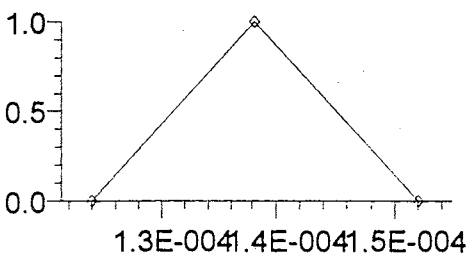
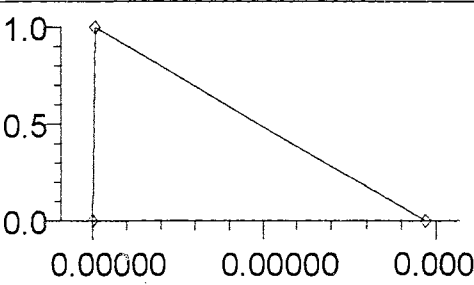
frac-trans	X=0.6 METERS					
				$((Por. * D) / (V * b)) * X$		
INPUT PARAMETERS		erfc			
0.01	- V (m/day)			$2[D * (t-x/v)]^{0.5}$		
1.00E-004	- b(m)					
0.6	- X (m)	erfc	➤	3.48E-003		
4.2E-005	- Porosity		➤	7.18E-001		
➤ 1.38E-004	- D (m ² /day)					
995	- t (days)	erfc = >	➤	0.486637		
COMPLEMENTARY ERROR FUNCTION APPROXIMATION						
➤ 0.48664	- beta					
➤ 0.80472	- t = 1/(1+.5* beta)					
➤ -0.68465	a1					
➤ 0.93751	a2	erfc(beta)=	➤	0.49358		
➤ -0.38050	a3	erf(beta)=	➤	0.50642		
➤ -0.02786	a4					
➤ -0.20910	a5					
➤ -0.07195	a6					
➤ 0.31575	a7					
➤ 1.25450	a8					
FUZZY "D "						
			LOW	0.000124		
			CENTROID	0.000138		
			HIGH	0.000152		
FUZZY RELATIVE CONCENTRATION ALONG FRACTURE						
			LOW	0.41733		
			CENTROID	0.49358		
			HIGH	0.56978		

frac-trans	X = 1.0 METERS						
					$((Por. * D) / (V * b)) * X$		
INPUT PARAMETERS			erfc			
0.01	= V (m/day)				$2[D * (t-x/v)]^{0.5}$		
1.00E-004	= b(m)						
1	= X (m)		erfc	➤	5.80E-003		
4.2E-005	= Porosity			➤	7.02E-001		
➤ 1.38E-004	= D (m^2/day)						
995	= t (days)		erfc = >	➤	0.828988		
COMPLEMENTARY ERROR FUNCTION APPROXIMATION							
	➤ 0.82899	= beta					
	➤ 0.70779	= t = 1/(1+.5* beta)					
	➤ -0.70121	a1					
	➤ 0.99211	a2	erfc(beta) =	➤	0.24610		
	➤ -0.43252	a3	erf(beta) =	➤	0.75390		
	➤ -0.02818	a4					
	➤ -0.20676	a5					
	➤ -0.05022	a6					
	➤ 0.33795	a7					
	➤ 1.23967	a8					
			</				

frac:trans	X=1.5 METERS					
					$((\text{Por.} \cdot D) / (V \cdot b)) \cdot X$	
INPUT PARAMETERS			erfc			
0.01	= V (m/day)				$2\{D \cdot (t-x/v)\}^{0.5}$	
1.00E-004	= b(m)					
1.5	= X (m)		erfc	➤	8.69E-003	
4.2E-005	= Porosity			➤	6.82E-001	
➤ 1.38E-004	= D (m^2/day)					
	995 = t (days)		erfc = >	➤	1.27974	
COMPLEMENTARY ERROR FUNCTION APPROXIMATION						
	➤ 1.27974	= beta				
	➤ 0.61106	= t = 1/(1+.5* beta)				
	➤ -0.71774	a1				
	➤ 1.04980	a2	erfc(beta)=	➤	0.07677	
	➤ -0.49308	a3	erf(beta)=	➤	0.92323	
	➤ -0.02363	a4				
	➤ -0.20124	a5				
	➤ -0.02690	a6				
	➤ 0.35706	a7				
	➤ 1.21860	a8				
FUZZY "D "						
				LOW	0.000124	
				CENTROID	0.000138	
				HIGH	0.000152	
FUZZY RELATIVE CONCENTRATION ALONG FRACTURE						
				LOW	0.03613	
				CENTROID	0.07677	
				HIGH	0.12437	

frac-trans	X = 2.2 METERS					
				$((\text{Por.} \cdot D) / (V \cdot b)) \cdot X$		
INPUT PARAMETERS		erfc			
0.01	= V (m/day)			$2[D \cdot (t-x/v)]^{0.5}$		
1.00E-004	= b(m)					
2.2	= X (m)	erfc	➤	1.28E-002		
4.2E-005	= Porosity		➤	6.54E-001		
➤ 1.38E-004	= D (m ² /day)					
995	= t (days)	erfc = >	➤	1.95989		
COMPLEMENTARY ERROR FUNCTION APPROXIMATION						
➤ 1.95989	= beta					
➤ 0.50674	= t = 1/(1+.5* beta)					
➤ -0.73556	a1					
➤ 1.11563	a2	erfc(beta) =	➤	0.00818		
➤ -0.56917	a3	erf(beta) =	➤	0.99182		
➤ -0.01086	a4					
➤ -0.19205	a5					
➤ -0.00116	a6					
➤ 0.37346	a7					
➤ 1.18953	a8					
FUZZY "D "						
				LOW	0.000124	
				CENTROID	0.000138	
				HIGH	0.000152	
FUZZY RELATIVE CONCENTRATION ALONG FRACTURE						
				LOW	0.00135	
				CENTROID	0.00818	
				HIGH	0.01834	
					Cf/Co	

frac-trans	X = 3.0 METERS					
					$\{(Por. * D) / (V*b)\} * X$	
INPUT PARAMETERS			erfc		
0.01	= V (m/day)				$2\{D * (t-x/v)\}^{0.5}$	
1.00E-004	= b(m)					
3	= X (m)		erfc	➤	1.74E-002	
4.2E-005	= Porosity			➤	6.19E-001	
➤ 1.38E-004	= D (m ² /day)					
995	= t { days)		erfc = >	➤	2.8222	
COMPLEMENTARY ERROR FUNCTION APPROXIMATION						
	➤ 2.82220	= beta				
	➤ 0.41668	= t = 1/(1+.5* beta)				
	➤ -0.75095	a1				
	➤ 1.17547	a2	erfc(beta) =	➤	0.00023	
	➤ -0.64475	a3	erf(beta) =	➤	0.99977	
	➤ 0.00900	a4				
	➤ -0.18236	a5				
	➤ 0.02033	a6				
	➤ 0.38290	a7				
	➤ 1.15973	a8				

frac-trans	X=4.0 METERS					
					$((\text{Por.} * D) / (V * b)) * X$	
INPUT PARAMETERS			erfc			
0.01	= V (m/day)				$2[D * (t-x/v)]^{0.5}$	
1.00E-004	= b(m)					
4	= X (m)		erfc	➤	2.32E-002	
4.2E-005	= Porosity			➤	5.73E-001	
➤ 1.38E-004	= D (m ² /day)					
995	= t (days)		erfc =>	➤	4.06688	
COMPLEMENTARY ERROR FUNCTION APPROXIMATION						
➤ 4.06688	= beta					
➤ 0.33167	= t = 1/(1+.5* beta)					
➤ -0.76548	a1					
➤ 1.23451	a2	erfc(beta)=	➤	2.88E-007		
➤ -0.72520	a3	erf(beta)=	➤	1.00000		
➤ 0.03733	a4					
➤ -0.17318	a5					
➤ 0.03904	a6					
➤ 0.38726	a7					
➤ 1.12856	a8					
FUZZY "D "						
				LOW	0.000124	
				CENTROID	0.000138	
				HIGH	0.000152	
FUZZY RELATIVE CONCENTRATION ALONG FRACTURE						
				LOW	2.98E-011	
				CENTROID	2.88E-007	
				HIGH	9.68E-007	

VITA²

Jon L. LaRue

Candidate for the Degree of
Doctor of Philosophy

Thesis: A FUZZY MODELING PLATFORM FOR FLOW AND
TRANSPORT IN ALLUVIAL AND FRACTURED PORUS MEDIA

Major Field: Civil Engineering

Biographical:

Education: Graduated from Sistersville High School, Sistersville, West Virginia in May 1974; received Bachelor of Science degree in Mechanical Engineering with an Industrial Engineering Option from the University of Cincinnati in May 1979; received a Masters in Business Administration from the University of Texas at Austin in May 1981. Completed the requirements for the Doctor of Philosophy degree with a major in Civil and Environmental Engineering at Oklahoma State University in July 1997.

Professional Memberships: Society of Petroleum Engineers, Gas Processors Association, Pipeliners.